JCBFM

Journal of Cerebral Blood Flow & Metabolism
2023, Vol. 43(1S) S1–S83

DOI: 10.1177/0271678X231176478
journals.sagepub.com/home/jcbfm
Sage

Oral Abstracts

The association of clinical outcome and cerebral autoregulation in acute stroke patients during early mobilization

Lisa Kobayashi Frisk[1], Jonas B. Fischer, Izaksun Belmonte-Jimeno[2], Jacqueline Martínez García[3], Ana Bosch de Basea Gomez[2], Clara Gregori-Pla[3], Daniel Guisado-Alonso[4], Joan Martí-Fàbregas[4], Marta Navarro-Roman[2], Udo M. Weigel[5], Turgut Durduran[6] and Raquel Delgado-Mederos[4]

[1]ICFO-Institut de Ciéncies Fotóniques, The Barcelona Institute of Science and Technology, Castelldefels, Barcelona, Spain
[2]Department of Rehabilitation and Physiotherapy, Hospital de la Santa Creu i Sant Pau
[3]ICFO – Institut de Ciències Fotóniques, The Barcelona Institute of Science and Technology, Spain
[4]Department of Neurology, Hospital de la Santa Creu i Sant Pau, Spain
[5]HemoPhotonics S.L
[6]1ICFO-Institut de Ciéncies Fotóniques, The Barcelona Institute of Science and Technology, Castelldefels, Barcelona, Spain; 2Institució Catalana de Recerca i Estudis Avançats (ICREA), Barcelona, Spain

Abstract

Background: Early mobilization in stroke patients is considered to be a safe and effective method for improving outcome. However, the AVERT trial challenged this view, leading to revisions in clinical guidelines. One culprit for complications could be impaired cerebral autoregulation (CAR) which increases the risk of hypoperfusion in acute stroke.

Aim: We hypothesized that optimal intensity of mobilization intervention depends on cerebral hemodynamic status, particularly CAR.

Method: Hemodynamic parameters including CAR and cerebral metabolic rate of oxygen were monitored in acute stroke (ischemic and hemorrhagic) patients using diffuse optics. Patients were monitored (at 24 ± 6 hours) during a protocol (Figure A) including first mobilization. After optical monitoring, patients were randomized to two groups receiving different intensities of mobilization. Clinical outcomes and safety parameters were recorded at discharge and at three months. Associations of outcome and hemodynamic parameters were measured using linear and logistic regression models. All models were corrected for baseline NIHSS (National Institutes of Health stroke scale) and age.

Results and Conclusions: We recruited 106 patients. 45% were female, and median age was 76 years (IQR [67 83]). Median NIHSS was six (IQR [3, 14]), CAR (independent of mobilization group) at first mobilization was associated ($p = 0.03$) with neurological deterioration ($\geq$4 point increase in NIHSS) and a threshold of CAR impairment was proposed (Figure B). Greater dose (minutes) of mobilization was associated with improvement in PASS (Postural Assessment Scale for Stroke) ($p < 0.05$), independent of CAR. A cerebral hemodynamic parameter for individualizing intensity of mobilization could not be found.

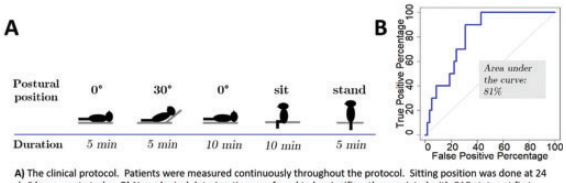

A) The clinical protocol. Patients were measured continuously throughout the protocol. Sitting position was done at 24 ± 6 hours post-stroke. **B)** Neurological deterioration was found to be significantly associated with CAR status at first mobilization (sitting position in **A**)

Fibroblasts repair blood-brain barrier damage and hemorrhagic brain injury in a TIMP2-dependent manner

Lingling Xu[1] and Yao Yao[1]

[1]University of South Florida

Abstract

Background: Fibroblasts are located in the meninges and perivascular space of large vessels in the CNS. Due to lack

of fibroblast-specific markers, their functions remain largely unknown.

Aim: We aim to investigate the function of fibroblasts using a newly identified fibroblast-specific marker–Col1α1.

Method: We generated fibroblast-ablated mice and assessed their intracerebral hemorrhage (ICH) outcomes, including neurological functions, hematoma volume, and blood-brain barrier (BBB) integrity. The paracellular and transcellular mechanisms of BBB disruption were further explored by transmission electron microscopy. Furthermore, the molecules that mediate the neuroprotective role of fibroblasts were screened using a proteomic approach, and their functions were validated *in vitro* and *in vivo* using both pharmacological and genetic approaches.

Results: Although grossly normal under homeostatic conditions, fibroblast-ablated mice demonstrated worse neurological function, enlarged injury volume, and exacerbated BBB damage after ICH. Similarly, fibroblasts significantly decreased endothelial permeability in an *in vitro* ICH model. Subsequent mechanistic studies revealed that fibroblasts repaired BBB damage mainly via up-regulating tight junction proteins without affecting transcytosis. Using LC-MS/MS, we identified ~20 fibroblast-secreted proteins that may mediate this neuroprotective effect. Further studies demonstrated that blockage or knockdown of TIMP2 in fibroblasts exacerbated BBB disruption in the *in vitro* ICH model. More importantly, we found that exogenous TIMP2 was able to attenuate BBB disruption in fibroblast-ablated mice after ICH.

Conclusions: These results suggest that Col1α1^{+} fibroblasts repair BBB damage in ICH via the paracellular pathway in a TIMP2-dependent manner, and that fibroblasts and TIMP2 may be targeted in the treatment of ICH.

Figure:

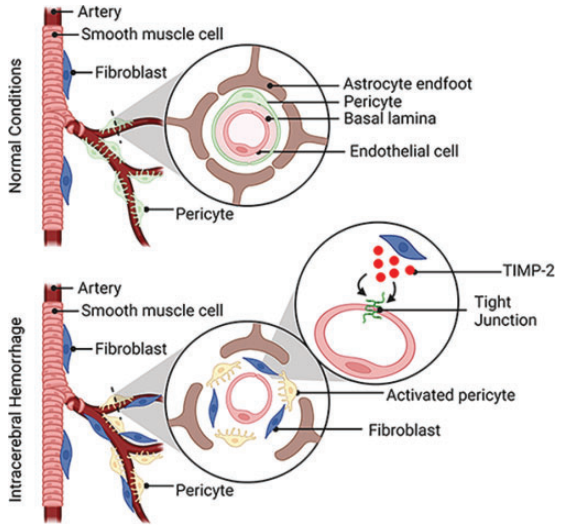

Triculture-based BBB microphysiological system and its application in the study of BBB-glioblastoma interaction

Hong Nam Kim[1]

[1]*Korea Institute of Science and Technology*

Abstract

Background: Physiologically, brain tumors interact with surrounding vascular and glial cells, and change their responses depending on the brain tissue-specific microenvironments. Therefore, mimicking the physiological environment of brain tumors on 3D engineered in vitro platforms can aid in predicting the cellular response to drugs.

Aim: We present a BBB-mimetic model by coculturing BBB-composing cells in the 3D microphysiological system, in other words, an organ-on-a-chip platform. Further, by incorporating brain tumor spheroids in the 3D BBB model, we analyze the structural and functional changes of both BBB and brain tumors.

Method: We prepared a 3D BBB structure by embedding astrocytes and pericytes in the hydrogel and by seeding the brain microvascular endothelial cells in the pre-formed microchannels. The brain tumor spheroids were mixed with the hydrogel and injected through the side channels, and thereby the BBB-glioblastoma interacting microenvironment was formed.

Results: First, we confirmed that three-types of BBB composing cells are definitely needed to ensure the tight barrier function by controlling the number of cell types in the BBB model. Further, the effectiveness of BBB opening agents were also validated by using our 3D BBB model. Next, the effect of BBB-glioblastoma interaction was evaluated by observing the cellular behaviors. In the view of BBB, the existence of tumor spheroids promoted the angiogenic sprouting, leaky barrier function, vasodilation, and vascular inflammation. In the view of brain tumor, the significant invasion of tumor cells towards the surrounding matrix was observed, and the tumor cells also acquired chemoresistance. We also could promote the delivery of anticancer drugs by opening the BBB with BBB opening agents.

Conclusions: In this study, we proposed a human cell-based BBB chip, confirmed its in vivo BBB-like functionality through a permeability assay, and showed the importance of triculture in the recapitulation of the barrier function.

Association of RNF213 polymorphism and cortical hyperintensity sign on FLAIR images after revascularization surgery for moyamoya disease

Haruto Uchino[1], Masaki Ito[2], Kikutaro Tokairin[2], Ryota Tatezawa[1], Taku Sugiyama[2], Ken Kazumata[2] and Miki Fujimura[1]

[1]*Department of Neurosurgery, Hokkaido University Graduate School of Medicine, Sapporo, Japan*
[2]*Hokkaido university*

Abstract

Background: A cortical hyperintensity on fluid-attenuated inversion recovery images (FLAIR cortical hyperintensity, FCH) is an abnormal finding after revascularization surgery for moyamoya disease.

Aim: This study aimed to investigate the pathophysiology of FCH through genetic analyses of *RNF213* p.R4810K polymorphism and perioperative hemodynamic studies using single photon emission computed tomography.

Method: We studied 96 hemispheres in 65 adults and 47 hemispheres in 27 children, who underwent combined direct and indirect revascularization. Early or late FCH was defined when it was observed on postoperative days 0–2 or 6–9, respectively. FCH scores (range: 0–6) were evaluated according to the extent of FCH in the operated hemisphere.

Results: FCHs were significantly more prevalent in adult patients than pediatric patients (early: 94% vs. 78%; late: 97% vs. 59%). In pediatric patients, FCH scores were significantly improved from the early to late phase regardless of the *RNF213* genotype (mutant median [IQR]: 2 [1–5] vs. 1 [0–2]; wild-type median: 4 [0.5–6] vs. 0.5 [0–1.75]). In adults, FCH scores were significantly improved in patients with the wild-type *RNF213* allele (median: 4 [2–5.25] vs. 2 [2–3]); however, they showed no significant improvement in patients with the *RNF213* mutation. FCH scores were significantly higher in patients with symptomatic cerebral hyperperfusion than those without it (early median: 5 [4–5] vs. 4 [2–5]; late median: 4 [3–5] vs. 3 [2–4]).

Conclusions: In conclusion, the *RNF213* p.R4810K polymorphism was associated with prolonged FCH, and extensive FCH was associated with symptomatic cerebral hyperperfusion in adult patients with moyamoya disease.

Altered brain metabolism in a mouse model of 16p11.2 deletion syndrome.

Alexandria Béland-Millar[1], Alexia Kirby[1], Yen Truong[1], Julie Ouellette[1], Sozerko Yandiev[2], Khalil Bouyakdan[3], Chantal Pileggi[1], Shama Naz[1], Micaël Carrier[4], Pavel Kotchetkov[1], Marie-Kim St-Pierre[4], Marie-Ève Tremblay[4], Julien Courchet[2], Mary-Ellen Harper[1], Thierry Alquier[3], Claude Messier[1], Adam J. Shuhendler[1] and Baptiste Lacoste[1]

[1]*University of Ottawa*
[2]*University of Lyon 1*
[3]*University of Montreal*
[4]*University of Victoria*

Abstract

Background: The brain is reliant on a continuous influx of energy substrates and is thus vulnerable to metabolic imbalance. We recently revealed a causal link between endothelial deficits and neuronal abnormalities in a mouse model of 16p11.2 deletion (*16p11.2*$^{df/+}$ mice), a mutation related to autism spectrum disorders (ASD). *16p11.2*$^{df/+}$ mice displayed similarities with models of glucose transporter-1 deficiency, including impaired brain angiogenesis, enhanced evoked neuronal activity and ASD-related behaviors.

Aim: We investigated key metabolic players in the cerebral cortex of adult male *16p11.2*$^{df/+}$ and wild-type (WT) mice to determine whether the previously-observed neurovascular deficits are associated with, or a cause of, changes in brain metabolism.

Method: Brain glucose entry was measured by positron emission tomography (PET) of FDG uptake in anesthetized mice. Extracellular metabolite fluctuations were quantified using biosensors in the cerebral cortex of anesthetized mice. Protein levels were measured by western blots. Mitochondrial number and structure were assessed by transmission electron microscopy.

Results: Anesthetized *16p11.2*$^{df/+}$ mice displayed higher brain glucose uptake than WT controls ($n = 5$; $p < 0.05$), which was recapitulated in mice with endothelial-specific 16p11.2 deletion ($n = 9$; $p < 0.001$). Awake *16p11.2*$^{df/+}$ mice displayed attenuated fluctuations of extracellular brain glucose following systemic glucose administration compared to controls ($n = 4$; $p < 0.001$). Metabolomics on cerebral cortex extracts measured enhanced metabolic responses to systemic glucose in *16p11.2*$^{df/+}$ mice ($n = 5$). The latter also displayed significantly reduced mitochondria number in brain endothelial cells (ECs) compared to

WTs ($n = 7$; $p < 0.05$). Reduced mitochondria content in 16p11.2-deficient ECs was associated with absence of NT-PGC1α protein ($n = 5$; $p < 0.01$), suggesting defective mitochondrial biogenesis.
Conclusions: Altered brain metabolism in *16p11.2*$^{df/+}$ mice appears as compensatory to endothelial dysfunction and is associated with reduced mitochondrial biogenesis. We propose a model whereby *16p11.2*$^{df/+}$ mice modulate their brain glycolytic pathway to shunt additional glucose towards the pentose phosphate pathway as a result of dysfunctional brain ECs.

PET measurement of cyclooxygenase-2 (COX-2) with 11C-MC1in healthy human brain

Xuefeng Yan[1], Andrea Zhang[1], Cheryl Morse[1], Jeih San Liow[1], Min Jong Kim[1], Jose Montero Santamaria[1], Maria Ferraris Araneta[1], Andrew Mannes[2], Ningping Feng[3], William Miller[1], Lester Manly[1], Madeline Jenkins[1], Maia Van Buskirk[1], Carson Knoer[1], Bruny Kenou[1], Sara Rubovitz[1], Sami Zoghbi[1], Victor Pike[1], Robert Innis[1] and Paolo Zanotti Fregonara[4]

[1]Molecular Imaging Branch, National Institute of Mental Health, National Institutes of Health
[2]Department of Perioperative Medicine, Clinical Center NIH
[3]Human Brain Collection Core, National Institute of Mental Health, National Institutes of Health
[4]Molecular Imaging Branch, National Institute of Mental Health, National Institutes of Health, Bethesda, MD, USA

Abstract
Background: ^{11}C-MC1 is a selective and high-affinity radioligand for COX-2.
Aim: This study investigated whether COX-2 can be measured by ^{11}C-MC1 in healthy human brain.
Method: Ten healthy participants received two brain ^{11}C-MC1 PET scans, at baseline and after blockade with celecoxib. A test-retest imaging was conducted in other 17 participants. Receptor occupancy was determined via Lassen plot. Time stability, test-retest variability and reliability were evaluated. To investigate the ability of ^{11}C-MC1 to image the human COX-2, baseline and blocked scans were performed in transgenic mice, which expressed human COX-2 in brain.
Results: Brain radioactivity peaked at 4.0 SUV at ~2.8 minutes and declined to 16% of the peak at 120 minutes. The brain time-activity curves visually fit well using 2TCM. V_Ts were stable after 80 minutes. Celecoxib decreased V_T in all 10 subjects by 18 ± 9% in cortical regions, and this translated into a low BP_{ND} (<0.2). No significant blockade was observed in the subcortical regions, which express lower levels of COX-2 mRNA transcripts. Celecoxib occupied all available COX-2 in the brain (slope = 1.07). V_T exhibited moderate test-retest reliability (ICC = 0.56) and variability (12%). In transgenic mice, about 70–90% of ^{11}C-MC1 uptake in brain could be blocked.
Conclusions: Both human and transgenic rodent data confirm that ^{11}C-MC1 specifically binds to the human COX-2 enzyme. The specific binding is higher in regions of the neocortex, which express higher levels of COX-2 mRNA transcripts.
Figure:

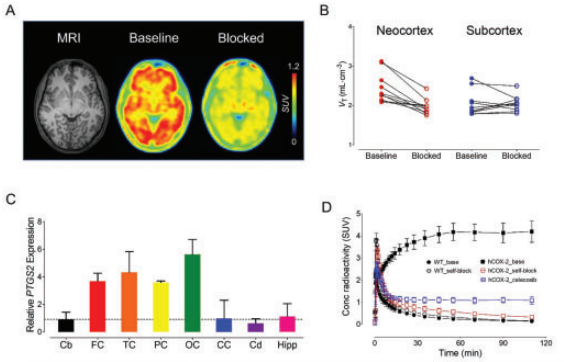

(A) Distribution of radioactivity in human brain at baseline and after blockade by Celecoxib, and the corresponding MRI slice (B) Total distribution volume (V_T) of ^{11}C-MC1 in neocortex and subcortex for 10 participants at baseline and after blockade. (C) Regional *PTGS2* mRNA transcript relative to cerebellum (Cb). (D) Whole brain time-activity curves from PET in wild-type (WT) and human COX-2 transgenic mice (hCOX-2).

Differences in Total Cognition and Cerebrovascular Function in Female Breast Cancer Survivors and Cancer-Free Women

Tahnee Downs[1], Eliza Whiteside[1], Dean Milss[1] and Edward Bliss[1]

[1]University of Southern Queensland

Abstract
Background: Cognitive decline is commonly reported in up to 75% of breast cancer patients and survivors. This reduces their quality of survivorship. Further, the mechanisms for this decline are yet to be determined but may be preceded by a reduction in cerebrovascular function.

Aim: We compared the differences in cerebrovascular function and cognition in breast cancer survivors and cancer-free women, matched by age and body mass index.
Method: Participants undertook anthropometric, mood, cardiovascular, exercise performance, strength, cerebrovascular, and cognitive assessments. Transcranial Doppler ultrasound was used to measure the cerebrovascular responsiveness (CVR) to physiological (hypercapnia; 5% carbon dioxide) and psychological stimuli.
Results: Breast cancer survivors ($n = 15$) had a lower CVR to hypercapnia (21.5 ± 12.8 vs $66.0 \pm 20.9\%$, $P < 0.001$), CVR to cognitive stimuli (15.1 ± 1.5 vs $23.7 \pm 9.0\%$, $P < 0.001$) and total composite cognitive score (100 ± 12 vs. 113 ± 7, $P = 0.003$) than cancer-free women ($n = 15$). These parameters remained statistically different between the groups following adjustments for covariates using an analysis of co-variance. We observed significant correlations between multiple measures and exercise capacity, the only variable positively correlated to all primary measures (CVR to hypercapnia, $r = 0.492$, $P = 0.007$; CVR to cognitive stimuli $r = 0.555$, $P = 0.003$; and total composite cognitive score, $r = 0.625$, $P < 0.001$).
Conclusions: Breast cancer survivors have lower cerebrovascular and cognitive function than age-matched cancer-free women, which is likely attributable to the detrimental effects of cancer and cancer treatment on brain health.
Figure:

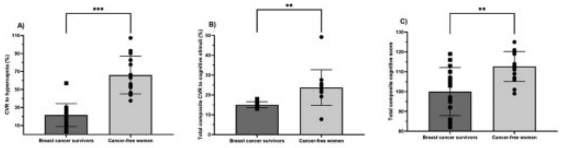

Cerebrovascular responsiveness (CVR) to hypercapnia (A), CVR to total composite of cognitive stimuli (B) and total composite cognitive score (C) for breast cancer survivors and cancer-free women. Significantly different between groups ** (P<0.005), *** (P<0.001).

ATF3 coordinated with lipid metabolism control a pro-inflammatory subpopulation of microglia function in brain injury

Yan Li[1] and Peiying Li[2]

[1]Renji Hospital Affiliated to Shanghai Jiao Tong University School of Medicine
[2]Renji Hospital, Shanghai Jiao Tong University School of Medicine

Abstract
Background: The pro-inflammatory phenotype change of microglia plays a key role in the neuroinflammation evolving following acute brain injuries. Recent evidence suggest that lipid metabolism could profoundly affect the pro-inflammatory phenotypic switch of microglia, however, the precise regulatory mechanism remains unclear.
Aim: The purpose of this study is to explore the regulatory mechanism of microglial pro-inflammatory phenotypic change and investigate its relationship with the lipid metabolism of microglia in the neuroinflammation evolving following acute brain injuries.
Method and Results: Using single-cell sequencing, we found a Ccl4+ subpopulation of microglia that was highly correlated with neuroinflammation and neurocognitive function in stroke, perioperative stroke (PIS), and traumatic brain injury (TBI). Transcriptome sequencing, flow cytometry analysis, and immunostaining revealed that pro-inflammatory microglia specifically express increased level of transcription factor 3 (ATF3) in the Ccl4+ microglia ($n = 4$, $P < 0.05$). Conditional deletion of ATF3 in microglia prohibited the phenotypic switch of Ccl4+ microglia and improves neuroinflammation and neurocognitive dysfunction following stroke, PIS and TBI ($n = 8$, $P < 0.05$). We further revealed that ATF3, as a metabolic checkpoint, could promote lipid decomposition and the generation of saturated free fatty acids, and control the microglia lipid metabolism, thus modulate the pro-inflammatory phenotype switch ($n = 6$, $P < 0.05$).
Conclusions: Our work reveals that ATF3 plays a key role in regulating the lipid metabolism and the pro- phenotypic switch of Ccl4+ pro-inflammatory microglia during neuroinflammation evolving, thus may serve as a novel therapeutic target for precise microglia modulation to combat detrimental neuroinflammation following acute brain injuries.

Figure:

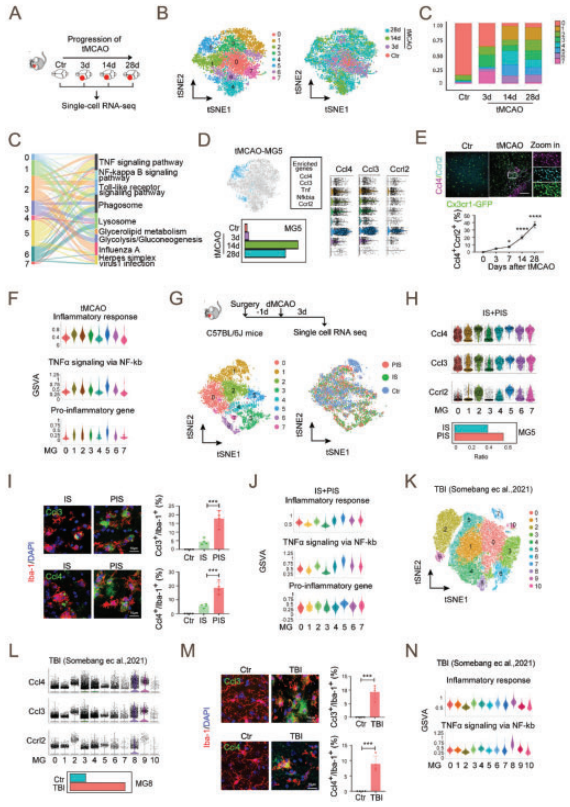

Is ASL perfusion MRI A Potential Alternative to 18F-FDG PET for Lateralization of Mesial Temporal Lobe Epilepsy?

Mohammad-Reza Nazem-Zadeh[1], Hossein Rahimzadeh[2], Hadi Kamkar[3], Pardis Ghafarian[4], Ben Sinclair[5] and Meng Law[1]

[1]Monash University
[2]Department of Biomedical Engineering and Medical Physics, Shahid Beheshti University of Medical Sciences, Tehran, Iran
[3]4Bioinformatics and Biophysics Department, Tarbiat Modares University, Tehran, Iran
[4]Chronic Respiratory Diseases Research Center, National Research Institute of Tuberculosis and Lung Diseases, Shahid Beheshti University of Medical Sciences, Tehran, Iran
[5]Monash University, Neuroscience Department

Abstract

Background: ^{18}F-fluorodeoxyglucose positron emission tomography (^{18}F-FDG-PET) is the primary interictal pre-surgical imaging for diagnosing focal hypometabolism in mesial temporal lobe epilepsy (mTLE) with a 60–90% sensitivity. Yet, it has significant limitations including radiation exposure, high cost, and limited availability. Arterial spin labelling (ASL) is a modality of magnetic resonance imaging (MRI) that provides fairly accurate quantitative measures of cerebral blood flow (CBF) by artificially magnetically labelling water in the arteries as endogenous contrast agent.

Aim: The purpose of this investigation is to determine whether there is a correlation between the perfusion data obtained from ASL-MRI and the metabolic data acquired from ^{18}F-FDG-PET in mTLE.

Method: Pulsed ASL MRI and ^{18}F-FDG PET were collected from 22 mTLE patients. Asymmetry index (AI) was measured for relative CBF (rCBF) from ASL-MRI, and standardized uptake values ratio (SUVr) maps from ^{18}F-FDG PET in bilateral vascular territories as well as in bitemporal structures including the amygdalae, hippocampi, and parahippocampi. The intra-group comparison between brain hemispheres for rCBF and SUVr was performed to detect hypoperfusion and hypometabolism in cases of mTLE.

Results: rCBF and SUVr showed a significant correlation in the associated AI at both middle and superior temporal gyri; and hippocampus ($r > 0.47$, $P < 0.03$, Fig. 1). They also showed a significant correlation in vascular territories of distal posterior, intermediate, intermediate middle, proximal anterior, and proximal middle cerebral arteries ($r > 0.44$, $P < 0.01$). Intra-group comparison showed significant interhemispheric differences for rCBF and SUVr in widespread brain regions for the right mTLE cohort ($P < 0.03$), while hypoperfusion and hypometabolism were not concurrently observed in any intracranial region for the left mTLE cohort.

Conclusions: Hypometabolism estimated from ^{18}F-FDG-PET and hypoperfusion determined from ASL MRI are in promising concordance. This gives rise to the hope that with prospective technical improvements, ASL perfusion MRI may be used as an alternative for ^{18}F-FDG-PET in future.

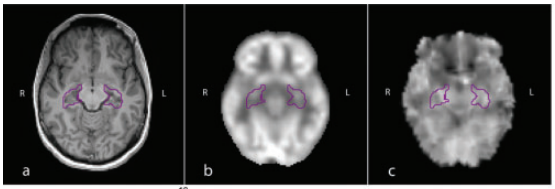

Fig. 1. T1-weighted, ASL MRI, and ^{18}F-FDG - PET images obtained from a patient with right mTLE patient. a) T1-weighted axial images registered in MNI atlas showing overlaid left and right hippocampi for calculation of hypoperfusion and hypometabolism. b) PET-CT axial image registered on MNI atlas showed hypometabolism with AI=-5.79 for the hippocampus. c) Pulsed ASL axial image registered on MNI atlas represented hypoperfusion for hippocampus with AI= -12.4.

The Association between Blood Pressure and Endovascular Treatment Outcomes Differs by Baseline Perfusion and Reperfusion Status

Beom Joon Kim[1], Wi-Sun Ryu[2], Joon-Tae Kim[3], Hyunjong Eom[4], Chi Kyung Kim[4] and Hee-Joon Bae[1]

[1]*Seoul National University Bundang Hospital*
[2]*JLK Inc., Seoul*
[3]*Chonnam National University Medical School*
[4]*Neurology Korea University Guro Hospital*

Abstract

Background: Leptomeningeal collateral after large vessel occlusion (LVO) maintains tissue viability by providing regional perfusion, the level of which may be affected by the changes and levels of blood pressure (BP) and the reperfusion status.

Aim: We hypothesized that the association between BP and endovascular treatment (EVT) outcomes would differ by baseline perfusion and recanalization status.

Method: From a prospective registry, we identified 388 ICA or M1 occlusion patients who underwent EVT $\leq$24 hours from the onset and achieved a post-EVT mTICI $\geq$2b. BP was measured at 5-minute intervals from arrival and during the procedure. Systolic BPs (SBP) were summarized as dropmax (the maximal decrease over two consecutive measurements), incmax (the maximal increase), mean, coefficient of variation (cv), and standard deviation. Adequate baseline perfusion was defined as HIR $\leq$ 0.5; infarct proportion as the volume ratio of final infarcts within the Tmax >6 seconds region.

Results: In the adequate perfusion patients, infarct proportion was correlated with BP indices during the pre-reperfusion period (beta $\pm$ standard error; SBPdropmax per 10 mm Hg, 1.22 $\pm$ 0.48; SBPincmax per 10, 1.12 $\pm$ 0.33; SBPcv, 0.61 $\pm$ 0.15; SBPsd, 0.66 $\pm$ 0.08) but not with SBPmean (per 10, 0.71 $\pm$ 0.37). During the post-reperfusion period, SBPdropmax (2.04 $\pm$ 0.35), SBPincmax (2.07 $\pm$ 0.46), and SBPmean (0.94 $\pm$ 0.42) showed significant associations. SBPincmax, SBPcv, SBPmean had associated with a greater mRS score at three months before the recanalization in adequate perfusion patients; but only SBPincmax was significant after reperfusion. None of the BP indices correlated with the infarct proportion and mRS score at three months in the poor baseline perfusion group. Significant hemorrhage was not significantly associated regardless of baseline perfusion and reperfusion.

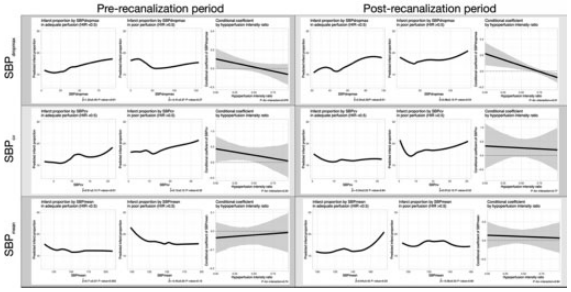

Conclusions: The role of BP fluctuations on aggravated ischemic injury after LVO may differ by baseline perfusion and reperfusion status.

Microglial activation and serotonin transporter in anorexia nervosa patients with and without weight recovery: [^{11}C] DPA713 and [^{11}C]DASB PET study

Masamichi Yokokura[1], Hidenori Yamasue[1], Kiyokazu Takebayashi[1] and Yasuomi Ouchi[1]

[1]*Hamamatsu University School of Medicine*

Abstract

Background: While microglial activation and serotonin transporter (SERT) are implicated in the pathophysiology of anorexia nervosa (AN), no study has examined in-vivo microglial activation concomitant with changes in SERT levels in either underweight or weight-recovered patients.

Aim: The contribution of microglial activation and its interaction with SERT to the pathophysiology of AN regarding body weight status were examined.

Method: In psychotropic-free underweight women with AN (UAN), weight-recovered women with AN (RAN), and age-matched healthy women (HCs), positron emission tomography (PET) with [^{11}C]DPA713 and [^{11}C]DASB tracers was used to assess microglial activation and SERT expression respectively.

Results: Twenty-seven UAN, 10 RAN, and 32 HCs were participated. The [^{11}C]DPA713 PET showed that the non-displaceable binding potential (BP_{ND}) values in anterior cingulate cortex (ACC), thalamus, orbitofrontal cortex, and dorsal raphe were significantly higher in UAN than in RAN and HCs; the BP_{ND} values in precuneus were significantly higher in both UAN and RAN than in HCs. The [^{11}C]DPA713 BP_{ND} values in ACC and thalamus of

UAN significantly correlated with their lowest body mass index (BMI) in their lives which suggests better outcomes, whereas in ACC and precuneus of RAN significantly correlated with mild AN symptoms and the brevity of both illness duration and time to recovery. The [^{11}C]DASB PET showed that the BP_{ND} values in ventral striatum and dorsal raphe were significantly higher in RAN than in UAN and HCs, and significantly correlated with longer illness duration in ACC and ventral striatum. The [^{11}C]DPA713 and [^{11}C]DASB BP_{ND} values significantly negatively correlated in orbitofrontal cortex and precuneus of RAN. All statistical significances were set at $P < 0.05$ adjusted for multiple comparisons.

Conclusions: The current in-vivo PET study of AN suggests that microglial activation leads to better outcomes by controlling increased SERT which might be resulted from malnutrition.

Diagnosis of mTBI using Molecular MRI

Alexia Kirby[1], Nicholas Calvert[2], Cian Ward[2], Ashwin Sharma[2], Emily Standen[1], Mojmir Suchy[2], Joseph Leung[1], Jing Wang[3] and Adam Shuhendler[2]

[1]*University of Ottawa, Department of Biology*
[2]*University of Ottawa, Department of Chemistry and Biomolecular Sciences*
[3]*Ottawa Hospital Research Institute*

Abstract

Background: Concussion is a form of mild traumatic brain injury (mTBI), defined by neurological impairment induced by biomechanical forces without structural brain damage. The diagnosis of mTBI relies on psychoneurological/cognitive testing *via* patient interviews, but there does not yet exist an objective diagnostic tool. Without such a tool, it is estimated that up to 90% of patients go undiagnosed. This has identified a need for molecular imaging probes targeted to the diagnosis of mTBI.

Aim: Downstream injury from mTBI stems from oxidative damage producing neurotoxic aldehydes. A novel CEST-MRI contrast agent, 5-propargyloxy-2-hydrazinobenzoic acid (PHBA), has been developed to map aldehyde production *in vivo* following mTBI. PHBA binds rapidly and irreversibly with aldehydes, affording the use of pathology-associated aldehydic load as an imaging biomarker for molecular MRI.

Method: A novel mouse model of closed-head, awake concussion was developed in a strain of aldehyde dehydrogenase 2 knockout ($ALDH2^{-/-}$) mice. Mice were separated into six cohorts by age and genotype. The mice were either used for behavioural testing and longitudinal CEST-MRI (n = 24), or histology (n = 36) at days -1, 2, and 7 after impact.

Results: Signal enhancement significantly increases at two days post-injury and decreases to near baseline by 7 days post-injury in all mice. The data suggest aged mice and ALDH2 deficient mice produce more aldehydes post-mTBI compared to young and wild type mice, respectively. Histology confirms a neuroinflammatory response at 2- and 7-days post-injury. Aldehyde production following impact was also supported in a corticomimetic scaffold using primary mouse neurons.

Conclusions: This novel MRI contrast agent represents the first objective diagnostic tool for concussion. If proven safe and effective, these probes may be used in a clinical setting, not only telling that mTBI occurred, but also mapping the location of damage to improve treatment outcomes on an individual patient basis.

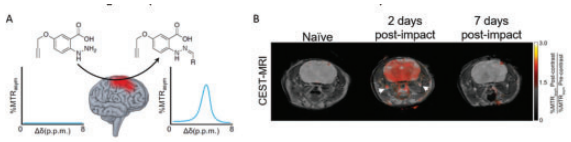

Fig. 1. Mapping of brain aldehydes by PHBA in a mouse model of concussion. (A) 5-propargyloxy-2-hydrazinobenzoic acid (PHBA) binds aldehydes rapidly and irreversibly for *in vivo* visualization of concussion *via* CEST-MRI. (B) CEST-MRI (average $\%MTR_{asym}$ normalized to pre-contrast) after PHBA injection mapped onto a coronal T_2-weighted image of an aged ALDH2 -/- mouse before, 2 days, and 7 days post-impact. Arrowheads indicate vascular signal derived from PHBA-aldehyde adducts.

Gut microbial-produced metabolites reverse adverse post-stroke outcomes in mice via G-protein coupled receptors

Alex Peh[1], Evany Dinakis[1], Charles Mackay[2], Tenghao Zheng[1], Bradley Broughton[3] and Francine Marques[1]

[1]*Hypertension Research Laboratory, School of Biological Sciences, Monash University, Melbourne, Australia*
[2]*Department of Medicine, School of Clinical Sciences, Monash Medical Centre, Clayton, Victoria, Australia*
[3]*Cardiovascular & Pulmonary Pharmacology Group, Department of Pharmacology, Monash University, Melbourne, Australia*

Abstract

Background: Evidence suggests higher intake of dietary fibre pre-stroke is associated with lower stroke risk, yet no data support whether high fibre (HF) or their gut microbial-produced metabolites, called short-chain fatty acid (SCFAs), improve adverse post-stroke outcomes.

Aim: To investigate whether HF or SCFAs supplementation post-stroke can reverse adverse outcomes in mice

and determine if the effects are mediated via GPR41/43/109A receptors.

Method: C57BL/6J mice (8–9 weeks, male, n = 8/group) were randomised into a low-fibre (LF) diet for four weeks before photothrombotic stroke surgery to mimic poor outcomes. Post-stroke, the mice were fed with LF, HF or LF+SCFAs for 7-days. GPR41/43/109A$^{-/-}$ (triple knockout, 3KO) mice were treated with HF pre- and post-stroke to assess the importance of their receptors in post-stroke recovery. Motor function, infarct volume and immunohistochemical analysis were performed.

Results: While no difference in infarct volume was observed across different diets at day 1 (D1) post-stroke, infarct volume was reduced in HF and LF+SCFAs group at D7 (mean ± SEM, LF:11.27 ± 1.51mm^2; HF:7.28 ± 0.90mm^2; LF + SCFAs:5.17 ± 1.11mm^2, $P < 0.001$). Consistent with these findings, wire-hanging motor ability was improved in mice treated with HF or SCFAs (LF:15.07 ± 2.32%; HF:62.83 ± 9.22%; LF+SCFAs:97.42 ± 1.54%, $P < 0.001$). Moreover, HF and SCFAs treatment led to less MPO+ neutrophils ($P < 0.001$), more DCX+ neuroblasts ($P < 0.001$) and increased tight junction expression ($P < 0.001$) in the infarct core. A positive correlation was found between the number of neuroblasts and the infarct recovery rate ($P < 0.001$; $R^2 = 0.376$). Conversely, 3KO mice fed HF had larger infarct volumes at D1 ($P = 0.047$) and D7 ($P = 0.020$) as compared to wild-type mice. 3KO mice also demonstrated poor wire-hanging ability ($P < 0.001$) as well as more neutrophils ($P = 0.044$), fewer neuroblasts ($P = 0.013$), and less tight junction expression ($P = 0.005$) in the infarct core.

Conclusions: An HF diet or SCFA supplementation post-stroke ameliorates brain injury and motor function impairment via GPR41/43/109A signalling, possibly via neurogenesis and immune cell suppression in the brain.

Modelling Tau PET Radiotracer Pharmacokinetics and Applications in Tauopathies

Callum Taylor[1], Cassandra Marotta[1], Craig Despott[2], Kelly Bertram[2], Terence O'Brien[1] and Lucy Vivash[1]

[1]*Monash University*
[2]*Alfred*

Abstract

Background: Tauopathies encompass a range neurodegenerative diseases which are characterized by the accumulation of the protein tau, however the link between tau and disease severity in tauopathies has not yet been established. [18F]-PI2620 is a novel positron emission tomography (PET) tracer which binds to tau with high specificity. Traditionally, in non-invasive modelling of PET, anatomically defined reference regions are used to determine tracer binding potential (BP) within given regions of interest. Recently, a data-driven method of determining individualized reference regions, the Parametric Estimation of Reference Signal intensity (PERSI) has been developed for reference region generation, demonstrating improved performance over anatomically defined reference regions in PET quantification.

Aim: The aim of this study was to investigate PERSI as an alternative reference region to the cerebellum for the pharmacokinetic modelling of [18F]-PI-2620 and to establish the link between tau and disease severity.

Method: Eight patients with PSP (n = 4 male, 47–73 years) underwent dynamic 60-minute tau PET scan with tracer [18F]-PI-2620. Pharmacokinetic modelling was performed using anatomical and data driven reference regions. Several pharmacokinetic models were investigated for both reference region methods to determine the best fitting models.

Results: PERSI was seen to have significantly lower χ^2 values and hence better goodness of fit compared to the cerebellum reference region in MRTM1 (0.173469 vs 0.564557, $p = 0.0049$) and MRTM2 (0.272943 vs 5.2382, $p = 0.0039$), but not SRTM (1.5262 vs 1.6190, $p = 0.4451$) or SRTM2 (1.5289 vs 2.4737, $p = 0.5$) whilst having less variability in goodness of fit in all models. BPnd was not seen to be linked to disease severity in any region of interest analyzed, as determined by any model.

Conclusions: PERSI provides a more robust methodology for quantifying tau PET in patients with PSP. PERSI has potential use for data-driven reference region determination for a wide range of tracers in future studies of disease.

Optical Imaging Measures Predict Functional Recovery after Stroke

Ryan Bowen[1], Jake Lee[1], Brendon Wang[1], Ping Yan[1], Qingli Xiao[1], Adam Bauer[2] and Jin-Moo Lee[3]

[1]*Washington University in St. Louis, Department of Neurology*
[2]*Washington University at Saint Louis*
[3]■

Abstract

Background: Recovery from stroke, a major cause of chronic disability in adults, is often incomplete and unpredictable. Remapping of affected local neuronal circuits and repair of brain networks have been associated with enhanced behavioral recovery. However, it is unclear

how stroke size affects remapping, network repair, and behavioral recovery.

Aim: The aim of this experiment was to determine how stroke size affects remapping, network repair, and functional recovery, and to find optical imaging measures that predict recovery.

Methods: We used *in vivo* wide-field optical imaging to examine longitudinal changes in local and global neuronal circuit activity in mice expressing the genetically encoded calcium indicator, GCaMP, after photothrombotic stroke of variable size in forepaw somatosensory cortex. Imaging and behavioral assays (cylinder rearing and grid walking) were performed before stroke, and at 1, 4, and 8 weeks after stroke. Local circuit activity was measured using evoked response recordings during anesthetized forepaw stimulation. Global network changes were measured using resting-state functional connectivity analysis in awake animals.

Results: Large ischemic lesions (2 mm diameter) in forepaw somatosensory cortex caused spatially diffuse remapping of forepaw somatosensory circuits compared to the more focal remapping observed in mice with smaller lesions (1 mm diameter). Relative change in GCaMP evoked response area following stroke was significantly negatively correlated to behavioral recovery ($n = 27$, $p = 0.0199$). Furthermore, the extent of stimulus-to-response latency was negatively correlated with behavioral recovery ($n = 24$, $p = 0.0264$). Larger strokes also disrupted global brain networks, causing hyperconnectivity within the contralesional hemisphere. The degree of contralesional hyperconnectivity was also significantly negatively correlated to behavioral recovery ($n = 22$, $p = 0.0345$).

Conclusions: These results indicate that infarct size affects both remapping of local neuronal circuits and repair of global neuronal networks. These data also reveal that aberrations in the spatiotemporal characteristics of remapped circuits and hyperconnectivity in the contralesional hemisphere predict worsened recovery.

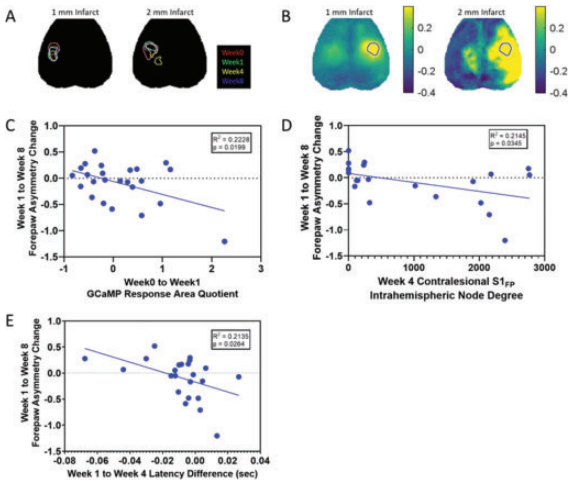

Figure 1. (A) Group-averaged evoked responses are outlined for each imaging timepoint. Outlined regions of interest were calculated by thresholding group-averaged, block-averaged, and stimulus-averaged fluorescence maps during affected forepaw stimulation at 50% of maximum activation. (B) Connectivity in the contralesional hemisphere is dramatically increased at 4 weeks after large photothrombotic lesion (2 mm diameter infarct, bottom) compared to smaller lesion (1 mm diameter infarct, top). (C) Linear regression analysis showing relative change in GCaMP response area from baseline to 1 week after stroke correlates negatively with change in forepaw asymmetry from 1 week to 8 weeks after stroke (n=27, p=0.0199). (D) Linear regression analysis shows intrahemispheric node degree of the contralesional forepaw somatosensory cortex 4 weeks after stroke correlates negatively with forepaw asymmetry change from 1 week to 8 weeks after stroke (n=22, p=0.0345). (E) Linear regression analysis showing change in average latency from 1 week to 4 weeks after stroke correlates negatively with change in forepaw asymmetry from 1 week to 8 weeks after stroke (n=24, p=0.0264).

Revascularization Improves Vascular Hemodynamics in Moyamoya Patients

Moss Zhao[1], Michael Moseley[1], Gary Steinberg[2] and Greg Zaharchuk[1]

[1]*Department of Radiology, Stanford University*
[2]*Department of Neurosurgery, Stanford University*

Abstract

Background: Cerebrovascular reserve (CVR) reflects the capacity of cerebral blood flow (CBF) to change. Decreased CVR implies poor hemodynamics and is linked to a higher risk for stroke. Revascularization has been shown to improve CBF in patients with vasculopathy such as Moyamoya disease. Arterial spin labeling (ASL) is a non-invasive technique for CBF, CVR, and arterial transit time (ATT) measurements.

Aim: Compare vascular hemodynamics before and after revascularization in 52 Moyamoya patients

Method: Images were collected using 3T MRI systems a week before and 4–12 months after the patient's bypass surgery. Diamox was administered to induce vasodilation. Single- and multi-delay (5 delays) ASL data were collected before and 15 minutes after the administration of Diamox. CVR, CBF, ATT were measured in different flow

territories. Paired t-tests were conducted to compare the mean values of CVR, CBF, and ATT before and after revascularization in regions affected by vasculopathy under the null hypothesis that the value of these parameters was the same.

Results: Figure 1 shows the changes in CVR and CBF after bypass surgeries within the regions affected by vasculopathy. CVR in the affected regions increased significantly (by $16 \pm 11\%$ and $25 \pm 13\%$ [both $p < 0.01$] for single- and multi-PLD PCASL) after bypass surgeries. A similar trend was observed in ΔCBF after vasodilation, whereby a significant increase (by $13 \pm 10\%$ and $19 \pm 12\%$ [both $p < 0.01$] for single- and multi-PLD PCASL) can be found after bypass, as shown in Figure 1B. In terms of the CBF measurements, revascularization caused CBF to increase before and after vasodilation, as shown in Figure 1C. Revascularization caused ATT to reduce significantly by $11 \pm 7\%$ ($p < 0.01$) and $13 \pm 7\%$ ($p < 0.01$) pre- and post-vasodilation, respectively (not shown in Figure 1).

Conclusions: Revascularization enhanced perfusion and transit time and that multi-delay ASL may enable non-invasive measurement of arterial arrival times in Moyamoya patients.

Figure

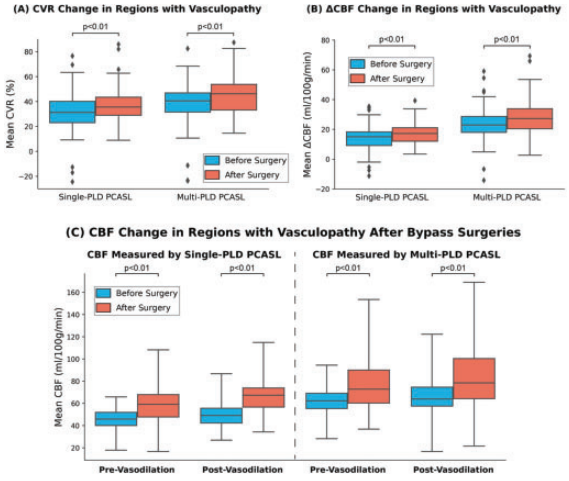

Initiation and formation of the spontaneous intracerebral hemorrhage

Radosław Rzepliński[1], Mikołaj Sługocki[2], Sylwia Tarka[3], Michał Tomaszewski[4], Michał Kucewicz[4], Jerzy Małachowski[4] and Bogdan Ciszek[5]

[1]*ISCBFM Student Early Career Investigator; Department of Descriptive and Clinical Anatomy, Medical University of Warsaw, Poland*

[2]*Department of Descriptive and Clinical Anatomy, Medical University of Warsaw, Poland*

[3]*Department of Neuropathology, Institute of Psychiatry and Neurology, Warsaw, Poland*

[4]*Institute of Mechanics and Computational Engineering, Faculty of Mechanical Engineering, Military University of Technology, Warsaw, Poland*

[5]*Department of Descriptive and Clinical Anatomy, Medical University of Warsaw, Poland; Department of Pediatric Neurosurgery, Bogdanowicz Memorial Hospital for Children, Warsaw, Poland*

Abstract

Background: Due to high epidemiologic and economic burden, spontaneous intracerebral haemorrhage (ICH) is a subject of thorough research. Better understanding of the disease will lead to therapy improvement, which is mainly supportive now. Knowledge about the initial hematoma expansion pathophysiology is limited due to lack of a suitable animal model and insufficient clinical data.

Aim: To create anatomical specimens-based model of intracerebral haemorrhage initiation and formation and investigate pattern of extravasation.

Method: Forty specimens of the human basal ganglia were injected with contrast medium, fixed and scanned with micro-computed tomography (CT) scanner. The results of radiological, direct and histological studies were analysed.

Results: In 9 out of 40 cases intraparenchymal contrast extravasations were revealed; perforating arteries rupture points were present in 7 cases (77%). In all cases the contrast medium filled the perivascular spaces and spread both proximally and distally along the vessels and its branches, detached the arterial tree from the adjacent neural tissue creating secondary extravasation points and destroying the tissue. In 3 cases contrast extravasations skipped to the perivascular spaces of unruptured perforators and aggravated the expansion of the artificial hematoma. There was no subarachnoid extension of any artificial hematoma.

Conclusions: The anatomical specimen-based model of the ICH can be used to study haematoma initiation and propagation. The model is reproducible and does not

require specialised equipment apart from the micro-CT scanner. The bleeding starts with the perforating artery rupture and blood extravasation to the perivascular space. Subsequently the arterial tree is detached from the neural tissue, which creates secondary bleeding sites. The mechanism explains extent of damage to the neural tissue, creation of secondary bleeding sites, variability of growth in time and space, and limited usefulness of surgical interventions. The perivascular spaces of the basal ganglia may not connect directly with the subarachnoid space.

Figure:

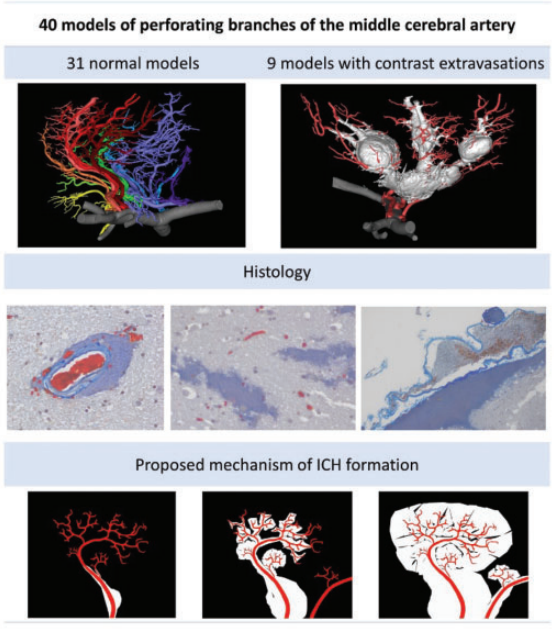

NOTCH3 mutation causes glymphatic dysfunction and brain presenility in CADASIL

Li Chunyi[1], Xiaohui Deng[2], Zhengqi Lu[1] and Wei Cai[3]

[1]*Department of Neurology, Mental and Neurological Disease Research Center, the Third Affiliated Hospital of Sun Yat-sen University*
[2]*Department of Neurology, Mental and Neurological Disease Research Center, the Third Affiliated Hospital of Sun Yat-sen University, Guangzhou, 510630, China*
[3]*the third affiliated hospital of sun yat-sen university*

Abstract

Background: Cerebral autosomal dominant arteriopathy with subcortical infarcts and leukoencephalopathy (CADASIL) is the most common monogenic small vessel disease which is caused by NOTCH3 mutation. Enlarged perivascular spaces (EPVS) and brain atrophy in CADASIL have been widely documented, which indicates the dysfunction of glymphatic system and brain presenility in CADASIL.

Aim: The aim was to explored functional alteration of glymphatic system and the consequences to brain senility in CADASIL.

Method: *Notch3*^{R170C} mice were used as CADASIL models and age- and sex-matched WT mice were set as controls. Alteration of glymphatic function was assessed with influx and efflux experiments. In influx experiment, fluorescent 3kDa dextran was injected into the cisterna magna, and its penetration into brain parenchyma was analyzed. Glymphatic efflux was evaulated by injection of Evans blue (EB) into the striatum and its outflow into the peripheral blood.

Results: Spearman correlation and ROC analysis revealed that EPVS was an effective indication of brain atrophy, emphasizing that glymphatic dysfunction contributed to brain presenility. In the glymphatic influx experiment, *Notch3*$^{R170C+/+}$ mice displayed ~56% less CSF tracer penetration at 30min ($N = 3$, $P = 0.028$). The glymphatic efflux experiment demonstrated reduced EB removal efficiency in CADASIL brains, which was ~65% lower in *Notch3*$^{R170C+/+}$ mice ($N = 4$, $P = 0.0009$), and ~35% lower in *Notch3*$^{R170C+/-}$ mice ($N = 3$, $P = 0.0355$) comparing to WT. With brain tissue of *Notch3*^{R170C} mice and the primary astrocyte cultures, we found that expression of AQP4 in astrocytes, the key glymphatic mediator, was reduced in CADASIL. Mechanistically, NOTCH3 mutation resulted in down-regulation of RUNX1-cMYB signaling, which was responsible for AQP4 transcription. Reinforcing AQP4 expression in astrocytes by AAV-based gene therapy resumed glymphatic functions and protected against brain senescence in CADASIL.

Conclusions: Low AQP4 expression in astrocytes resulted from NOTCH3 mutation leads to glymphatic dysfunction and brain presenility. Reinforcing AQP4 expression represents a novel gene therapy against CADASIL.

Figure:

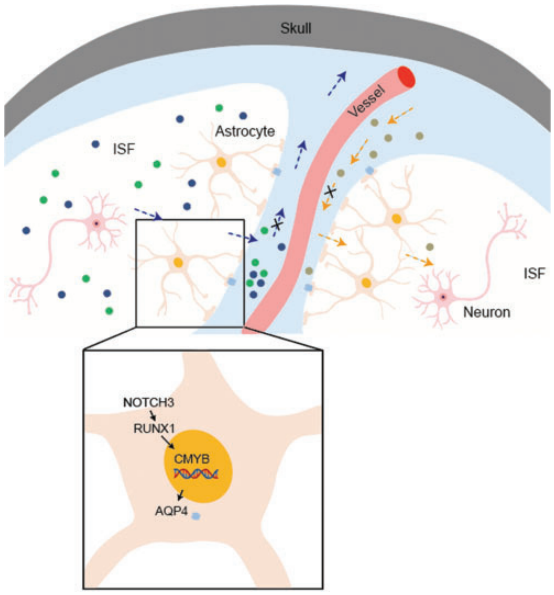

Reduced adenosine receptor availability and increased blood flow in the human brain during acute normobaric hypoxia: a multimodal PET-MRI study

Manuel Michno[1], Henning Weis[2], Jan Schmitz[3], Anna L Foerges[1], Simone Beer[1], Bernd Neumaier[4], Alexander Drzezga[1], Daniel Aeschbach[3], Andreas Bauer[1], Jens Tank[2], Eva-Maria Elmenhorst[3] and David Elmenhorst[1]

[1]Institute of Neuroscience and Medicine (INM-2), Forschungszentrum Jülich, 52425Jülich, Germany
[2]Institute of Aerospace Medicine, Cardiovascular Aerospace Medicine, German Aerospace Center, Cologne, Germany
[3]Institute of Aerospace Medicine, Human Factors Research, German Aerospace Center, Cologne, Germany
[4]Institute of Neuroscience and Medicine (INM-5), Forschungszentrum Jülich, 52425Jülich, Germany

Abstract

Background: Cerebral blood flow, metabolism, and electrical activity are altered during normobaric hypoxia. Adenosine is present in excessive amounts during severe hypoxia and inhibits neurons. Silencing of the A_1 adenosine receptor (A_1AR) attenuates this inhibition.

Aim: We investigated the hypothesis that a short period of hypoxia compared to an interval of normoxia reduces the availability of A_1AR in the human brain due to hypoxia-induced rise of endogenous adenosine. As exploratory objectives, we tested the hypotheses that psychomotor vigilance is affected during hypoxia and that cerebral blood flow is altered.

Method: Healthy volunteers ($n = 10$, 32 ± 13 years, 3f) completed an 110-minute bolus plus constant infusion [F-18]CPFPX PET-MRI experiment: Subjects spent the first 60 minutes of the scan in normoxia followed by 30 minutes of individually adapted normobaric hypoxia to achieve an oxygen saturation of 70–75%, followed by 20 minutes of normoxia. Blood samples were used to calculate metabolite-corrected steady-state distribution volumes of A_1AR (i. e., 40–100 min after start of [F-18] CPFPX administration). Brain perfusion was measured via arterial spin labelling continuously. A 3-minute psychomotor vigilance test (PVT) was conducted every 10 minutes. Heart rate and peripheral blood oxygen saturation were measured throughout.

Results: Compared to normoxia, 30 minutes of hypoxia reduced A1AR availability in the cerebral cortex by 11% ($p = 0.033$). Brain perfusion increased during hypoxia by 25% in cortical gray matter ($p < 0.001$). Heart rate increased by 22% ($p < 0.001$). PVT mean reaction time was 7 ms longer ($p = 0.027$).

Conclusions: Intermittent reduction of the blood oxygen saturation to 70–75% (equivalent to an oxygen saturation at 6000 m) increases cerebral blood flow and impairs cognitive performance while A_1AR availability is reduced. This indicates that acute hypoxia exposure increases cerebral adenosine concentration and receptor occupancy.

Exploring the spatio-temporal and functional dynamics of the neurovascular coupling during cortical slow wave

Sumana Chetia[1], Diana Casas-Torremocha[2], Alejandro Suarez-Perez[2], Maria V. Sanchez-Vives[2] and Turgut Durduran[3]

[1]ICFO-Institut de Ciéncies Fotóniques, The Barcelona Institute of Science and Technology, Castelldefels, Barcelona, Spain
[2]Institut d'Investigacions Biomèdiques August Pi i Sunyer (IDIBAPS)
[3]1ICFO-Institut de Ciéncies Fotóniques, The Barcelona Institute of Science and Technology, Castelldefels, Barcelona, Spain; 2Institució Catalana de Recerca i Estudis Avançats (ICREA), Barcelona, Spain

Abstract

Background: Synchronous, low frequency (0.1–2 Hz) neural fluctuations observed during unconsciousness (slow-wave sleep, deep-anesthesia) are called "slow oscillations" (SO). Apart from being a good predictor of conscious brain-states, its alterations often appear during various pathologies making its understanding relevant for diagnostic and therapeutic clinical translations. To date, the fundamentals of underlying neuro-vascular coupling during this activity is not entirely known.

Aim: Explore the spatio-temporal and functional relationship between neuronal and hemodynamic activity during cortical SO and understand: (1) How hemodynamics correlate to neural fluctuations in this state? (2) Does hemodynamics show functional connectivity which is expected from electrophysiology? (3) Can functional complexity (that can explain state of consciousness) be determined using hemodynamics?

Method: A synchronized, custom-built laser speckle flowmetry (LSF) and a 32-channel multielectrode array (MEA) setup was developed to monitor relative cerebral blood flow (rCBF) and local field potential (LFP) simultaneously in deeply anesthetized mice (*C57BL/6J*, N = 10 animals) during both spontaneous SO activity and electrically-evoked activity.

Results: We have detected and quantified the rCBF fluctuations generated during cortical SO. The neurovascular coupling is studied through spontaneous (data from one of N = 8 animals shown in figure1(a)) and electrically evoked (mean ± S.E.M. plot considering N = 5 animals shown in figure 1(c)) waveform comparisons of rCBF and LFP. Functional connectivity matrices plotted for different cortical positions show a highly coordinated rCBF for deep anesthesia as expected from electrophysiology (data from one animal shown in figure 1(b)). We also compared the functional complexity values in LFP and rCBF to understand the neurovascular coupling better (plot not included in this abstract).

Conclusions: Our results are enlightening on the understanding of cortical dynamics during the default cortical activity regime, creating bridges between neuronal activity and hemodynamics with promising implications for basic and clinical neuroscience.

Figure:

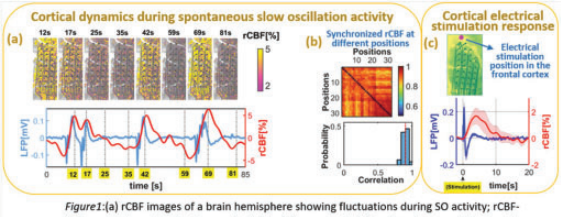

Figure1:(a) rCBF images of a brain hemisphere showing fluctuations during SO activity; rCBF-LFP comparisons implicating cortical SO; (b) coordinated functional connectivity matrix observed in rCBF during deep-anesthesia as expected from electrophysiology; (c) rCBF-LFP comparisons of electrically-evoked responses.

Leptomeningeal collaterals regulate reperfusion in ischemic stroke

Nadine Felizitas Binder[1], Mohamad El Amki[2], Chaim Glueck[3], William Middleham[4], Anna Maria Reuss[5], Adrien Bertolo[6], Patrick Thurner[7], Thomas Deffieux[6], Hannah-Lea Handelsmann[4], Philipp Baumgartner[4], Cyrille Orset[8], Zsolt Kulcsar[7], Adriano Aguzzi[5], Mickael Tanter[9], Denis Vivien[10], Matthias Wyss[11], Andreas Luft[1], Michael Weller[4], Bruno Weber[11] and Susanne Wegener[1]

[1]*Department of Neurology, University Hospital Zurich and University of Zurich, Zurich, Switzerland*
[2]*Yes*
[3]*Institute of Pharmacology and Toxicology, University of Zurich, Winterthurerstrasse 190, 8057Zürich, Switzerland*
[4]*Department of Neurology, University Hospital and University of Zurich, and Zurich Neuroscience Center, Zurich, Switzerland*
[5]*Institute of Neuropathology, University Hospital Zurich, University of Zurich, Schmelzbergstrasse 12, 8091Zurich, Switzerland*
[6]*Iconeus, 6rue Jean Calvin, Paris, France*
[7]*Department of Neuroradiology, University Hospital and University of Zurich, and Zurich Neuroscience Center, Zurich, Switzerland*
[8]*Normandie University, UNICAEN, INSERM, UMR-S U1237, Physiopathology and Imaging of Neurological Disorders (PhIND), Institute Blood and Brain @ Caen Normandie, GIP Cyceron, France*
[9]*Physics for Medicine, INSERM U1273, ESPCI Paris, CNRS UMR 8063, PSL Research University, 17rue Moreau, Paris, France*
[10]*UNICAEN, INSERM U1237, Physiopathology and Imaging of Neurological Disorders (PhIND), Cyceron, Institut Blood and Brain @ Caen-Normandie (BB@C), Normandie University, Caen, France*
[11]*Institute of Pharmacology and Toxicology, University of Zurich*

Abstract

Background: Leptomeningeal collaterals (LMC) are important determinants of ischemic stroke severity. However, the underlying mechanisms of protection are still unknown.

Aim: We hypothesized that LMCs lead to a controlled gradual reperfusion after thrombolytic treatment preventing reperfusion injury.

Method: We compared three mouse strains with differences in their natural collateral network (C57BL/6, Rabep2–/–, Balb-C). Stroke was induced by injecting thrombin into the M2 bifurcation of the middle cerebral artery (MCA). Thirty minutes later, thrombolysis was initiated through rt-PA. Changes in CBF were monitored using laser speckle imaging and ultrafast ultrasound for two hours during stroke and reperfusion. Cerebrovascular reactivity was assessed using CO_2 challenges. In a subset of animals, functional deficits were evaluated during the chronic phase and on day seven, infarct volumes were quantified. In addition, reperfusion pace of stroke patients, who underwent thrombectomy after M2 occlusion, were retrospectively analyzed using DSA and correlated with collateral status and 3-months outcome.

Results: In mice with poor (Balb-C; $n = 10$) and intermediate (Rabep2–/–; $n = 10$) LMCs, rt-PA led to significant reperfusion in the area supplied by the MCA-M4/M5 segment. In mice with abundant (C57BL/6, $n = 10$) LMCs, irrespective of rt-PA administration, we observed only minor CBF recovery. However, regions more proximal (MCA-M3) showed considerable reperfusion in all three strains ($n = 8$/strain). While C57BL/6 displayed a gradual reperfusion reaching 100% of baseline, Balb-C and Rabep2–/– showed steep reperfusion resulting in an uncontrolled hyperemic response. Challenging cerebrovascular reactivity ($n = 8$/strain) we observed that integrity was preserved in C57BL/6 but altered in the other strains after stroke. In the chronic phase after ischemia (7d), only mice with poor and intermediate LMCs suffered hemorrhages and mortality. In addition, data of stroke patients ($n = 33$) suggest that fast reperfusion is associated with poor collateral status and complications after mechanical thrombectomy.

Conclusions: Our findings suggest that LMCs allow a controlled, gradual reperfusion after thrombolysis.

Neuroprotection targeting ischemic penumbra by novel lipid mediators after experimental stroke

Nicolas G Bazan[1], Andre Obenaus[2], Madigan M Reid[1], Pranab K Mukherjee[1], Larissa Khoutorova[1] and Ludmila Belayev[1]

[1]*LSUHSC*
[2]*Pediatrics, Univ. of California, Irvine, Irvine, CA*

Abstract

Background: Neuroprotection to attenuate or block the ischemic cascade and salvage neuronal damage has been extensively explored for treating ischemic stroke. However, despite our increasing knowledge of the physiologic, mechanistic, and imaging characterizations of the ischemic penumbra, no effective neuroprotective therapy has been found to treat ischemic stroke. We recently showed that a combinatory treatment with Neuroprotectin D1 (NPD1) and Resolvin D1 (RvD1) was more effective than the single therapy administered 3 h after stroke. These lipid mediators are biosynthesized "on-demand" in response to stroke onset to resolve neuroinflammation and restore homeostasis and functional integrity.

Aim: This study aimed to determine the neuroprotection of NPD1 + RvD1 on the ischemic penumbra.

Methods: Male Sprague-Dawley rats (270–360g) were anesthetized and received 2 h of middle cerebral artery occlusion (MCAo). Behavior was evaluated at 60 min on days 1, 2, 3, 7, 14. Rats treated IV with NPD1 (222 μg/kg at 3 h) and RvD1 (222 μg/kg at 3.15 h) or vehicle ($n = 6$–10 group). Four groups: NPD1+RvD1 and vehicle, 7 and 14 days survival ($n = 6$–10/group). Rats were perfused with 4% paraformaldehyde on days 7 and 14, and an *ex vivo* brain MRI was conducted using an 11.7 T MRI. Hierarchal region splitting was used to distinguish the core from the penumbra.

Results: Behavior was improved on days 1, 2, 3, and 7 in 7-day NPD1 + RvD1 (by 26, 31, 36, 37%) and 14-day (by 29, 31, 32, 34, and 34%) groups compared to the vehicle. Ischemic penumbra, core, and total lesion volumes (computed from T2WI) were reduced by NPD1+RvD1 treatment on days 7 (by 80, 55, 68%) and 14 (by 69, 39, 51%; $p < 0.05$), respectively.

Conclusion: Combining treatment by NPD1+RvD1 affords synergistic neuroprotection in the post-ischemic brain. These findings open avenues for ischemic stroke therapeutics. We are currently exploring the cell-specific and molecular mechanisms involved.

[^{11}C]PS13 shows high specific and displaceable binding to COX-1 enzyme in the human brain

Nafiseh Ghazanfari[1], Min Jeong Kim[1], Carson Knoer[1], Jinsoo Hong[1], Fatemeh Ahmadi[1], Jose Montero Santamaria[1], Sami Zoghbi[1], Jeih San Liow[1], Victor Pike[1], Robert Innis[1] and Paolo Zanotti Fregonara[1]

[1]*Molecular Imaging Branch, National Institute of Mental Health, National Institutes of Health, Bethesda, MD, USA*

Abstract

Background: Neuroinflammation is associated with various neurodegenerative forms of dementia, including Alzheimer's disease. Such diseases may be associated with neuroinflammation. Cyclooxygenases (COX) produce inflammatory mediators Thus, PET radioligands for COX are potentially useful for the study of neuroinflammation. We recently developed [^{11}C]PS13, a highly selective radioligand for COX-1, a major isoform of COX

Aim: To accurately estimate the specific binding of [^{11}C]PS13 to COX-1 in healthy human brain using scans performed at baseline and after treatment with ketoprofen.

Method: Eight healthy volunteers underwent two 90-minute [^{11}C]PS13 PET scans (injected activity 743 ± 37 MBq) at baseline and at least two hours after oral administration of ketoprofen (75 mg). During each scan, the radiometabolite-corrected arterial input function was measured. V_T values were obtained with both a two-tissue compartmental model (2TCM) and Logan graphical analysis.

Results: Brain radioactivity concentration peaked at about 3 minutes after [^{11}C]PS13 injection, with SUV values of 2.9 ± 0.7 at baseline and 3.3 ± 0.8 after ketoprofen treatment. The time-activity curve for parent radiotracer in plasma had a higher peak after ketoprofen treatment (12.5 ± 5.1 SUV) than at baseline (7.5 ± 2.0 SUV). 2TCM analysis fitted the brain time-activity curves well at both baseline and after ketoprofen treatment (SE $< 5\%$). V_T values were 2.7 ± 0.5 at 1.6 ± 0.5 for baseline and after treatment, respectively. The Lassen plot revealed an occupancy of 80% by ketoprofen and a V_{ND} of 1.4. Whole brain BP_{ND} was calculated at 1.3.

Conclusions: [^{11}C]PS13 binds specifically to COX-1 in the human brain and can be blocked by the selective inhibitor ketoprofen.

Figure:

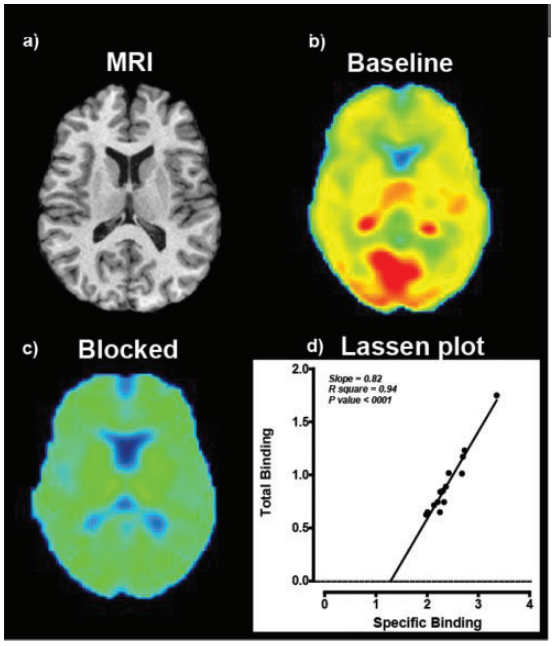

Figure. MRI (a) and PET of a representative healthy subject injected with ^{11}C-PS13 at baseline (b) and after blockade by Ketoprofen (c). Ketoprofen induced about 40% decrease of ^{11}C-PS13 uptake and occupied about 80% of COX-1 binding sites, as measured with a Lassen plot (d).

Cathepsin B Knockout Offers Significant Brain Protection in the Mouse Model of Stroke

Kurt Hu[1], Yujung Park[2], Yamileck Olivas-Garcia[2], Chunli Liu[2] and Bingren Hu[2]

[1]Department of Medicine, Division of Pulmonary and Critical Care Medicine, Medical College of Wisconsin, Milwaukee, WI
[2]Departments of Emergency Medicine and Neurosciences, University of California San Diego, La Jolla, CA

Abstract

Background: Recent research has advanced our understanding of the endolysosomal cycle and its disruption can lead to cathepsin B (CTSB) release resulting in cell death.

Aim: The objective of this study is to investigate the role of the endolysosomal damage and CTSB release in brain ischemia-reperfusion injury in a mouse model of stroke.

Methods: A total of 50 mice were randomly assigned into four experimental groups: (i) wt sham; (ii) wt middle cerebral artery occlusion (MCAO); (iii) CTSB knockout (KO) sham; and (iv) CTSB KO MCAO. Mice were subjected either to 0 min (sham) or 40 min of MCAO, followed by 1- and 7-day reperfusion. In the 7-day reperfusion group, mice underwent physical and behavioral examinations until the day-7 endpoint after MCAO. Confocal microscopy was used to analyze key endolysosomal markers proteins, including their levels, redistributions, and co-localizations. Light and electron microscopy (EM) were utilized to examine the histopathology and endolysosomal ultrastructures.

Results: Relative to those in sham, the level of CTSB was drastically accumulated while N-ethylmaleimide sensitive factor ATPase (NSF) was irreversibly depleted primarily in post-ischemic penumbral neurons. Furthermore, CTSB-immunostained structures were enlarged and diffusely distributed in both the cytoplasm and extracellular space, indicating the CTSB release from post-ischemic neurons. EM showed a significant increase in the number of endolysosomal structures with various sizes in post-ischemic neurons. CTSB KO mice had a decreased hippocampal injury area, increased number of survival neurons in the striatal core area, and improved physical and functional performance in post-MCAO mice compared to wild-type (wt) mice after MCAO.

Conclusion: Brain ischemia triggers a cascade of events, including inactivation of NSF, disruption of the endolysosomal cycle, endolysosomal structural damage, and release of CTSB in post-ischemic neurons. CTSB KO provides protection against brain ischemia-reperfusion injury.

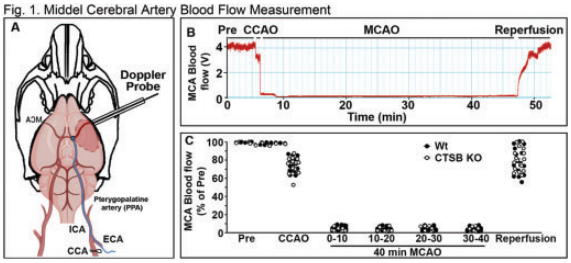

Fig. 2. Graphical Abstract

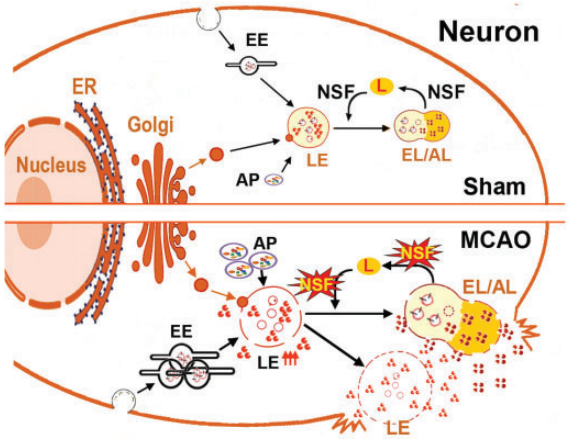

Free-Water Imaging in Friedreich's Ataxia using Multi-compartment Models

Lara Fernandez[1], Louise Corben[2], Hiba Bilal[1], Martin Delatycki[2], Gary Egan[3] and Ian Harding[1]

[1]*Monash University*
[2]*Murdoch Childrens Research Institute*
[3]*Turner Institute for Brain and Mental Health, Monash University; Monash Biomedical Imaging, Monash University; and Australian Research Council Centre of Excellence for Integrative Brain Function, Melbourne*

Abstract

Background: Individuals with Friedreich's Ataxia (FRDA) show marked and progressive neurodegeneration and neuroinflammation in the cerebellum and brainstem. Work in other neurodegenerative diseases indicates that neuronal atrophy and inflammation is associated with increased free-water in the extracellular space surrounding axons. Regional alterations in free-water and other microstructural tissue properties can be quantified *in vivo* using multi-compartment modelling of diffusion magnetic resonance imaging (dMRI).

Aim: To quantify the extent of free-water and microstructural change in disease-relevant brain regions in individuals with FRDA relative to healthy controls using both neurite orientation dispersion and density imaging (NODDI), and bitensor diffusion tensor imaging (DTI) models.

Method: Multi-shell dMRI was acquired from 14 FRDA patients (mean mFARS 48.15 ± 15.19) and 14 healthy controls. Mean values within ROIs in the cerebellum and brainstem were extracted for each NODDI (isotropic volume [FISO], intracellular volume [FICVF], orientation dispersion [ODI]), and DTI metric (free-water volume [FW], fractional anisotropy [FA], and free-water corrected fractional anisotropy [FW-FA]). Group differences in each ROI were inferred using ANCOVA (controlling sex and age).

Results: In FRDA, elevated FW was observed in all cerebellar cortex, cerebellar peduncles (excluding middle), dentate and brainstem ROIs ($p < 0.05$). Elevations in FISO occurred primarily in the cerebellar lobules ($p \leq 0.01$). FA was reduced in all ROIs ($p \leq 0.01$), aside from the dentate and MCP. Reduced FW-FA and FICVF in FRDA were observed in all white-matter regions ($p < 0.05$). The largest effect sizes (XXXXX $>$ .14) occurred in the midbrain, superior-cerebellar-peduncle, anterior cerebellar lobe, and dentate, with FW showing the largest effects (max XXXXX $= 0.41$).

Conclusions: Multi-compartment diffusion measures of free-water and neurite integrity distinguish FRDA from healthy controls with large effects. The extent of free-water in the brainstem and cerebellum provided the greatest distinction between groups. This study indicates that further investigation of free-water as a potential biomarker for disease progression in FRDA is warranted.

A spatially varying multi-compartment model of the regulation of cerebral blood flow and volume

Stephen Payne[1]

[1]*National Taiwan University*

Abstract

Background: The maintenance of adequate cerebral perfusion is key to healthy brain function. Dynamic cerebral autoregulation is the mechanism that acts to maintain

cerebral blood flow constant in response to short-term changes in arterial blood pressure and is impaired in many cerebrovascular and neurodegenerative diseases.

Aim: However, little is known about its spatial variability due to the difficulties in measurement of flow/perfusion in the human brain and no mathematical model yet exists of this. A new framework for considering the regulation of perfusion and blood volume is thus presented and the different types of behaviour that are exhibited are highlighted.

Method: Three blood compartments (arterial, capillary, and venous) are assumed. Conservation of mass gives three governing equations in terms of volume fraction, pressure, and velocity field. It is assumed that perfusion coupling between compartments is linearly proportional to the volume fraction and the driving pressure difference. Darcy flow is assumed with a linear relationship between changes in volume fraction and pressure in each compartment. Three cases are considered: first, the pressure-volume relationship is purely passive; second, volume fractions remain constant; third, assuming typical/baseline values for each compartment. Parameter values and boundary conditions are taken from previous studies. The equations are solved in a spherically symmetric annular shell.

Results: A drop in inlet arterial pressure of 10% at time 0 is used to illustrate the model behaviour, as shown in Figure 1 for (spatially averaged) grey matter perfusion. The response times are very different, and a biphasic response is shown for two of the three conditions.

Conclusions: A new multi-compartmental framework for spatially varying regulation of cerebral blood flow and volume is presented. Future work will extend this to integrate more active mechanisms of control.

Figure:

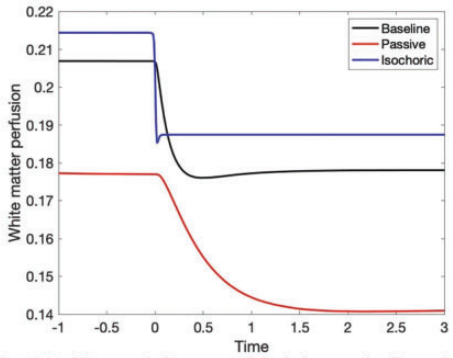

Figure 1: Spatially averaged white matter perfusion in three cases: baseline, passive and isochoric.

Figure 1: Spatially averaged white matter perfusion in three cases: baseline, passive and isochoric.

Stimulus-evoked cerebrovascular responses fluctuate over minutes to hours

Deepa Issar[1], Emily C. Crane[1], Emily E. Skog[1], Matthew A. Smith[1] and Jana M. Kainerstorfer[1]

[1] *Carnegie Mellon University*

Abstract

Background: Many neurodegenerative diseases, including Alzheimer's disease, are associated with impaired or altered arousal, such as abnormal drifts in wakefulness. Understanding the link between impaired arousal and disease requires first the study of how typical arousal fluctuations, naturally occurring over many hours and across the day, change neural and cerebrovascular activity.

Aim: We investigated how evoked neural and cerebral hemodynamic activity changed with arousal-linked parameters at multiple timescales, including over many minutes and across the circadian cycle.

Method: A healthy rhesus monkey (*Macaca mulatta*) performed a simple fixation task where the goal was to detect and then look at a target. Some trials had a full-field flashing stimulus (natural image or radial checkerboard), while others had a blank screen. Each session was several hours long (2 to 6 hours), and sessions started at different times of day (between 6:00 and 22:00). Arousal fluctuations were quantified using heart rate, respiration, pupil diameter, and reaction time. Changes in oxy- and deoxy-hemoglobin concentrations were measured using near-infrared spectroscopy with a probe placed on the scalp over visual cortex (source-detector distances: 16 mm, 21 mm, 26 mm; wavelengths: 760 nm, 850 nm). In several sessions, neural activity was measured simultaneously using a 96-channel intracortical electrode array in left hemisphere visual area V4.

Results: We recorded over 40 sessions from one subject. The figure shows visually-evoked hemodynamic responses averaged in 30-minute bins at different times over a single multi-hour session. The amplitude and latency of these evoked responses changed over hours during each session. Arousal-linked variables, such as heart rate and reaction time, as well as neuronal spiking activity varied over a similar timescale. We also observed circadian-related arousal fluctuations.

Conclusions: The evoked hemodynamic responses, neural population activity, and arousal-linked measures fluctuated over many minutes and across the circadian cycle.

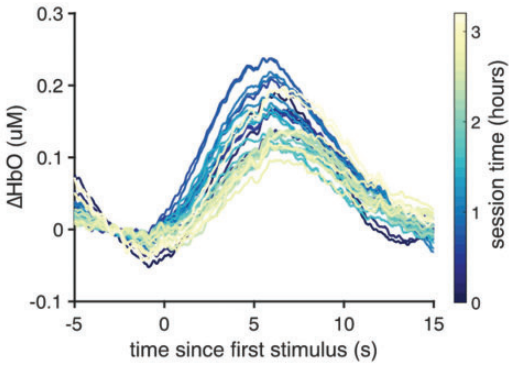

Photobiomodulation Therapy Restores Olfactory Function Impaired by Photothrombosis in Mouse Olfactory Bulb

Euiheon Chung[1], Reham A. Shalaby[2], Muhammad Mohsin Qureshi[3], Mohd. Afzal Khan[2], S. M. Abdus Salam[4], Hyuk Sang Kwon[2], Kyung Hwa Lee[4] and Young Ro Kim[5]

[1]ISCBFM
[2]Gwangju Institute of Science and Technoloy
[3]Princess Margret Cancer Center
[4]Chonnam National University, Hwasun Hospital and Medical School
[5]Harvard Medical School

Abstract

Background: Ischemic stroke typically accompanies numerous disorders ranging from somatosensory dysfunction to cognitive impairments, inflicting its patients with various neurologic symptoms. Among pathologic outcomes, post-stroke olfactory dysfunction is frequently observed. Despite the well-known prevalence, therapy options for such compromised olfaction are limited, likely due to the complexity of olfactory bulb (OB) architecture, which encompasses both peripheral and central nervous systems. As photobiomodulation (PBM) emerged for treating stroke-associated symptoms, the effectiveness of PBM on stroke-induced impairment of olfactory function was explored

Aim: To address the efficacy of PBM therapy on OB damage caused by ischemic stroke using both behavioral and histologic analyses with inflammatory markers in stroke mice models.

Method: A novel mouse model with olfactory dysfunction was prepared using photothrombosis (PT) in the OB. Subsequently, post-PT PBM was performed daily from day 2 to 7 by irradiating OB using an 808 nm laser with fluence of 40 J/cm^2 (325 mW/cm^2 for 2 minutes/day). Buried food test (BFT) was used for scoring behavioral acuity in food-deprived mice to assess olfactory function before and after PT, and after PBM. Histopathological examinations and cytokine assays were performed on mice brains harvested on day 8.

Results: The BFT results were specific to the individual, with positive correlations between baseline latency time measured before PT and alterations at the ensuing stages for PT ($n = 11$) and PT+PBM ($n = 10$) groups ($p = .0001$). Also in both groups, the correlation analysis showed a significant positive relationship between early and late latency time changes independent of PBM, implicating a common recovery mechanism. PBM treatment accelerated the recovery of impaired olfaction after PT with suppression of inflammatory cytokines ($n = 3$/group) while enhancing glial and vascular factors (e.g., GFAP, IBA-1, and CD31 $n = 6$/group).

Conclusions: The PBM therapy during the acute phase of ischemia improves the compromised olfactory function by modulating microenvironment and tissue inflammation

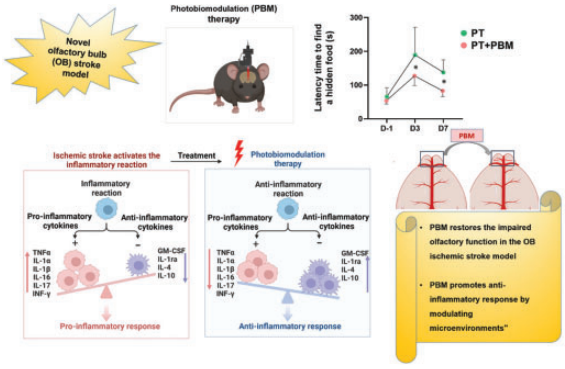

CCL5 mediated astrocyte-T cells interaction disrupts blood-brain barrier in mice after hemorrhagic stroke

Shiyi Zhou[1], Chang Liu[1], Jing Ye[1], Qianyuan Lian[1], Tongtong Xu[1], Shiyu Deng[1], Lin Gan[1], Yiyan Guo[1], Wanlu Li[1], Zhijun Zhang[1], Guo-Yuan Yang[1], Yaohui Tang[2] and Jixian Wang[3]

[1]School of Biomedical Engineering, Shanghai Jiao Tong University
[2]Shanghai Jiao Tong University
[3]Department of Rehabilitation Medicine, Ruijin Hospital, School of Medicine, Shanghai Jiao Tong University

Abstract

Background: The interaction between astrocytes and immune cells plays critical roles in maintaining blood-brain barrier (BBB) integrity. However, how astrocytes interact with immune cells and the effect of their interaction on BBB integrity after stroke are still unclear.

Aim: To investigate the effect and mechanism of astrocytes-immune cells interaction on BBB integrity in hemorrhagic stroke mice.

Method: RNA sequencing of reactive astrocytes that induced by IL-1α, TNFα, and C1q treatment was performed. Astrocytic CCL5 knockout mice (n = 102) underwent collagenase-induced intracerebral hemorrhage. Flow cytometry was performed to investigate the number of immune cells that infiltrated into the brain. BBB disruption was evaluated by western blot, Evans blue, and immunostaining. Neurobehavioral tests were used to assess the neurological function of mice. bEnd.3 cells were co-cultured with immune cells in the presence or absence of EGTA. The apoptosis of bEnd.3 cells was assessed by TdT-mediated dUTP Nick End Labeling staining.

Results: RNA sequencing results showed high expression of CCL5 in reactive astrocytes. Flow cytometry results showed knockout astrocytic CCL5 reduced the infiltration of $CD8^+$ but not $CD4^+$ T and myeloid cells into the brain ($p < 0.05$). In addition, knockout CCL5 in astrocytes increased ZO-1 and occludin expression, reduced Evans blue leakage and expression of perforin and granzyme B, and lowered modified neurologic severity score and improved the performance of elevated body swing test, rotarod test and grid walking test of hemorrhagic stroke mice ($p < 0.05$), while transplantation of $CD8^+$ T cells reversed the protective effects. Moreover, co-culture of $CD8^+$ T with bEnd.3 cells induced bEnd.3 cells apoptosis, which was rescued by inhibiting perforin.

Conclusions: Our study demonstrates that astrocytes interact with $CD8^+$ T cells through CCL5, leading to endothelial apoptosis and BBB disruption through perforin, suggesting a novel mechanism of crosstalk between astrocytes and $CD8^+$ T cells.

Figure:

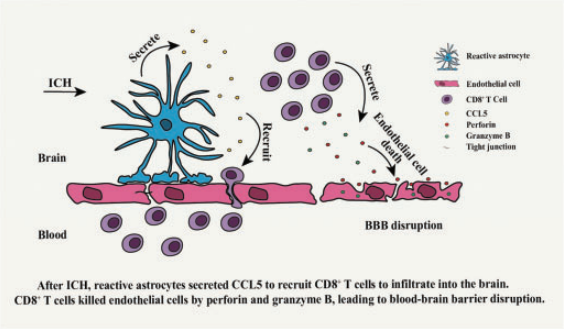

After ICH, reactive astrocytes secreted CCL5 to recruit $CD8^+$ T cells to infiltrate into the brain. $CD8^+$ T cells killed endothelial cells by perforin and granzyme B, leading to blood-brain barrier disruption.

Astrocytic MEGF10/MERTK-mediated myelin phagocytosis differentially affects white matter injury in mice after chronic cerebral hypoperfusion

Tongtong Xu[1], Lin Gan[2], Shiyu Deng[2], Chang Liu[1], Shiyi Zhou[1], Zhijun Zhang[1], Guo-Yuan Yang[1], Won-Suk Chung[3], Jixian Wang[4] and Yaohui Tang[5]

[1]*School of Biomedical Engineering, Shanghai Jiao Tong University*
[2]*School of Biomedical Engineering Shanghai Jiao Tong University*
[3]*Department of Biological Sciences, Korea Advanced Institute of Science and Technology*
[4]*Department of Rehabilitation Medicine, Ruijin Hospital, School of Medicine, Shanghai Jiao Tong University*
[5]*Shanghai Jiao Tong University*

Abstract

Background: Chronic cerebral hypoperfusion (CCH) causes white matter injury and leads to vascular cognitive impairment and dementia. After CCH, astrocytes are activated and engulf myelin debris. However, the effect of astrocyte-mediated myelin engulfment on white matter injury and cognitive impairment is unclear.

Aim: To explore the effect and mechanism of astrocyte-mediated myelin phagocytosis on white matter injury and cognitive impairment in mice after CCH.

Methods: Astrocyte-specific MEGF10 or MERTK knockout mice (n = 102 respectively) were subjected to bilateral common carotid artery stenosis (BCAS). White matter injury was evaluated by Luxol fast blue (LFB) staining and transmission electron microscope (TEM). Myelin phagocytosis was assessed by immunostaining, TEM and pHrodo dye. 8-arm maze test and novel object recognition were conducted to determine neurobehavioral outcomes. RNA sequencing was performed for further mechanistic study.

Results: Astrocytes in the corpus callosum activated and engulfed myelin after BCAS from day 7 to 21 in a time-dependent manner. Phagocytosis-associated receptors MEGF10 and MERTK were upregulated in astrocytes. Conditional knockout of MEGF10 or MERTK in astrocytes reduced astrocyte-mediated myelin engulfment compared with control group in vivo and in vitro. Interestingly, LFB staining and TEM data showed that knockout of MEGF10 in astrocytes alleviated white matter injury while knockout of MERTK in astrocytes aggravated white matter injury after BCAS. Astrocytic MEGF10 knockout mice showed better working memory and exploration tendency, but conditional knockout of MERTK in astrocytes worsened

cognitive function. Mechanistically, RNA sequencing data revealed that knockout of MEGF10 in astrocytes reduced cell cycle-related genes including CCNA2, CCNB1, etc., further reduced astrogliosis and myelination inhibitors such as CSPG, fibronectin, etc. However, knockout of MERKT in astrocytes activated inflammatory pathways.
Conclusion: Our study demonstrated that astrocytic MEGF10/MERTK-mediated myelin phagocytosis distinctively contributed to white matter injury in mice after BCAS via different mechanisms, suggesting novel therapeutic targets for treating CCH.
Figure:

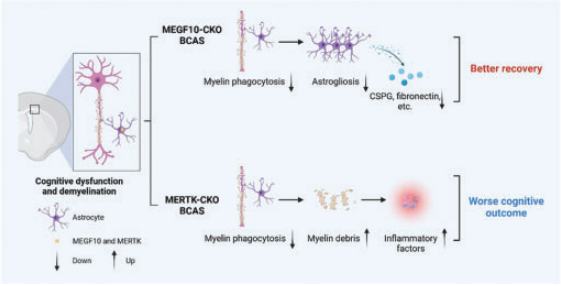

A Stroke-induced Phenotype of Neuroinflammatory Astrocytes Disrupts Blood-Brain Barrier Integrity via Matrix Metalloproteinase-3

Chang Liu[1], Shiyu Deng[1], Shiyi Zhou[1], Yiyan Guo[1], Tongtong Xu[1], Hanlai Li[1], Zhijun Zhang[2], Jixian Wang[3], Yaohui Tang[2] and Guo-Yuan Yang[2]

[1]School of Biomedical Engineering, Shanghai Jiao Tong University
[2]Shanghai Jiao Tong University
[3]Department of Rehabilitation Medicine, Ruijin Hospital, School of Medicine, Shanghai Jiao Tong University

Abstract
Background: Astrocytes undergo transcriptomic changes and become heterogenous after stroke. However, phenotypic changes of astrocytes and their function remain unclear in hemorrhagic stroke.
Aim: To investigate phenotypic changes of astrocytes and the function on blood-brain barrier (BBB) integrity in hemorrhagic stroke mice.
Method: Adult male C57BL/6 mice (n = 36) underwent collagenase-induced intracerebral hemorrhage. Single cell RNA-sequencing was used to reveal the heterogeneity of astrocytes in hemorrhagic stroke mice. PLX5622 or F70101C-A was used to delete microglia or macrophages in mice, respectively. Hemorrhage-specific neuroinflammatory astrocytes were induced *in vitro* with conditioned medium from lipopolysaccharides- or Hemin-stimulated microglia. RNA-sequencing was further conducted to determine the function and mechanism of hemorrhage-specific neuroinflammatory astrocytes. Astrocytic matrix metalloproteinase 3 (MMP3) knockout mice (n = 60) underwent hemorrhagic stroke. BBB disruption was assessed by Evans blue, IgG staining, and western blot. Transmission electron microscopy was used to quantify the thickness of base membrane. Gelatin zymography was used to evaluate the activity of matrix metalloproteinase 9 (MMP9).
Results: Hemorrhagic stroke induced phenotypic changes of astrocytes. A specific phenotype of astrocytes was detected at 3rd day after hemorrhagic stroke, and neuroinflammatory genes such as *Lcn2*, *Vim*, *C3*, *S100a10*, and *S100a6*, were highly expressed. Furthermore, the hemorrhage-specific neuroinflammatory astrocytes were partially induced by microglia but not infiltrated macrophages. BBB disruption related gene MMP3 was highly upregulated in the hemorrhage-specific neuroinflammatory astrocytes ($p < 0.01$). Inhibiting MMP3 activity in astrocytes reduced tight junction protein loss *in vitro* ($p < 0.01$). Conditional knockout of MMP3 in astrocytes reduced Evans Blue and IgG leakage, alleviated parenchymal base membrane expansion, decreased the activity of MMP9, and improved neurological outcomes in hemorrhagic stroke mice ($p < 0.01$).
Conclusions: Our findings highlight the critical role of hemorrhage-specific neuroinflammatory astrocytes in disrupting BBB through MMP3, which suggests a potential therapeutic strategy for hemorrhagic stroke.
Figure:

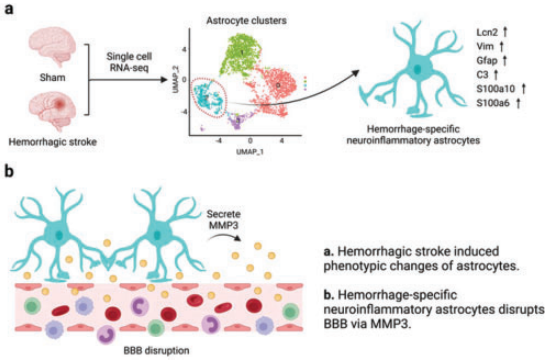

Senile perivascular macrophage promotes microglial senescence through CD5L-containing large extracellular vesicles in CAA

Mengyan Hu[1], Tiemei Li[2], Xinmei Kang[2], Zhengqi Lu[2] and Wei Cai[2]

[1]*Department of Neurology, Mental and Neurological Disease Research Center, the Third Affiliated Hospital of Sun Yat-sen University*
[2]*the Third Affiliated Hospital of Sun Yat-sen University*

Abstract

Background: Microglial senescence results in impairment of the scavenging function, leading to accumulation of metabolic wastes and the progression of cerebral amyloid angiopathy (CAA). Deposition of Aβ40 in brain blood vessel is the pathological signature of CAA. Perivascular macrophages (PVM) are the first to encounter the deposited Aβ40. Interaction between PVM and microglia and the impacts on CAA development are worth studying.
Aim: This study aims to unveil the impacts of Aβ40-stimulated PVM on microglial senescence and CAA outcomes.
Method: Tg-SwDI/B mice were used as CAA models. Microglia were depleted with PLX5622-containing chow. Blood-brain barrier (BBB) integrity was assessed with the permeability to fluorescent dextran. Cellular senescence was evaluated with the ageing markers including SA-β-gal and P16. Protein content of large extracellular vesicles (LEVs) was identified by ITRAQ.
Results: Senility of microglia preceded other brain cells in CAA models ($N = 8$, 6 m vs. 12 m, $P < 0.01$). Renewing the microglial pool by microglia depletion reduced Aβ deposition and protected against BBB injury ($N = 8$, $P < 0.05$). Senility of PVM was evident even earlier than microglia ($N = 8$, 3 m vs. 6 m, $P < 0.01$). *In vitro* study revealed that macrophages suffered replicative senescence when stimulated by Aβ40 ($N = 3$, $P < 0.05$), which further promoted microglial ageing ($N = 3$, $P < 0.01$). Among the cell products of senile macrophages, LEVs displayed pro-ageing effects. Mechanistically, CD5L loaded in the LEVs bound to CD16 on microglia, which advanced the microglial senescence through ARF-dependent signaling. Knock-out of CD5L in macrophage or blocking CD16 on microglia effectively suppressed microglial senescence, thus attenuating amyloid angiopathy and BBB damage in CAA mice ($N = 8$, $P < 0.05$).
Conclusions: PVM undergo replicative ageing and release CD5L-loaded LEVs in CAA, which promote microglia senescence through activating CD16-ARF signaling. CD5L-containing LEVs represent novel senescence associated secretary phenotype (SASP). Clearing the SASP and blocking CD5L-CD16 interaction are promising therapeutic strategies against microglial senescence in CAA.

Figure:

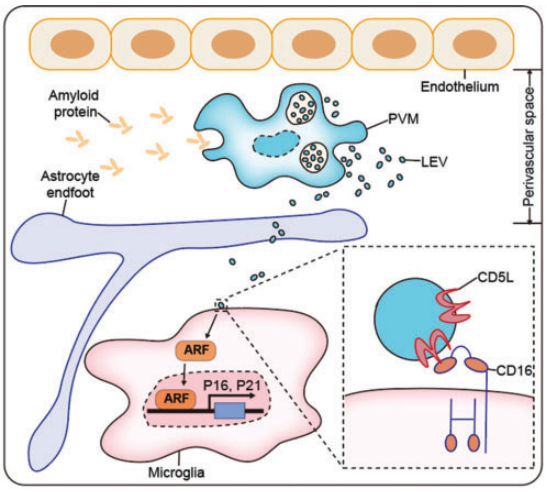

Bone Marrow Mesenchymal Stem Cell Inhibits Enterobacterial Translocation after Ischemic Stroke via Liver-Gut Axis

Xiaotao Su[1], Wei Cai[1] and Zhengqi Lu[2]

[1]*The Third Affiliated Hospital of Sun Yat-sen University*
[2]*Department of Neurology, Mental and Neurological Disease Research Center, the Third Affiliated Hospital of Sun Yat-sen University*

Abstract

Background: Enterobacterial translocation mediates post-stroke infection and is thus a leading contributor to mortality of acute ischemic stroke (AIS). Accumulative evidence suggests that bone marrow-derived mesenchymal stem cells (BM-MSC) effectively improve stroke outcomes. Whether BM-MSC could inhibit post-stroke enterobacterial translocation remains elusive.
Aim: To unveil the protective effect of BM-MSC against post-stroke enterobacterial translocation and the underlying mechanisms.
Method: AIS patients (within 7 days after stroke) and age- and sex-matched healthy individuals were enrolled in the study. Male C57BL/6J mice were subjected to transient middle cerebral artery occlusion (tMCAO) as AIS models and were treated with BM-MSC (2×10^6, i.v.) right after reperfusion. Enterobacterial translocation was assessed with stroke dysbiosis index and circulating endotoxin. Thickness of mucus was evaluated with Alcian-blue staining. Hepatic metabolism of glucocorticoid was

assessed by the catabolic products and expression of HSD11B2, HSD11B1, and SRD5A1.

Results: Pronounced enterobacterial translocation were evident in both AIS patients (34 HC *vs* 54 patients, $P < 0.0001$) and mice models ($N = 3$, $P = 0.0069$). Attenuation of the gut mucus layer in tMCAO mice was recorded. Transfer of BM-MSC restored the mucus thickness and subsequently inhibited enterobacterial translocation. Gut tissue RNAseq and *in vitro* experiments revealed that mucin production by gut goblet cells was impaired after stroke in response to elevation of glucocorticoid, which was reversed by BM-MSC therapy. However, *in vivo* tracing showed that BM-MSC was largely stationed in the liver but hardly infiltrated into gut. Liver resident BM-MSC activated PPARγ in hepatocyte, leading to increased expression of HSD11B2 and SRD5A1 but down-regulation of HSD11B1. Consequently, the hepatic metabolism of glucocorticoid was enhanced, which inhibited the injurious effect of glucocorticoid on gut barrier integrity.

Conclusions: BM-MSC improves post-stroke gut barrier integrity and inhibits enterobacterial translocation by enhancing the hepatic metabolism of glucocorticoid. BM-MSC represents a protective modulator of the brain-liver-gut axis after AIS.

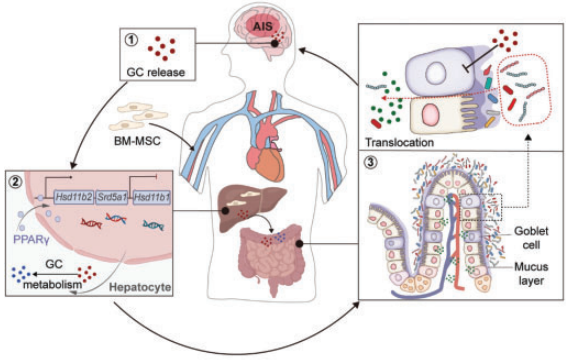

Bone Marrow Mesenchymal Stem Cell Inhibits Enterobacterial Translocation after Ischemic Stroke via Liver-Gut Axis

NX210c: a disease-modifying peptide for the treatment of Alzheimer's Disease

Sighild Lemarchant[1], Juliette Le Douce[1], Valérie Bourdès[1] and Yann Godfrin[2]

[1]*Axoltis Pharma, Lyon, France*
[2]*Axoltis Pharma, Lyon, France; Godfrin Life-Sciences, Caluire-et-Cuire, France*

Abstract

Background: Alzheimer's Disease (AD) is a common progressive neurodegenerative disease that slowly impairs cognitive functions. Current standards of care (such as donepezil) are mainly symptomatic while recently approved disease-modifying treatments (DMT) can lead to safety issues (notably amyloid-related imaging abnormalities). Hence, there is an urgent need to develop a new and safe DMT.

Aim: Here, we sought to evaluate the effect of a subcommissural organ-spondin-derived peptide, NX210c, on AD progression and on learning and memory deficits in a mouse model of AD.

Method: Mice were subjected to an intracerebroventricular injection of $A\beta_{25-35}$ oligomers and treated with daily intraperitoneal injections of NX210c at different doses (ranging from 0.1 to 30 mg/kg) or its vehicle (water for injection) and therapy paradigms (early or late stand-alone treatments, combination with donepezil or second-line treatment). Cognitive functions were evaluated using the Y-Maze, the step-through latency passive avoidance (STPA) and the Morris water maze (MWM) tests for up to 4 months.

Results: Early-stage daily treatment with NX210c decreased the levels of common markers of AD such as $A\beta_{1-42}$, phosphorylated Tau and TNF-α, and increased synaptogenesis. Regardless of the experimental paradigm used, NX210c prevented AD-induced decreased spontaneous alternations (Y-Maze) and step-through latency into the dark compartment (STPA), and AD-induced increased time to find the immersed platform during the learning phase and decreased time in the target quadrant during the retention phase (MWM).

Conclusions: This study provides the first evidence that a clinical-stage drug candidate peptide reduces common hallmarks of AD pathology and restores learning and memory at both early and late pathological stages. Moreover, results from first-in-human trial showed that NX210c peptide was safe irrespective of the dose. Overall, we shed light on the therapeutic potential of this innovative disease-modifying peptide to restore memory function in AD patients.

Anakinra negatively affects thrombolysis treatment in ischemic stroke

Ioana-Emilia Mosneag[1], Marina Rubio[2], Ben Dickie[3], Yolanda Ohene[4], Eloise Lemarchand[2], Graham Coutts[1], Denis Vivien[2], Craig J Smith[5] and Stuart M Allan[1]

[1]*Geoffrey Jefferson Brain Research Centre, School of Biological Sciences, Faculty of Biology, Medicine and Health, University of Manchester, United Kingdom*

[2]UNICAEN, INSERM U1237, Physiopathology and Imaging of Neurological Disorders (PhIND), Cyceron, Institut Blood and Brain @ Caen-Normandie (BB@C), Normandie University, Caen, France
[3]Division of Imaging, Informatics and Data Science, University of Manchester
[4]Geoffrey Jefferson Brain Research Centre, School of Health Sciences, Faculty of Biology, Medicine and Health, University of Manchester, United Kingdom
[5]Geoffrey Jefferson Brain Research Centre, Manchester Centre for Clinical Neurosciences, Northern Care Alliance National Health Service Foundation Trust, Salford Royal Hospital, UK

Abstract

Background: Inflammation is detrimental in ischaemic stroke, with the proinflammatory cytokine interleukin-1 (IL-1) a key mediator of neuronal injury. Inhibition of IL-1 has been targeted therapeutically in preclinical and clinical trials for both ischaemic and haemorrhagic stroke, with IL-1 receptor antagonist (IL-1Ra, anakinra) successfully decreasing inflammation. In the most recent Phase 2 trial, IL-1Ra was co-administered with tissue plasminogen activator (tPA) for the first time. Despite the confirmation of IL-1Ra's anti-inflammatory effect, secondary mediation analysis uncovered an alternative pathway leading to no overall improvement in functional outcome.
Aim: We hypothesise that there is an interaction between IL-1Ra and tPA in ischaemic stroke that could impact on drug efficacy. Therefore, we aim to uncover and understand the combined effects of IL-1Ra and tPA preclinically with different dosing regimens.
Methods: See figure below.
Results: tPA administered alone decreased lesion volume by 55% compared to control (**$p < 0.01$) as measured three days post-stroke by T2 MRI in both studies. IL-1Ra administered alone did not decrease lesion volume in the thrombin stroke model, contrary to beneficial effects seen previously in other murine models. However, when the two drugs were co-administered acutely (Study 2), the thrombolytic effect of tPA was diminished two-fold compared to the effect obtained with the longer dosing regimen. Additionally, co-treatment in Study 2 led to 52% lower (**$p < 0.01$) cerebral blood flow in the stroke lesions and increased haemorrhagic transformation, compared to the group receiving thrombolysis only.
($n = 10–13$/group, One-way ANOVA **$p < 0.01$ for all outcomes)
Conclusions: These data suggest that there is an acute negative interaction between IL-1Ra and tPA at the vascular level within 3 h after stroke induction. Ongoing experiments aim to provide further insights into anti-inflammatory treatment post-stroke and possible drug-drug interactions between tPA and IL-1Ra. Understanding the potential differences of prolonged versus acute anti-inflammatory treatment is of importance for clinical translation.

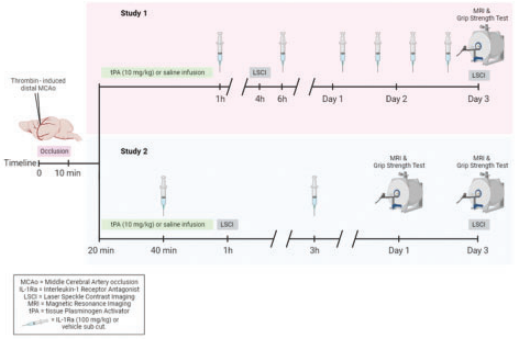

Figure: Experimental timelines. Thrombin-induced middle cerebral artery occlusion was used for stroke induction in both preclinical studies. In Study 1 - the SCIL-STROKE regimen was mimicked, with six doses of IL-1Ra (100 mg/kg) twice daily following tPA (10 mg/kg) administration. In Study 2 - IL-1Ra was administered during tPA infusion (30 min post-occlusion) with one more dose 3h after, replicating previous preclinical studies in stroke. The main outcomes were measured at 3 days post-occlusion using MRI scans, but secondary measurements were taken at either 4h, or 1h and day 1 post-occlusion in Study 1 and 2, respectively.

NOTCH3 mutation promotes microglial presenility through the inactivation of Hippo pathway in CADASIL

Xiaohui Deng[1], Chunyi Li[1], Huipeng Huang[1], Zhengqi Lu[2] and Wei Cai[3]

[1]Department of Neurology, Mental and Neurological Disease Research Center, the Third Affiliated Hospital of Sun Yat-sen University, Guangzhou, 510630, China
[2]Department of Neurology, Mental and Neurological Disease Research Center, the Third Affiliated Hospital of Sun Yat-sen University
[3]the third affiliated hospital of sun yat-sen university

Abstract

Background: Senescence of microglia, the brain resident scavenger, leads to accumulation of metabolic wastes. White matter injury is one of the fundamental pathological issues in CADASIL (Cerebral Autosomal Dominant Arteriopathy with Subcortical Infarcts and Leukoencephalopathy), which causes injury of neurovascular unit (NVU) and requires timely myelin debris clearance. Whether microglial senescence is implicated in CADASIL progression remains elusive.
Aim: To reveal the implication of microglial senescence in CADASIL progression and the underlying mechanisms.
Methods: *Notch3^{R170C}* C57BL/6J mice were used as CADASIL models. Cellular senescence was assessed with the ageing markers including SA-β-gal and P16, while cell proliferation was analyzed with Ki67 expression. NVU injury was evaluated with white matter integrity, tight junction protein expression and neuronal loss.

Results: Microglial senescence was recorded in CADASIL brain as early as 4 m of age, which was not detected in WT mice until 8 m ($N = 8$, $P < 0.05$). Both human ($N = 3$, $P < 0.05$) and mice ($N = 4$, $P < 0.01$) microglia with NOTCH3 mutation displayed vulnerability against the stimulus of myelin debris which underwent cell cycle arrest and got into aging process. Mechanistically, NOTCH3 mutation inactivated Hippo signaling, leading to deficiency in proliferation and programmed cell death, which resulted in failure of cell renewal. Reinforcing Hippo activation reversed the pro-ageing effect of NOTCH3 mutation in microglia and ameliorated NVU injury in CADASIL.
Conclusions: Inactivation of Hippo signaling due to NOTCH3 mutation causes microglial senescence, which promotes CADASIL progression. Reinforcing the function of Hippo signaling represents a promising therapeutic strategy against microglial presenility in CADASIL.

Regional differences in LPS-induced microglial programmed cell death following immature brain injury

Tiantian He[1], Jinjin Zhu[1], Zilong Yi[1], Yiran Xu[1] and Changlian Zhu[2]

[1]Institute of Neuroscience and Third Affiliated Hospital of Zhengzhou University, Zhengzhou, Henan Province, China
[2]Center for Brain Repair and Rehabilitation, Institute of Neuroscience and Physiology, University of Gothenburg, Gothenburg, Sweden

Abstract
Background: Inflammation is a principal cause of preterm birth and is frequently associated with preterm brain injury. Microglia are key players in the development of neuroinflammation. However, there are limited studies on the role of programmed cell death (PCD) of microglia. Furthermore, aberrant activation of PCD such as apoptosis, necroptosis, and ferroptosis is a common feature of neurological diseases, particularly in the developing brain, and recent evidence indicates complex interplay and crosstalk between these processes.
AIM: To investigate the various types and characteristics of microglia PCD induced by LPS in immature brain injury, and to identify potential key convergence point that can regulate multiple types of PCDs.
Methods: To establish an immature brain injury mouse model, mice were given LPS (10mg/kg) via intraperitoneal injection. $CD45^+$ cells from the whole brain and conducted RNA-seq to analyze different types of PCDs. The type, expression characteristics, and possible upstream key points of PCD were validated using various techniques, including gene, protein, and morphology analyses, through a series of in vitro and in vivo experiments.
Results/Conclusions: RNA-seq analysis and validation revealed that LPS-induced preterm mice exhibited activated microglia cell death pathways, including apoptosis, necroptosis, and ferroptosis at 24 h post-injury. STRING data analysis identified ZBP1 as a potential key control points (figure 1). Furthermore, using Tunel and Prussian blue iron staining in brain section at 24 hours, we observed that positive cells were mainly concentrated in the subcortical white matter of the LPS group, indicating brain region-specific expression. LPS exposure also decreased MBP staining at the corpus callosum area at P12. Overall, our finding demonstrate the existence of multiple types of microglial PCDs and underscore the pivotal role of ZBP1 in immature brain injury induced by bacterial infection.

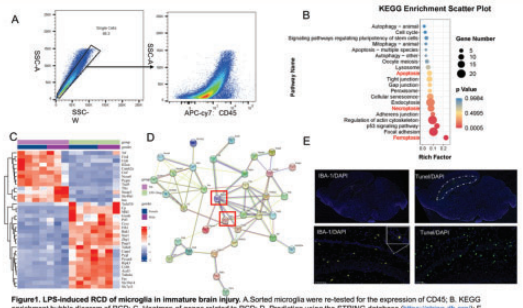

Figure1. LPS-induced RCD of microglia in immature brain injury. A.Sorted microglia were re-tested for the expression of CD45; B. KEGG enrichment bubble diagram of RCD; C. Heatmap of genes related to RCD; D. Prediction using the STRING database (https://string-db.org/); E. Representative images show Tunel and Iba-1 staining results (blue, DAPI; green, Tunel; yellow, Iba-1). Insets are enlarged, representative images of activated microglia morphology.

Automated detection of severe cerebral edema in cardiac arrest survivors

Zihao Wang[1], Annelise M Kulpanowski[2], William A. Copen[3], Brandon L. Hancock[1], Eric S. Rosenthal[4], Jacob A. Dodelson[2], Brian L. Edlow[5], W. Taylor Kimberly[5], Edilberto Amorim[4], M. Brandon Westover[6], Ming Ming Ning[5], Pamela W. Schaefer[3], Rajeev Malhotra[7], Joseph T. Giacino[8], David M. Greer[9] and Ona Wu[2]

[1]Athinoula A. Martinos Center for Biomedical Imaging, Department of Radiology, Massachusetts General Hospital, Harvard Medical School
[2]Athinoula A. Martinos Center for Biomedical Imaging, Department of Radiology, Massachusetts General Hospital, Harvard Medical School, Charlestown, MA 02129, USA
[3]Department of Radiology, Neuroradiology Division, Massachusetts General Hospital, Boston, MA, 02114, USA

[4]Department of Neurology, Massachusetts General Hospital
[5]Department of Neurology, Massachusetts General Hospital, Boston, MA, 02114, USA
[6]Beth Israel Deaconess Medical Center
[7]Department of Medicine, Cardiology Division, Massachusetts General Hospital
[8]Department of Physical Medicine and Rehabilitation, Spaulding Rehabilitation Hospital, Harvard Medical School, Charlestown, MA 02129, USA
[9]Department of Neurology, Boston University School of Medicine, Boston Medical Center, Boston, MA, 02118, USA

Abstract

Background: Significant knowledge gaps remain in predicting neurological outcomes for comatose cardiac arrest patients. Outcomes studies focus on survival, a measure confounded by withdrawal of life-sustaining therapy (WLST) decisions. Severe cerebral edema (SCE) development offers an objective imaging surrogate for neurologic injury.

Aim: We aim to automate the detection of SCE on CT scans using machine learning. We focus on CT since many cardiac arrest patients are contraindicated for MRI.

Method: We retrospectively analyzed CT data from comatose cardiac arrest patients admitted between 2007–2019. SCE classifications were made by review of radiology reports. Datasets were randomly split (balancing for SCE) into training, validation, and testing cohorts. We used transfer learning with a 3D residual neural network (ResNet) framework initially designed for CT image segmentation (MedicalNet) to train our model. We performed experiments with pre-trained models (see Figure) for hyperparameter optimization (i.e., learning rate [LR] and model selection). Model selection was based on maximum accuracy (number of correctly classified datasets/number of datasets) and minimum cross-entropy loss (CEL, measure of differences) for the validation cohort.

Results: We analyzed CT data from 299 patients (55 ± 17 years, 71% male). SCE was identified on CT scans from 65 patients. The distribution of patients in training, validation, and testing cohorts was 178/60/61. The distribution of SCE patients in the cohorts was 39/13/13. Based on our experiments (see Figure), the optimal model was ResNet-34 using LR = 0.001 (CEL: 0.015 vs. 0.016 for ResNet-18, LR = 0.01), with a validation accuracy of 84% [95% CI: 78–89%]. The model's accuracy on the reserved test cohort was 83% [95% CI: 76 to 89%], comparable to the validation cohort.

Conclusions: Our result shows that transfer learning is a promising method to automate SCE detection on CT images. We expect that with larger data cohorts, we can further improve the model's performance.

Figure: Classification accuracy (in percentage) / cross-entropy loss of different models on the validation dataset.

		Pre-trained Model Name			
		ResNet 10	ResNet 18	ResNet 34	ResNet 50
Learning Rate	0.01	81.46 / 0.052	84.27 / 0.016	79.78 / 0.12	75.84 / 0.23
	0.001	75.84 / 0.19	81.46 / 0.061	**84.27 / 0.015**	75.84 / 0.18
	0.0001	75.84 / 0.21	75.84 / 0.19	75.84 / 0.16	75.84 / 0.19

Apolipoprotein e4 impairs cerebrovascular regulation via perivascular macrophagesand Nox2-Derived radicals

Antoine Anfray[1], Yorito Hattori[2], James Seo[1], Monica Santisteban[1], Sung Ji Ahn[1], Gang Wang[1], Josef Anrather[1], Laibaik Park[1] and Costantino Iadecola[3]

[1]Weill Cornell Medicine
[2]Feil Family Brain and Mind Research Institute, Weill Cornell Medicine; Department of Neurology, National Cerebral and Cardiovascular Center
[3]Feil Family Brain and Mind Research Institute, Weill Cornell Medicine

Abstract

Background: Apolipoprotein E4 (ApoE4) is associated with marked alterations in cerebral blood flow (CBF) and regulatory mechanisms. Using ApoE4 targeted replacement mice (ApoE4-TR), we found that cerebrovascular regulation is altered by vascular oxidative stress. However, the cellular bases of the detrimental effects of ApoE4 on cerebrovascular regulation remain undetermined. Perivascular macrophages (PVM) mediate vascular oxidative stress in models of hypertension and amyloid accumulation through reactive oxygen species (ROS) produced by Nox2.

Aim: To investigate whether PVM are responsible for the vascular oxidative stress and cerebrovascular dysregulation induced by ApoE4.

Methods: CBF was assessed by laser-Doppler flowmetry in the somatosensory cortex of ApoE3/4-TR and C57BL/6 mice anesthetized with urethane-chloralose (n = 5/group). PVM were depleted by intracerebroventricular (i.c.v.) administration of clodronate and examined seven days later.

Results: In C57BL/6 mice, we found that neocortical superfusion with recombinant ApoE4 (rApoE4), but not rApoE3, attenuates the increase in CBF produced by whisker stimulation (WS) or by topical application of the endothelium-dependent vasodilator acetylcholine (WS,

$-62 \pm 3\%$; ACh, $-48 \pm 8\%$; $p < 0.05$) and not by the smooth muscle relaxant adenosine, as observed in ApoE4-TR mice. PVM depletion completely prevented the cerebrovascular dysfunction induced by rApoE4 superfusion ($p > 0.05$) and ameliorated cerebrovascular responses in ApoE4-TR mice. In brain cells isolated from ApoE4-TR mice, ROS production, assessed by flow cytometry using dihydroethidium, was increased in PVM ($+64 \pm 11\%$; $p < 0.05$), but not in microglia or endothelial cells. Furthermore, neocortical superfusion of the Nox2 peptide inhibitor gp91ds-tat (1μM), but not its scrambled control peptide, counteracted the cerebrovascular dysfunction produced by rApoE4 ($p < 0.05$).

Conclusions: These findings suggest that PVM are the source of the ApoE4 causing cerebrovascular dysfunction via Nox2-derived ROS. We conclude that PVM ApoE4 may be a therapeutic target to counteract the cerebrovascular alterations associated with the ApoE4 genotype.

Supported by NIH grants R01-NS126467; R01-NS037853; R01-NS097805

The role of the VWF/ADAMTS13 axis in the outcome of ischaemic stroke after SARS-CoV2 infection

Nadim Luka[1], Kieron South[1], Graham Coutts[1], Rachel Jones[1], Chloe Quigley[2], Siew yan Wong[2], Amy Bradley[2], Craig Smith[2] and Stuart Allan[1]

[1]Geoffrey Jefferson Brain Research Centre, School of Biological Sciences, Faculty of Biology, Medicine and Health, University of Manchester, United Kingdom

[2]Geoffrey Jefferson Brain Research Centre, Manchester Centre for Clinical Neurosciences, Northern Care Alliance National Health Service Foundation Trust, Salford Royal Hospital, UK

Abstract

Background: Respiratory tract infections increase risk of ischaemic stroke (IS), potentially through a thromboinflammatory cascade driven by an imbalance in the ratio of Von Willebrand Factor (VWF) and a disintegrin and metalloproteinase with a thrombospondin type 1 motif, member 13 (ADAMTS13), leading to ultra-large VWF (UL-VWF) and thrombus formation.

Aim: To investigate the effect of SARS-CoV2 infection on the post-stroke thromboinflammatory response.

Methods: Blood was collected from patients 2–3 days post-stroke and from matched controls. Respiratory failure was used to assess SARS-CoV2 severity. Thromboinflammatory factors were measured using ELISAs and Legendplex multiplex assays. Statistical analyses were performed using the Kruskal-Wallis test and non-parametric Spearman correlation.

Results: Seventy-one individuals (age, sex and stroke severity matched) were divided in non-stroke controls ($n = 23$), IS ($n = 24$) and SARS-CoV2 + IS ($n = 24$). VWF ($p < 0.0001$) and UL-VWF ($p < 0.05$) **(Figure 1A–B)** were elevated and ADAMTS13 **(Figure 1C)** was decreased ($p < 0.05$) in SARS-CoV2 + IS, suggesting a VWF/ADAMTS13 axis imbalance. Interleukin-6 (IL-6) was elevated in SARS-CoV2 + IS ($p < 0.05$), correlated with VWF ($p < 0.001$) and negatively correlated with ADAMTS13 ($p < 0.001$) suggesting that IL-6 drives this imbalance. Fibrinogen was elevated in IS ($p < 0.001$) and SARS-CoV2 + IS ($p < 0.05$), while Factor IX (FIX) was elevated in IS ($p < 0.05$). Tissue plasminogen activator (tPA) was elevated in SARS-CoV2 + IS ($p < 0.05$) and D-Dimer in IS ($p < 0.01$) and SARS-CoV2 + IS ($p < 0.001$) suggesting active fibrinolysis. Matrix Metalloproteinase-2 (MMP-2) ($p < 0.0001$) and Intracellular Adhesion Molecule-1 (ICAM-1) ($p < 0.01$) were elevated in IS, suggesting leukocyte recruitment and infiltration.

Conclusions: This is the first study assessing effects of SARS-CoV2 in thromboinflammation post-stroke. SARS-CoV2 drives an IL-6-mediated VWF/ADAMTS13 axis imbalance and increases tPA, while decreasing FIX, MMP-2 and ICAM-1 post-stroke. SARS-CoV2 thromboinflammatory data from different databases will be integrated to this study. The effect of SARS-CoV2 on interaction among the plasma, leukocytes and the vasculature, as well as the plasma environment's role in the transmigration of neutrophils, will be further investigated.

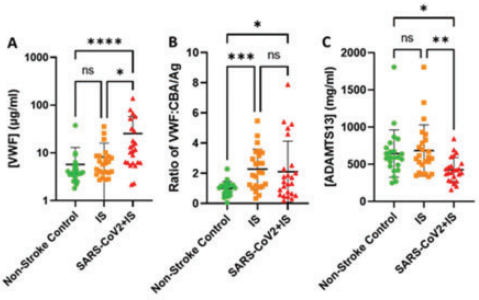

Figure 1: Plasma from SARS-CoV2+Ischaemic stroke patients show an imbalance in the VWF/ADAMT13 axis. **(A)** The plasma concentration of VWF was quantified using a previously optimised in-house ELISA. **(B)** The presence of UL-VWF was assessed by collagen binding assay. UL-VWF was quantified in comparison to the non-stroke control group. UL-VWF was normalised by the VWF antigen to obtain the VWF:CBA/Ag ratio. **(C)** The plasma concentration of ADAMTS13 was quantified using an in-house ELISA

Loss-of-microRNA-15a/16-1 function promotes neuropathological and functional recovery in experimental traumatic brain injury

Chao Zhou[1], Ping Sun[1], Milton H. Hamblin[2], C. Edward Dixon[1], Jun Chen[1] and Kejie Yin[1]

[1]*University of Pittsburgh School of Medicine; GRECC Veterans Affairs Pittsburgh Healthcare System*
[2]*Tulane University Health Sciences Center*

Abstract

Background: MicroRNAs (miRs) have been implicated in a variety of human central nervous system (CNS) diseases, and the function and mechanisms of miRs in regulating long-term neurological outcomes are poorly understood in traumatic brain injury (TBI). Dysregulated plasma miR-15a/16-1 levels have been found in TBI individuals. However, the essential role and therapeutic potential of the miR-15a/16-1 cluster in TBI are poorly understood.

Aim: To determine whether genetic deletion and pharmacological inhibition of the miR-15a/16-1 cluster improve the functional recovery in TBI.

Method: Experimental TBI was induced in miR-15a/16-1 knockout mice and wild-type controls by unilateral controlled cortical impact (CCI) for four weeks. A total of 8 μg miR-15a/16-1 antagomir or scramble control was intranasally administered in each mouse at 2 h, 5d, 10d, 15d, 20d, and 25d after TBI. The cognitive and sensorimotor neurobehavioral disorders, white matter injury, and neuronal loss were then extensively evaluated by multiple approaches and quantitatively analyzed. The parenchymal inflammatory cytokines were detected by inflammation antibody array.

Results: Mice underwent CCI for 28 days developed remarkable cognitive impairments, myelin loss and axonal damage in corpus callosum and external capsule, and neuronal death in cerebral cortex and hippocampal CA1 region. Genetic deletion of the miR-15a/16-1 cluster or intranasal delivery of miR-15a/16-1 antagomir significantly reduced CCI-induced neuronal loss, demyelination, and axonal injury, and improved long-term neurobehavioral outcomes in TBI mice. Inhibition of miR-15a/16-1 significantly decreased the expression of the proinflammatory cytokines interleukin-6, interleukin-9, monocyte chemoattractant protein-1, tumor necrosis factor alpha levels in the perilesional brain regions.

Conclusions: The present study has demonstrated that genetic deletion and pharmacological inhibition of the miR-15a/16-1 cluster improve histological and functional outcomes in an experimental TBI model. The miR-15a/16-1 cluster may be a novel therapeutic target for the treatment of TBI.

Selective loss of the mitochondrial protein prohibitin in neurons exacerbates ischemic brain injury and induces neurodegeneration in mice

Jasmine Fels[1], Diane Lane[1], Anja Kahl[1], Liping Qian[1], Belem Sanchez[1], Alexander Galkin[1], Giovanni Manfredi[1], Costantino Iadecola[2] and Ping Zhou[1]

[1]*Weill Cornell Medicine*
[2]*Feil Family Brain and Mind Research Institute, Weill Cornell Medicine*

Abstract

Background: Mitochondrial dysfunction is a major hallmark of neurodegeneration and ischemic brain injury. However, how mitochondrial dysfunction contributes to brain injury is not fully understood. Here, we present a novel mouse model generated by conditional deletion of the mitochondrial protein prohibitin (PHB KO) in neurons, which recapitulates many features of human neurodegeneration.

Aim: We used the PHB KO model to elucidate the early biochemical and molecular events through which neuronal mitochondrial dysfunction may lead to neurodegeneration and increased susceptibility to ischemia/reperfusion injury.

Method: PHB KO mice were generated by crossing floxed mice (exon 4–5) with a CamKIIα Cre line (JAX# 005359). These mice underwent longitudinal, biochemical, transcriptional, metabolic, and behavioural characterizations, as well as brain ischemia by transient middle cerebral artery occlusion (MCAO).

Results: At 26 weeks of age PHB KO mice manifested a progressive weight loss ($-25 \pm 2\%$; $p < 0.001$, @1 yr), reduced brain volume ($-34 \pm 2.2\%$; $p < 0.001$), and memory impairment (Barnes maze). MCAO produced larger infarct in PHB KO mice ($58 \pm 3.1\,mm^3$) than controls ($28 \pm 5.6\,mm^3$, $p = 0.0004$, $n = 9$/group; age 14 weeks). Mitochondrial defects, before brain atrophy and cognitive impairment, included decreased respiration, enhanced ROS, and reduced respiratory complex activity (CI:$-44.7 \pm 2.4\%$; CIV:$-29.4 \pm 2.1\%$, $p < 0.001$). Furthermore, these mice exhibited astrocyte and microglia activation, tau hyperphosphorylation (AT8), ubiquitinated protein aggregation, and accumulation of lipid droplet, first in neurons and then in microglia. Transcriptomic and lipidomic analyses revealed a sustained

integrated stress response (*Eif2α, Trib3, Atf4*) and dysregulation of cardiolipin and triacylglyceride metabolism.
Conclusions: Neuronal PHB deletion leads mitochondrial dysfunction, neurodegeneration, and enhanced vulnerability to cerebral ischemia in mice. The mechanisms likely involve mitochondrial respiratory chain impairments, leading to a sustained metabolic and oxidative stress, neuroinflammation, protein aggregation, lipid accumulation and brain atrophy. The PHB KO model could be a viable tool to dissect the early pathological events leading to brain injury in encephalopathies associated with mitochondrial dysfunction.

Targeted temperature management alters spatial characteristics of glucose metabolism and improves neurological function in rats after cardiac arrest

Zhuoran Wang[1], Mark Smith[1] and Xiaofeng Jia[2]
[1]*University of Maryland Baltimore*
[2]*University of Maryland School of Medicine, Johns Hopkins University School of Medicine*

Abstract
Background: Targeted temperature management (TTM) remains one therapeutic strategy with definitive protection against post-cardia arrest (CA) neurological damage with extensive evidence. TTM may not only affect the overall level of cerebral glucose metabolism but also affect the spatial heterogeneity of glucose metabolism, which might be related to TTM neuroprotection but remains unelucidated.
Aim: To conduct a hypothermia-based dynamic ^{18}F-FDG PET investigation in the injured brain after CA, to explore the mechanism of glucose metabolism related to TTM and neural outcomes.
Method: Twenty-two Wistar rats were randomly assigned into 8min-CA+hypothermia (CH, $n = 7$), 8min-CA+normothermia (CN, $n = 7$), sham+hypothermia (SH, $n = 4$), and sham+normothermia (SN, $n = 4$) groups. MicroPET/CT scans were performed for 60 minutes in sham groups or after resuscitation. Standardized uptake value was used to evaluate the glucose metabolisms in brain regions.
Results: Aggregate 72hr-NDS in the CH group was significantly higher than that in the CN group ($p < 0.05$), indicating a better neurological functional recovery. In all quantified regions, the SUV of the SN group had the highest SUV (In the cortex, thalamus, and hypothalamus: $p < 0.01$; in the hippocampus: SN VS. SH, $p < 0.05$, VS. CH, $p < 0.05$, and VS. CN $p < 0.01$). In the area with enriched neurons, particularly in the cortex and hippocampus, SUV in the CH group decreased less compared to the CN group (both $p < 0.01$). The normalized comparison showed that the CH group had higher radioactivity uptake in the cortex and hippocampus normothermia compared to the CN group (both $p < 0.01$).
Conclusions: Hypothermia contributes to the recovery of neurological function in rats after CA, and its mechanism may be related to the reconstruction of spatial homeostasis of cerebral glucose metabolism.
Funding: Supported by R01HL118084, and partially by R01NS110387 and R01NS125232 from the United States National Institute of Health (All to Xiaofeng Jia).

In chronic traumatic encephalopathy (CTE) synapse loss (SV2A-PET) and altered functional connectivity (BOLD-fMRI) overlap in "spared" brain regions

Marija Markicevic[1], Francesca Mandino[2], Takuya Toyonaga[3], Arman Fesharaki-Zadeh[4], Xilin Chen[1], Jason Cai[1], Stephen Strittmatter[5] and Evelyn Lake[1]
[1]*Department of Radiology and Biomedical Imaging, School of Medicine, Yale University, USA*
[2]*Yale University*
[3]*Yale University, Department of Radiology and Biomedical Imaging*
[4]*Department of Neurology; Department of Psychiatry, School of Medicine, Yale University, USA*
[5]*Department of Neurology; Department of Neuroscience, School of Medicine, Yale University, USA*

Abstract
Background: Chronic Traumatic Encephalopathy (CTE) is a neurodegenerative disorder caused by repetitive mild traumatic brain injuries (rmTBIs). Although famous for affecting football players, high incidences of CTE arise in victims of domestic violence and the general population. The neurobiological characteristics of CTE include tauopathies, synaptic density alterations, and neuroinflammation. Clinically, CTE symptoms can take decades to manifest and can only be definitely diagnosed post-mortem. Yet, neurological alterations must begin shortly after injury which theoretically represents a long therapeutic window. Better means to diagnose and treat CTE requires research aimed at uncovering underlying mechanism (treatment targets) and early markers of disease.

Aim: Our overarching aim is to use fMRI (11.7T) and PET in an animal model of CTE to characterize emergent abnormalities indicative of future neurodegeneration.
Method: We combine rmTBI, using closed head injury (CHI), with chronic variable stress (CVS) to exacerbate neurodegeneration (Fig.1A). C57BL/6J mice (n = 10) underwent 2-weeks of daily randomized aversive stimuli (CVS) followed by CHI. Imaging outcomes are compared to uninjured/unstressed animals (n = 10). BOLD-fMRI was measured using gradient-echo, echo-planar-imaging: TR = 1.8sec, TE = 9.1 ms, 334 repetitions isotropic (0.275 mm^3), with 35 slices. Data were preprocessed with RABIES. Structural images were obtained with a multi-spin-multi-echo (MSME) sequence. [^{18}F]SynVesT-1 PET data measured synapse density. Standardized uptake values (SUV) are normalized to the striatum.
Results: Structural MRI revealed heterogeneous hyper/hypo-intense lesions in targeted somatosensory cortices, an overlap of segmented lesions is illustrated in Fig.1B. PET results indicate a decrease in synaptic density in midbrain and cerebellum (Mann-Whitney U tests with Bonferroni correction, $p_{corr} < 0.01$) (Fig.1C). From BOLD fMRI, an increase in regional homogeneity was also observed in the cerebellum (Mann-Whitney U tests with Bonferroni correction $p_{corr} < 0.01$) (Fig.1D).
Conclusion: These preliminary results indicate that a decrease in synaptic density overlaps with increased activity synchronization in regions that are physically distant from the impacted sites.

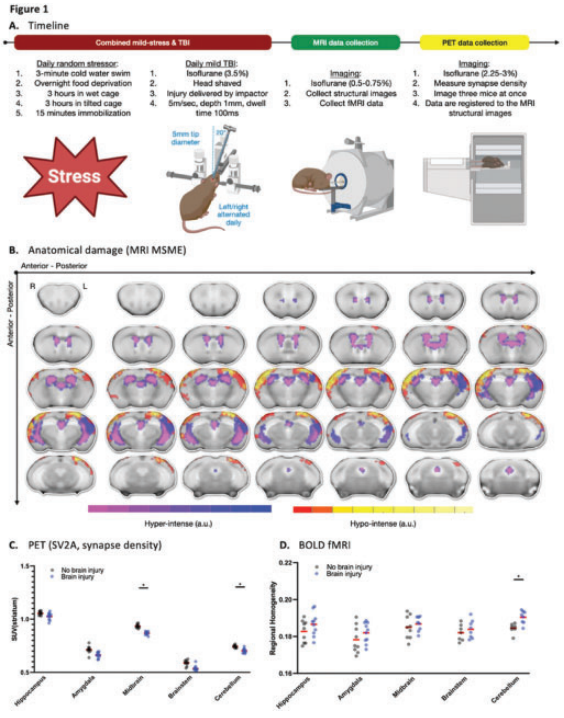

Spreading depolarization impairs neurovascular coupling in ischemia/reperfusion in mice

Ferenc Dr. Bari[1], Armand Bálint[1], Ákos Menyhárt[1] and Eszter Farkas[1]

[1] *University of Szeged, Albert Szent-Gyorgyi Faculty of Medicine*

Abstract
Background: Neurovascular coupling (NVC) is weak or absent upon acute ischemia/reperfusion. The mechanistic basis of NVC dysfunction might be the evolution of spreading depolarization (SD), that causes vasoconstriction and ischemic lesion progression.
Aim: We set out to explore the contribution of SD to NVC dysfunction in ischemia/reperfusion.
Method: C57BL/6 mice (n = 18) were anesthetized with isoflurane (0.6–1.2%). First, global forebrain ischemia was induced by transient (45 min) bilateral common carotid artery occlusion (2VO), followed by reperfusion (n = 6). SHAM-operated mice served as control (n = 7). Second, SD was induced in the optimally perfused cortex (n = 5). NVC function was evaluated under isoflurane (0.1%)-medetomidine (0.1 mg/kg) anesthesia by whisker stimulation (~2 Hz) either once 60 min into post-ischemic reperfusion, or repeatedly at 10–15 min intervals after SD in the otherwise intact cortex. Cerebral blood flow (CBF) was recorded using laser speckle contrast imaging/laser Doppler flowmetry combined with EEG recording.
Results: Spontaneous SD occurred in each hemisphere shortly after ischemia onset only below a CBF threshold of ~20%. Subsequent reperfusion was insufficient after the occurrence of SD (n = 8), but optimal after the absence of SD (n = 2) (51.07 ± 14.83 vs. 90.93 ± 3.08, presence vs. absence of SD). In concert, NVC was severely impaired when superimposed on reperfusion failure, but moderately impaired when superimposed on optimal reperfusion (hyperemia amplitude: 8.73 ± 3.01 vs. 17.16 ± 6.21 vs. 16.71 ± 5.41%, reperfusion failure vs. optimal reperfusion vs. SHAM). The absolute amplitude of functional hyperemia was reduced in the intact cortex after SD (14.8 ± 10.1 vs. 27.1 ± 13.1%, 10 min after vs. before SD), and recovered to control over 75 min.
Conclusions: SD is known to be followed by a persistent vasoconstrictive tone, probably mediated by prostanoids. We postulate that the post-SD vasoconstriction contributes to reperfusion failure and the graded impairment of NVC function after ischemia.
Funding: EU H2020-HCEMM (739593), NKFIH (K134377, K134334, FK142218, TKP2021-EGA-28), Hungarian Brain Research Program 3.0.

Multimodal imaging reveals evidence of neurovascular uncoupling along the Alzheimer's disease trajectory and response to synapse-rescuing treatment

Francesca Mandino[1], Xilin Shen[1], Gabriel Desrosiers-Gregoire[2], David O'Connor[1], Bandhan Mukherjee[1], Kristin DeLuca[1], Ali Hamodi[1], Daniel Barson[1], Ashley Owens[1], Yonghyun Ha[1], An Qu[1], John Onofrey[1], Xenophon Papademetris[1], Mallar Chakravarty[2], Michael C. Crair[1], Stephen M. Strittmatter[1] and Evelyn M.R. Lake[1]

[1]*Yale University*
[2]*McGill*

Abstract

Background: Alzheimer's (AD) is a devastating disease with high personal and societal costs that we have a limited ability to detect or treat. Neuroimaging in animal models stands to improve our understanding of clinically accessible biomarkers and to help us discover actionable disease-related processes (treatment targets). Here, in a double-knock-in murine model, we implement simultaneous wide-field calcium (WF-Ca^{2+}) and fMRI spanning disease-relevant timepoints (4–22M) and test a synapse-rescuing treatment. The co-acquisition of multimodal data sheds light on the widespread neural activity that underlies AD-related changes in the clinically accessible BOLD-fMRI signal.

Methods: We implement a novel technique for fluorophore expression in excitatory neurons in animals bearing disease-relevant mutations. This enables whole-brain labeling, whilst circumventing costly crossbreeding schemes (Fig.1a). Animals undergo longitudinal simultaneous WF-Ca^{2+} and fMRI at 4, 6, and 9M (Fig.1b, c). In a second cohort, we test treatment with a silent allosteric mGluR5 (metabotropic glutamate receptor five) modulator (Fig.1d). Mice undergo fMRI at 20 and 22M (before/after treatment). Whole-brain and cortical (WF-Ca^{2+}) functional connectivity (FC), measured using Pearson's correlation, is computed at each timepoint. Differences in FC (wild-type, WT, subtract AD) are shown (T-statistic) as matrices.

Results: fMRI-FC in AD deviates from WT in select circuits (e.g., somatosensory/motor) beginning at 9M and becomes more profound (20–22M, $p < 0.05$). These changes are rescued with treatment (no difference between AD-treated and WT, $p > 0.05$). Unlike the fMRI-FC, WF-Ca^{2+} imaging shows large AD-related FC differences at 4M that shift and dissipate (6–9M) before changes in fMRI-FC appear (Fig.1e, green panel).

Conclusion: We have established an experimental paradigm for simultaneous WF-Ca^{2+} and fMRI in an AD model at AD-relevant timepoints. This has enabled us to capture a trajectory of AD-related changes in fMRI-FC, evidence of treatment response, and a marked difference in excitatory neuron, relative to BOLD-fMRI, FC in early-stage disease which could indicate neurovascular uncoupling.

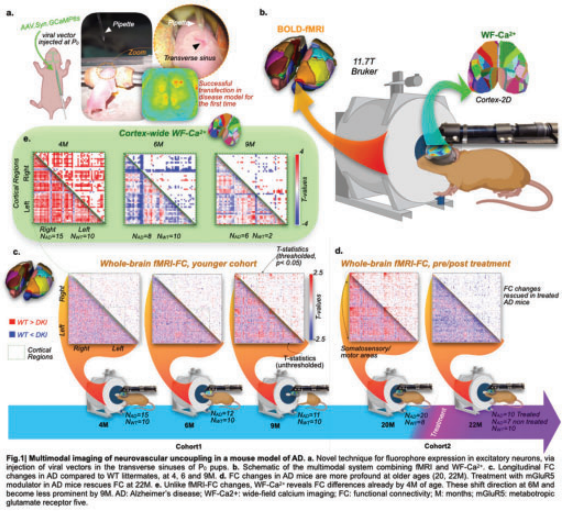

Fig.1| Multimodal imaging of neurovascular uncoupling in a mouse model of AD. a. Novel technique for fluorophore expression in excitatory neurons, via injection of viral vectors in the transverse sinuses of P_0 pups. b. Schematic of the multimodal system combining fMRI and WF-Ca^{2+}. c. Longitudinal FC changes in AD compared to WT littermates, at 4, 6 and 9M. d. FC changes in AD mice are more profound at older ages (20, 22M). Treatment with mGluR5 modulator in AD mice rescues FC at 22M. e. Unlike fMRI-FC changes, WF-Ca^{2+} reveals FC differences already by 4M of age. These shift direction at 6M and become less prominent by 9M. AD: Alzheimer's disease; WF-Ca2+: wide-field calcium imaging; FC: functional connectivity; M: months; mGluR5: metabotropic glutamate receptor five.

Non-invasive vagus nerve stimulation (nVNS) reduces BBB disruption, neuron-derived IL-1ß, and neuroinflammation in a rat model of ischemic stroke

Yi Yang[1], Yirong Yang[2], Lisa Yang[3], Jeffrey Thompson[3], Kiran Bhaskar[4], Kelsey Duval[1] and Michel Torbey[5]

[1]*Department of Neurology, University of New Mexico School of Medicine*
[2]*University of New Mexico College of Pharmacy*
[3]*Department of Neurology, University of New Mexico School of Medicine*
[4]*Department of Molecular Genetics and Microbiology, University of New Mexico School of Medicine*
[5]*University of New Mexico*

Abstract

Background: nVNS significantly reduces infarct volume in rat models of cerebral ischemia, while VNS is the first neuromodulation technology FDA approved for post-

stroke upper limb recovery. However, the mechanisms underlying remains open.

Aim: To test the hypothesis that nVNS delivered during middle cerebral artery occlusion (MCAO) protects the BBB integrity and attenuates neuroinflammation, leading to reduction of neuronal death in ischemic brain.

Method: Spontaneously hypertensive rats were subjected to a 90-minute MCAO with 24-hour reperfusion (RP). nVNS treated rats received 5 doses of nVNS (duration: 2min; every 10 min) beginning 30 min after MCAO onset.

Results: Compared with the control group, anatomic MRI T2-weighted images showed significantly smaller infarct sizes in the nVNS group. Dynamic contrast-enhanced-MRI showed a significantly decreased BBB transfer rate in the lesion area in the nVNS group, which was spatially correlated with the attenuation of the infarct size. nVNS also protected vascular tight junction proteins from disruption in microvessels, and reduced expression of matrix metalloproteinases-2/9 (MMP-2/9) in reactive astrocytes surrounding these compromised microvessels. Further study indicated that MCAO/RP induced a significant increase of active IL-1ß level and ischemic neurons were the main resource of the IL-1ß, which were significantly attenuated by nVNS. The activation of the neuronal IL-1ß was non-caspase-1-dependent. Both in *vivo* and *in vitro* data showed a correlation of intracellular MMP-9 activation with IL-1ß expression in ischemic neurons. nVNS significantly reversed stroke-induced decrease of neuronal nicotinic acetylcholine receptor a7 subtype (a7nAChR) and reduced neurodegeneration.

Conclusions: Our data suggest that the neuroprotective role of nVNS administrations during MCA occlusion spatially correlates with the protection of BBB integrity and reduction of infarct extent. Acute ischemic insult triggers a unique molecular injury cascade involving in activation of the MMPs/IL-1ß signalling pathway in injured neurons. nVNS downregulates this signalling pathway via a7nAChR to reduce neuronal death.

Effect of body temperature on selective brain cooling in traumatic brain injuries

Olivia Tong[1], Kevin J. Chung[1], Daniel Mendes[2], Laura Morrison[2], Lise Desjardins[2], Susan Tyler[2], Marcus Flamminio[2], Lynn Keenliside[2] and Ting-Yim Lee[1]

[1]Lawson Health Research Institute; Robarts Research Institute; Western University

[2]Lawson Health Research Institute

Abstract

Background: Traumatic brain injuries (TBI) pose a substantial public health burden. Both acute and sub-acute injuries can lead to long-term disabilities. Selective brain cooling (SBC) could prevent secondary (subacute) brain injuries after the initial trauma, and minimize the adverse effects of whole-body cooling. However, the influence of body temperature on the effectiveness of SBC is unknown.

Aim: We aim to determine the influence of body temperature, delivered by our in-house developed Vortex tube IntraNasal Cooling Instrument (VINCI), in TBI.

Method: 21 pigs were subjected to three >75 psi blasts from a fluid percussion injury device to induce lesions. The animals were then assigned to normothermia/control (n = 5) and two treatment groups. The treatment groups had body temperatures either below (BBT, N = 8) or above (ABT, N = 8) 37.5°C. Brain cooling (2–5°C below normothermia) by VINCI was maintained for 17 h before rewarming at a rate of 0.5°C. Throughout the study, online vitals, blood samples, and brain hemodynamics by CT perfusion were collected.

Results: All control animals had intracranial pressure (ICP) > 50 mmHg with severe neuronal damage as determined by blood markers. Importantly, ABT had better ICP during rewarming than BBT (24.9 ± 4.4 mmHg vs 33.5 ± 5.4 mmHg, $p < 0.005$). Although the average brain temperature in ABT was higher than BBT (36.3 ± 1.1°C vs 33.8 ± 0.6°C), the ICPs of the two treatment groups before rewarming did not have a significant difference (23.9 ± 4.6 mmHg vs 26.5 ± 5.4 mmHg, $p = 0.2$). BBT subjects also had episodes of abnormal heart rate (< 65 bpm) and compromised blood-brain barrier integrity.

Conclusions: Our work demonstrated the need to maintain the body temperature within normothermia for successful brain cooling. This finding might explain the lack of benefits in past clinical trials of hypothermia for TBI. Our study also demonstrated the feasibility of VINCI-enabled brain cooling.

Shear-Activated Nanotherapeutics to selectively increase cerebral collateral perfusion during ischaemic stroke- an update

Magdalena Litman[1], Sara Azarpeykan[1], Alastair Buchan[2], Neil Spratt[1], Donald Ingber[3] and Daniel Beard[1]

[1]School of Biomedical Sciences and Pharmacy, University of Newcastle, Australia

[2]Radcliffe Department of Medicine, University of Oxford

[3]Wyss Institute of Biologically Inspired Engineering, Harvard University

Abstract

Background: Enhancing collateral flow is an appealing therapeutic approach, given their demonstrated importance in stroke outcome. Vasodilators have failed to show benefits in treatment of acute ischaemic stroke due to systemic side effects such as hypotension and intracranial pressure rise. We have shown in experimental stroke, collaterals have fluid shear stress that is 3–7 times higher (100 dyne/cm2) than systemic vessels. This unique feature provides a novel way to selectively deliver vasodilators to collaterals, using nanoparticle aggregates, containing nitroglycerin (NG-NPAs), that only release drug in areas of high shear-stress.

Aims: We aim to:

1. Confirm the efficacy of NG-NPAs in dilating collateral vessels and enhancing perfusion during stroke.
2. Determine the effect of NG-NPAs on cerebral vein diameter and intracranial pressure (ICP)

Method: Middle cerebral artery occlusion (MCAo) was induced for 70 min in male hypertensive rats ($n = 26$). Laser speckle contrast imaging was used to measure collateral perfusion and cerebral vein diameter. ICP was measured before and during drug/control infusion. Brain injury was assessed at 24 h. 1, 2: Animals were randomized to receive blank-NPAs (control) or NG-NPAs (4μg/kg/min of NG) I.V., 25 minutes after MCAo.

Results: 1: NG-NPAs significantly increased collateral perfusion by 44% vs. 11% for B-NPAs at 40 minutes post-infusion ($p = 0.026$), without reducing blood pressure (NG-NPAs: 161 mmHg, B-NPAs: 163 mmHg, $p = 0.99$). NG-NPAs significantly reduced infarct volume at 24 hours (NG-NPA: 70 mm^3, B-NPAs: 121 mm^3, $p = 0.005$). 2. NG-NPAs had no statistically significant effect on vein diameter at 40 minutes post-infusion ($p > 0.9$) and did not affect ICP ($p = 0.48$).

Conclusions: Shear-activated nanoparticles selectively enhanced collateral perfusion and resulted in smaller infarcts at 24 hours. This is accomplished without causing significant drop in systemic blood pressure, altering intracranial pressure and cerebral veins. Our innovative nanoparticle therapy may provide an accurate and effective way of artificially enhancing collateral perfusion.

GFH312 attenuates ischemic neuronal death via inhibiting RIPK1-mediated apoptosis and necroptosis in mice

Ze Liu[1], Shengju Wu[2], Qian Suo[3], Chang Liu[2], Xiaojing Shi[3], Jing Ye[2], Yaohui Tang[1], Zhijun Zhang[2], Wanlu Li[2] and Guo-Yuan Yang[2]

[1]Shanghai Jiao Tong University
[2]School of Biomedical Engineering, Shanghai Jiao Tong University
[3]School of Biomedical Engineering, Shanghai Jiao Tong University, Shanghai 200030, China

Abstract

Background: The receptor-interacting serine/threonine protein kinase 1 (RIPK1) is a pivotal mediator of cell death and neuroinflammation during ischemic stroke. RIPK1 could cause neuronal apoptosis, RIPK3-mixed lineage kinase-like (MLKL)-dependent necroptosis, inflammatory gene expressions, and pro-inflammatory factor release. Therefore, RIPK1 has emerged as an important target in the neuropathology of ischemic stroke.

Aim: To identify the therapeutic effects of a new RIPK1 inhibitor GFH312 on ischemic stroke and investigate the underlying mechanisms.

Method: Adult male ICR mice ($n = 60$) underwent 90-min transient middle cerebral artery occlusion (tMCAO). GFH312 (15 mg/kg) was administered to ischemic mice 15 min before reperfusion and twice a day for three days via oral delivery. Nissl staining and the neurobehavioral tests were performed to evaluate the outcomes after three days of tMCAO in mice. The neuronal apoptosis, necroptosis and neuroinflammation factors were detected by immunostaining, Western blot analysis, and Real-Time PCR.

Results: Our results showed that neurobehavioral outcomes were improved in the GFH312 treated mice compared to the control ($p < 0.01$). Infarct volume was reduced in the GFH312 treated mice ($p < 0.05$). Further studies demonstrated that GFH312 inhibited the neuronal apoptosis and necroptosis-associated proteins PRIPK1/PRIPK3/PMLKL expression in tMCAO mice ($p < 0.05$). Moreover, necroptosis was activated rapidly after tMCAO and peaked at 2–6 hours, while apoptosis peaked at 24–72 hours. In addition, inflammatory genes such as TNFα, IL-1α, IL-1β, IL-6, IL-17 expression in the brain were down-regulated in the GFH312 treated mice compared to vehicle-treated mice ($p < 0.05$), which was also confirmed in the immunostaining.

Conclusions: The occurrence of apoptosis and necroptosis are time-dependent after tMCAO. Our studies have shed light on a new RIPK1 inhibitor GFH312 for its

potential role in ischemic stroke and highlighted the importance of administration time of neuroprotective agents.

Figure:

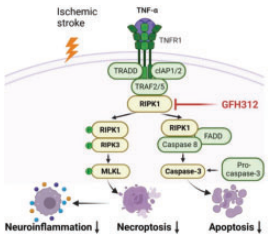

Figure 1. Schematic representation shows the role of GFH312 in RIPK1-dependent neuronal apoptosis, necroptosis and neuroinflammation after ischemic stroke.

After ischemic reperfusion, secreted TNF-α binds to TNF receptor on neurons, activating RIPK1-dependent necroptosis and apoptosis, releasing plenty of inflammatory cytokines. GFH312 decreased neuroinflammation, RIPK1/RIPK3/MLKL-mediated necroptosis and RIPK1-dependent apoptosis through inhibiting the activation of RIPK1.

Identification and functional prediction of fibrous and protoplasmic astrocytes after ischemic stroke in rats

Qian Suo[1], Lin Qi[2], Shengju Wu[2], Ze Liu[3], Cheng Wang[2], Wanlu Li[2], Yaohui Tang[3], Guo-Yuan Yang[2] and Zhijun Zhang[2]

[1]School of Biomedical Engineering, Shanghai Jiao Tong University, Shanghai 200030, China
[2]School of Biomedical Engineering, Shanghai Jiao Tong University
[3]Shanghai Jiao Tong University

Abstract

Background: Fibrous astrocytes (FAS) have different morphology, gene expression and function compared to protoplasmic astrocytes (PAS) of the brain. This heterogeneity of astrocytes results in the different susceptibility of grey and white matter to ischemic stroke. However, the distinction of astrocyte subtypes and their effect and molecular mechanism in ischemic stroke remains obscure.
Aim: To determine specific markers and investigate the role and underlying mechanism of astrocyte subtypes in ischemic stroke.
Method: Astrocytes were isolated from the cortex of neonatal SD rats and induced differentiation into FAS and PAS. The differentially expressed genes of astrocytes subtypes were analysed by RNA-sequencing. Adult male SD rats (n = 40) were subjected to 0, 3, 7, 14 and 28 days of MCAO. Astrocytes labelled ACSA-1 were separated from cortex, corpus callosum, and striatum by flow cytometry after MCAO, and verified the specific markers of FAS and PAS by RNA array. The expression and distribution of FAS and PAS were determined by immunostaining. Protein and metabolic analysis were performed by single-cell microdissection to examine the role of astrocyte subtypes after MCAO.
Results: We successfully cultured FAS and PAS *in vitro*, which both expressed GFAP. RNA-sequencing results showed that 3055 genes up-regulated and 2649 genes down-regulated in the FAS compared to that in the PAS. We found that the expression of Wnt7b was high in the FAS ($p < 0.001$), and Slc6a2 was high in the PAS ($p < 0.05$), with the greatest difference at 7 days *in vivo* after MCAO ($p < 0.05$). Protein and metabolic analysis demonstrated that astrocyte subtypes showed different roles in neuronal differentiation and metabolic regulation after MCAO in rats.
Conclusions: Our findings demonstrate that Wnt7b and Slc6a2 could be used as specific markers of FAS and PAS, respectively. The different abilities of astrocyte subtypes in neuronal differentiation and metabolic regulation contributed to the different susceptibility after MCAO.

Melatonin Protects against Prolonged Cerebral Ischemia by Resolving Refractory Stress Granules in Endothelial Cells

Yuxin Liu[1], Danli Lu[1], Tingting Lu[1], Wei Cai[2] and Zhengqi Lu[1]

[1]Department of Neurology, Mental and Neurological Disease Research Center, the Third Affiliated Hospital of Sun Yat-sen University
[2]the third affiliated hospital of sun yat-sen university

Abstract

Background: Ischemic-reperfusion injury of blood brain barrier (BBB) limits the time window of recanalization therapy in acute ischemic stroke (AIS). Endothelial cells (ECs) are the first to encounter the ischemic-reperfusion injury among BBB cells. It is reported that melatonin protects against AIS while whether melatonin could ameliorate the Ischemic-reperfusion injury of ECs in prolonged cerebral hypoxia remains elusive.
Aim: To unveil the injurious mechanisms of ECs during prolonged cerebral ischemia and the protective effects of melatonin.
Methods: *In vivo:* Wild type C57BL/6J mice (male, 8–10 week old) were subjected to 1–6 h of middle cerebral artery occlusion (tMCAO). *In vitro:* Brain vessel endothelial cells were treated with or without melatonin during both the ischemic phase (2 or 6 h of oxygen and glucose deprivation) and the reperfusion phase (5, 30, or 240 min of reperfusion after 6h-OGD).
Results: Prolonged ischemia resulted in pronounced ER stress, which subsequently mediated programmed cell

death of ECs. The ER stress in prolonged-hypoxic ECs could be attributed to accumulation of stress granules (SGs). SGs in ECs arose early after the onset of ischemia, and turned to be refractory as the ischemia extened. The refractory SGs, as a pool of RNA and proteins, activated PKR-EIF2α signaling and thus provoked ER stress and the subsequent cell death. Melatonin effectively resolved the refractory SGs in ECs by enhancing cellular autophagy both *in vitro* and *in vivo*. In prolonged tMCAO models, treatment of melatonin efficiently reduced infarct volume, alleviated brain edema, ameliorated neurological deficits, and protected BBB integrity ($N = 5$, $P < 0.05$).

Conclusions: Refractory SGs provoked ER stress thus mediated programmed cell death of ECs in prolonged cerebral ischemia which could be reversed by melatonin. Melatonin is a potential treatment to extend the time window of delayed recanalization therapy in AIS.

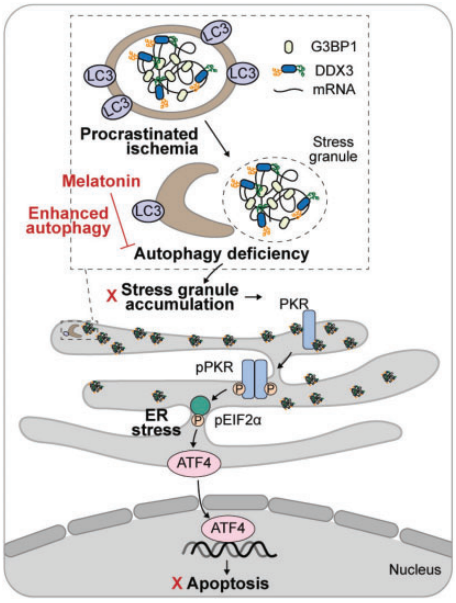

Arresting the Bad Seeds: HDAC3 Regulates Proliferation of Different Microglia Subsets after Ischemic Stroke

Jiaying Li[1], Yue Zhang[1], Yichen Huang[1], Ziyu Shi[1], Hui Cao[1] and Yanqin Gao[1]

[1]*Fudan University*

Abstract

Background: Self-renewed polarized microglia accumulated soon after stroke, leading to secondary demyelination and neuronal loss. HDAC3 modifies chromatin and regulates microglia-mediated neuroinflammation as revealed by recent studies. Notably, in these studies, deletion of HDAC3 reduces microglia number, suggesting its simultaneous involvement in microgliosis. Accordingly, it remains elusive how HDAC3 affects stroke outcomes, and under this premise, how it orchestrates the probable complex functions in microglia after stroke.

Aim: The roles of microglial HDAC3 and the underlying mechanisms in ischemic stroke.

Method: Transient middle cerebral artery occlusion (tMCAO) was induced in CX3CR1$^{CreER(-/-)}$HDAC3$^{flox/flox}$ (WT) and CX3CR1$^{CreER(+/-)}$HDAC3$^{flox/flox}$ (HDAC3-miKO) mice. Flow cytometry was used to monitor the change of cell-specific HDAC3 expression after stroke. Several behaviours were used to assess neurofunction. MRI, immunostaining and electrophysiology were employed to examine histological or functional integrity after stroke. RNA-seq and ATAC-seq were performed on flow-isolated microglia to elucidate potential mechanisms, as validated by qPCR, immunostaining, cell cycle analysis, and protein microarray. EdU was consecutively administrated to mice up to 3 days after tMCAO.

Results: Microglial HDAC3 expression increased after stroke ($n = 4$/group, $p = 0.0398$). HDAC3-miKO ameliorated long-term outcome ($n = 15$–17/group, $p < 0.05$). RNA-seq ($n = 3$) identified mitosis as the most significant process reversed by deleting HDAC3. Indeed, microglia were arrested at G2/M cell cycle phase in HDAC3-miKO mice after stroke ($n = 4$–5/group, $p < 0.0001$). Interestingly, CD16+ microglia ($n = 6$/group, $p = 0.0009$), but not CD206+ ones, were inhibited to proliferate by HDAC3 deletion, resulting in restoration of stroke-induced proinflammatory phenotype transition of microglia ($n = 5$/group, $P = 0.0317$). Furthermore, by ATAC-seq ($n = 3$), PU.1 was identified to modulate microglial biological processes under the regulation from HDAC3.

Conclusions: In ischemic stroke, HDAC3 depletion arrests microglia at G2/M phase by which microglia, especially the CD16+ ones, are impeded to undertake self-renewal and thereby fail to transition to a pro-inflammatory phenotype. These processes, probably mediated by PU.1, ameliorate histological and functional outcome.

Figure: (optional)

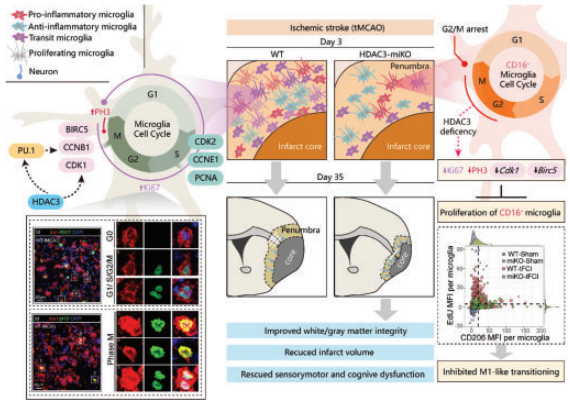

Timely assessment of cerebral blood flow autoregulation dynamics after subarachnoid haemorrhage

Edvinas Chaleckas[1], Vytautas Petkus[2], Vilma Putnynaite[2], Indre Lapinskiene[3], Aidanas Preiksaitis[3], Mindaugas Serpytis[3], Saulius Rocka[4], Laimonas Bartusis[5] and Arminas Ragauskas[1]

[1]Health Telematics Science Institute, Kaunas University of Technology, Lithuania
[2]Kaunas University of Technology
[3]Vilnius University Hospital Santaros Klinikos
[4]Clinic of Neurology and Neurosurgery, Faculty of Medicine, Vilnius University
[5]Health Telematics Science Institute, Kaunas University of Technology

Abstract

Background: Cerebral blood flow autoregulation (CA) is critical factor associated with clinical course of subarachnoid haemorrhage (SAH) patients. Timely CA assessment is necessary to choose appropriate personalized management before cerebral vasospasms and delayed cerebral ischemia occur.

Aim: The aim was to explore the ability to predict clinical course of SAH patients according to early examination of cerebral blood flow dynamics following after artificially induced arterial blood pressure (ABP) changes.

Method: Ongoing pilot study included CA status assessment in 18 SAH patients (1–3 days after aneurysmal rapture) and 15 healthy volunteers (control group). Study conducted in Vilnius University Hospital Santaros Klinikos. Air compression boots (ReBoots) were used for fast assessment of CA dynamics. The boots were continuously inflated and deflated within safe controlled pressure limits to generate slow ABP increase and fast drop per ~10 mmHg within ~10 sec deflation cycle. ABP delay in relation to cerebral blood flow (measured in middle cerebral artery by using Multi-DopT DWL, Viasonix Dolphin 4D TCD monitors) was used to estimate transient response time τ of cerebral blood flow regulation during deflation cycle. At least 5 inflation-deflation cycles with 2–3 min period were used to estimate average transient response time.

Results: Statistically significant differences were found between CA response time in SAH patients with unfavourable outcome ($\tau = 0.9 \pm 0.7$ sec) and favourable outcome ($\tau = 4.3 \pm 1.7$ sec) ($p < 0.001$). CA response time in control group ($\tau = 2.9 \pm 0.7$ sec) also significant differed from patients with unfavourable outcome ($p < 0.001$) but not from patients with favourable outcome.

Conclusions: Proposed methodology allows fast and safe assessment of CA response time within 10...15 minutes. Preliminary results showed that small transient time of cerebral blood flow autoregulation (< 1 sec) could be early warning factor associated with unfavourable outcome of SAH patients.

PTEN contributes to neurological impairment after TBI through ferroptosis and blockage of axonal regeneration

Ziyu Shi[1], Jiaying Li[1], Yichen Huang[1] and Yanqin Gao[1]

[1]Fudan University

Abstract

Background: Ferroptosis has been found to be involved in the acute phase of traumatic brain injury (TBI). Axonal damage in the chronic phase of TBI is difficult to repair. PTEN plays an important role in neuronal survival, but its expression and function after TBI remain unclear. In this study, PTEN was specifically deleted in neurons to investigate its protective role and mechanism.

Aim: To investigate the role of PTEN in neuronal ferroptosis and axonal regeneration after TBI.

Method: TBI was induced by a cortical controlled impact (CCI) method. Several Behavioral tests were performed to evaluate neurofunctional outcomes. MRI-DTI and electrophysiology were employed to evaluate white matter integrity. BDA tracing and calcium fiber photometry recording were performed for neural remodelling. Immunohistochemistry/fluorescence staining, Western Blot and PTEN/Raptor

double knockout mice were performed to elucidate mechanisms.

Results: Neuron-specific PTEN knockout mice (PTEN-nKO) showed ameliorated long-term outcome after TBI. They showed a significant recovery in the number of SYN and PSD95($n = 5$, $p < 0.05$) and a significant elevation in the number of newborn neurons long term after TBI. Moreover, PTEN-nKO enhanced white matter structural (MRI-DTI, $n = 5$, $p < 0.05$) and functional (callosal complex action potential, $n = 8$, $p < 0.05$) integrity, and remarkably promoted CNS plasticity (BDA tracing) and accelerated long-term neural remodelling (calcium fiber photometry recording). Mechanistically, neuronal death was significantly reduced in PTEN-nKO mice, along with reduced iron deposition (Perl's staining) in the injured area, lower concentrations of 4-HNE($n = 6$, $p < 0.05$), and restored GPx4 activity, suggesting ferroptosis in PTEN-nKO mice was reduced in the acute phase. Double depletion of PTEN/Raptor reversed the effects of PTEN-nKO on anti-ferroptosis, neural remodelling, and neurofunction recovery, suggesting that mTOR signalling was involved in the neuroprotection of PTEN deficiency.

Conclusions: PTEN-nKO improves neurological outcomes after TBI by inhibiting neuronal ferroptosis in the acute phase and promoting regenerative recovery of damaged axons in the chronic phase.

Figure: (optional)

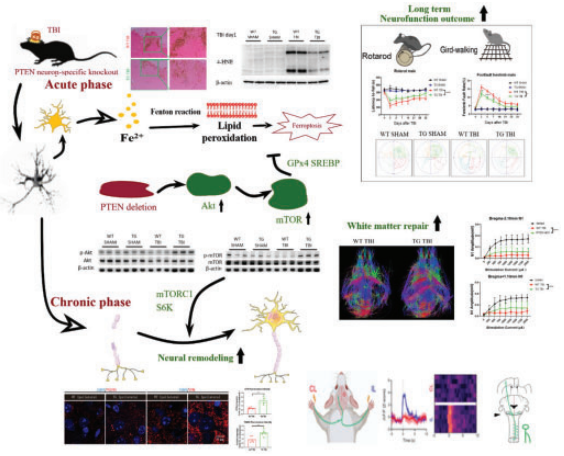

Mapping interactions between parvalbumin inhibitory interneurons and excitatory neurons over the cortex in awake mice

Xiaodan Wang[1], Annie Bice[1], Jin-Moo Lee[2] and Adam Bauer[3]

[1]*Washington University in Saint Louis*
[2]■
[3]*Washington University at Saint Louis*

Abstract

Background: Parvalbumin interneurons(PV-INs) are the largest subpopulation of GABAergic neurons. Coherent infraslow fluctuations in blood oxygenation (reflected in resting-state functional connectivity maps) are coupled in phase and amplitude to gamma brain rhythms. These patterns emerge from the rhythmic output of reciprocally-coupled PV-INs to synchronize excitatory activity over long distances (>1mm). Recent evidence suggests PV-INs exhibit long-range, transcallosal projections in select cortical regions. Whether transcallosal PV-INs feature prominently over the cortex, and the extent to which their local influences affects global excitatory activity is unknown.

Aim: Map the interactions between PV-INs and excitatory neurons over the cortex in awake mice.

Method: We created a novel imaging system and mouse line to allow for optogenetic targeting of PV-INs and mesoscopic imaging of excitatory activity via the red-shifted calcium indicator jRGECO1a (**Fig.1A**). Photostimuli were delivered over a grid in the left hemisphere (**Fig.1A**). Regional effective connectivity (EC) was determined by correlating the time course at the photostimulated site with all other time courses in our field-of-view and mapping the resulting correlation coefficients over the cortex.

Results: Photostimulation of PV-INs resulted in local reductions of jRGECO1a fluorescence, consistent with local inhibition of excitatory activity. Photostimulating primary somatosensory cortex(S1b) reduced S1b activity and ipsilateral motor (M2) activity (**Fig.1B**). Similarly, photostimulation of left M2 resulted in reciprocal, ipsilateral inhibition of left S1b, and right M2(**Fig. 1B**). EC mapping reveals the extent of regional PV-based inhibition (**Fig.1C**). Systematically scanning photostimulti over the left hemisphere allowed for visualizing the cortical "PV connectome" (**Fig.1D**) and site-wise homotopic EC (**Fig.1E**).

Conclusions: We used novel technology to examine the interaction between PV-INs and excitatory cells over the cortex in awake mice. PV-based inhibition extended several mm locally and into more distant, ipsilateral regions. Further, PV-INs exhibit region-specific interhemispheric inhibitory influences. Future work will examine whether these observations are mediated mono- or polysynaptically.

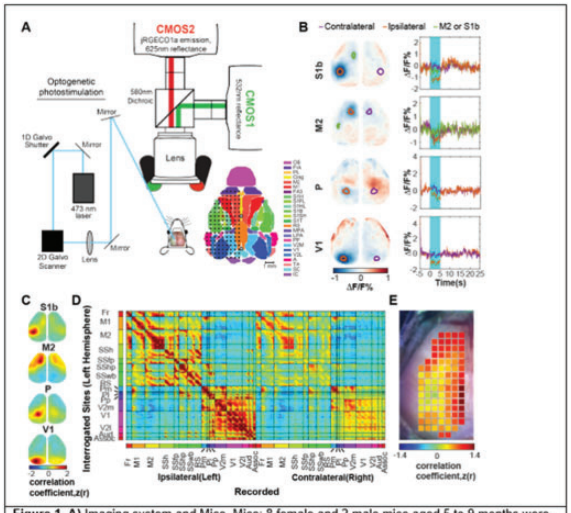

Figure 1. A) Imaging system and Mice. Mice: 8 female and 2 male mice aged 5 to 9 months were used for experimentation. All mice expressed the red-shifted GECI jRGECO1a driven by the *Thy1* promotor [Tg(Thy1-jRGECO1a) GP8.20Dkim/J; JAX Stock #: 030525] and serve as the "reporter" line for imaging. Homozygous jRGECO1a mice were crossed with a PV-Cre strain [B6.129P2-Pvalb$^{tm1(cre)Arbr}$/J, Jax Stock #: 017320] whose offspring were crossed with a Lox-ChR2 strain [B6;129S-Gt(ROSA)26Sortm32 (CAG- COP4*H134R/ EYFP) Hze/J, Jax Stock #: 012569] so that ChR2 is expressed in PV-INs. Imaging system: A custom light engine consisting of 530nm and 625nm LEDs illuminated the skull. Diffuse reflected light for optical intrinsic signal imaging and fluorescence emission were collected by a lens, split by a 580nm dichroic and sampled by two CMOS cameras. Calcium and hemodynamic activity were imaged at 20 Hz. Optogenetic photostimuli (PS, 473nm, 5mW, 20Hz, 5ms pulses) were delivered over a rectilinear grid consisting of 160 sites separated by 500 μm coregistered to each mouse. Sites were photostimulated at random, and each site was stimulated 3 times. **B)** Left: Maps of peak fluorescence change following PV photostimulation in select sites. Right: Time courses of jRGECO1a fluorescence within regions indicated in maps. **C)** Effective connectivity map resulting from correlating photostimulus evoked time courses in panel B with all other time courses in the brain reported as Fisher Z scores. Note, local PV stimulation reduces excitatory activity, thus positive correlations imply inhibition. **D)** PV-based effective connectivity matrix averaged across mice. Here, rows indicate sites interrogated while columns indicate recording sites. Note the richness of ipsilateral PV-based EC within the somatomotor system and separately more posterior regions including left parietal, retrosplenial and visual cortices. The off-diagonal in the contralateral hemisphere reveals region-specific inhibitory influences that extend across hemispheres. **E)** A map of this influence reports strong interhemispheric PV-based EC in motor and retrosplenial regions, but weak interhemispheric EC in parts of S1, parietal, an visual cortices.

Hallucinogenic 5-HT2A Receptor Agonism Alters Cortical Organization, Function, and Neurovascular Coupling

Jonah Padawer-Curry[1], Joshua Siegel[1], Jordan McCall[1], Adam Bauer[1] and Ginger Nicol[1]

[1] *Washington University at Saint Louis*

Abstract

Background: Psychedelics are an appealing potential therapeutic for neuropsychiatric conditions due to their rapid, sustained, results. These effects appear to be mediated by serotonin (5-hydroxytryptamine) receptor agonism, especially at the 5-HT2A receptor (5-HT2AR). Serotonin has potent vasoactive effects and is involved with regulating neuronal plasticity and arousal. Recent human functional neuroimaging studies evaluating acute effects of psychedelics show dramatic 5-HT2AR-dependent changes in functional network organization. However, these studies have not accounted for acute neurovascular effects of hallucinogenic 5-HT2AR agonists.

Aim: Determine whether hallucinogenic 5-HT2AR activation, using 2, 5-Dimethoxy-4-iodoamphetamine (DOI), affects cortical neuronal and hemodynamic activity and neurovascular coupling (NVC).

Method: Eight Thy1-jRGECO1a mice were imaged for 30-minutes before and after injection of either saline or DOI, under awake, resting-state conditions using wide-field optical imaging (**Fig. 1A, B**). Changes in cortical activity between 0.01 Hz–5 Hz were determined through power spectral density estimates (PSDE). NVC was estimated using deconvolution and resulting hemodynamic response/transfer functions (HRF, TF) were evaluated pre- and post- injection. Full-width-at-half maximum (FWHM) was calculated for HRFs and compared across conditions. Statistical differences were determined using a one-way ANOVA and post-hoc t-tests corrected for multiple comparisons.

Results/Conclusions: Canonical HRFs were observed for pre- and post- saline injection (**Fig 1C**). Conversely, DOI caused profound alterations to the HRF shape, with a smaller FWHM ($p = 0.018$), and a secondary peak occurring prior to time zero. TFs after DOI showed significant increases in delta-band transduction compared to saline ($p = 0.004$). Calcium PSDEs revealed significant increases in power from 0.32–1.28 Hz ($p = 0.009$) and 1.28–5.12 Hz ($p = 0.0002$). Similarly, significant changes were observed in hemodynamic activity from 0.32–1.28 Hz ($p = 0.002$). Results suggest that hallucinogenic 5-HT2AR agonists differentially alter neuronal versus hemodynamic activity, potentially driven by changes in NVC. Future work will examine other models for NVC and differentiate the effects of hallucinatory and non-hallucinatory 5-HT2AR activation.

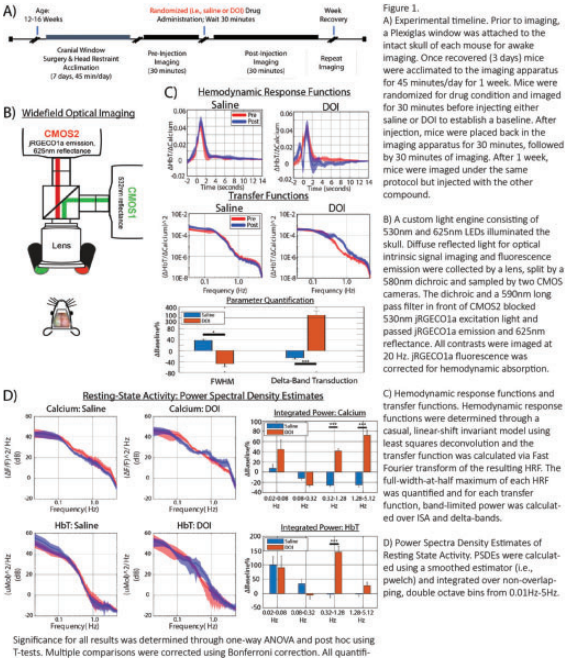

Figure 1.
A) Experimental timeline. Prior to imaging, a Plexiglas window was attached to the intact skull of each mouse for awake imaging. Once recovered (3 days) mice were acclimated to the imaging apparatus for 45 minutes/day for 1 week. Mice were randomized for drug condition and imaged for 30 minutes before injecting either saline or DOI to establish a baseline. After injection, mice were placed back in the imaging apparatus for 30 minutes, followed by 30 minutes of imaging. After 1 week, mice were imaged under the same protocol but injected with the other compound.

B) A custom light engine consisting of 530nm and 625nm LEDs illuminated the skull. Diffuse reflected light for optical intrinsic signal imaging and fluorescence emission were collected by a lens, split by a 580nm dichroic and sampled by two CMOS cameras. The dichroic and a 590nm long pass filter in front of CMOS2 blocked 530nm jRGECO1a excitation light and passed jRGECO1a emission and 625nm reflectance. All contrasts were imaged at 20 Hz. jRGECO1a fluorescence was corrected for hemodynamic absorption.

C) Hemodynamic response functions and transfer functions. Hemodynamic response functions were determined through a casual, linear-shift invariant model using least squares deconvolution and the transfer function was calculated via Fast Fourier transform of the resulting HRF. The full-width-at-half maximum of each HRF was quantified and for each transfer function, band-limited power was calculated over ISA and delta-bands.

D) Power Spectra Density Estimates of Resting State Activity. PSDEs were calculated using a smoothed estimator (i.e., pwelch) and integrated over non-overlapping, double octave bins from 0.01Hz-5Hz.

Significance for all results was determined through one-way ANOVA and post hoc using T-tests. Multiple comparisons were corrected using Bonferroni correction. All quantifi-

Exercise and Brain Energetics in Parkinson's Disease

Connor Bevington[1], Ju-Chieh (Kevin) Cheng[2], Rebecca Williams[3], G. Bruce Pike[4], A. Jon Stoessl[5] and Vesna Sossi[6]

[1]*Department of Physics & Astronomy, University of British Columbia*
[2]*Department of Physics & Astronomy, University of British Columbia; Pacific Parkinson's Research Centre, University of British Columbia*
[3]*Faculty of Health, School of Human Services, Charles Darwin University*
[4]*Department of Radiology, Department of Clinical Neuroscience, Hotchkiss Brain Institute, University of Calgary*
[5]*Djavad Mowafaghian Centre for Brain Health, Pacific Parkinson's Research Centre, University of British Columbia & Vancouver Coastal Health; Division of Neurology, Department of Medicine, University of British Columbia, Vancouver, British Columbia*
[6]*Department of Physics & Astronomy, University of British Columbia; Djavad Mowafaghian Centre for Brain Health, Pacific Parkinson's Research Centre, University of British Columbia & Vancouver Coastal Health*

Abstract

Background: Alterations in mitochondrial function (related to brain energetics) may play an important role in Parkinson's disease (PD). Exercise slows PD progression, but the neurophysiological underpinnings are unclear. Pre-clinical models suggest exercise may ameliorate mitochondrial dysfunction, but this has not been tested in humans.

Aim: To characterize brain energetics in PD vs. age-matched healthy controls (HC) and its modulation by exercise using pattern analysis.

Method: Cerebral metabolic rates of glucose (CMR_{glu}) and oxygen ($CMRO_2$) were obtained from 16 PDs and 11 HCs during a single scan on the GE SIGNA PET/MR. Seven of the PDs completed a six-month stationary cycling intervention before repeated scanning. Discordance between CMR_{glu} and $CMRO_2$, compared to HC, may be a marker of mitochondrial dysfunction in PD; this was computed using a novel relative aerobic cost metric (rCST, Fig. 1a). Scaled Subprofile Modelling Principal Component Analysis (SSM-PCA) and regional t-tests were used to investigate brain energetics as a function of disease and exercise.

Results: In addition to the well-known regional SSM-PCA CMR_{glu} pattern that separates PDs vs. HCs ($p < 0.00005$), we identified an additional CMR_{glu} pattern partially overlapping with the PD-related pattern (Fig. 1b), in which the expression is decreased in PDs post-exercise ($p < 0.005$, Fig. 1c); the reduction of pattern expression trends with aerobic fitness improvement (ΔVO2peak, $\rho = -0.67$, $p = 0.1$). t-tests of rCST in these affected regions reveal a significant increase for PDs in the posterior putamen only ($p < 0.001$, more affected side). Moreover, rCST in this region for PDs declines in concert with post-exercise increases in VO2peak ($\rho = -0.76$, $p = 0.08$).

Conclusions: Glucose/oxygen metabolism is modified in PD. Using pattern analysis and a novel metric to identify $CMR_{glu}/CMRO_2$ discordance, early results suggest that brain energetics in a subset of affected regions may be modulated by aerobic exercise, providing a neurophysiological basis for clinical observations of exercise slowing disease progression.

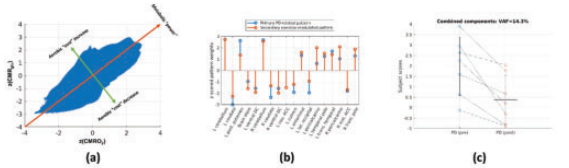

Figure 1: (a) computation of relative aerobic cost (rCST). Voxelwise measures of z-scored CMR_{glu} and $CMRO_2$ (restricted to grey matter) are plotted on orthogonal axes. A 45° rotation yields new axes of metric accordance, i.e. metabolic power, and metric discordance, i.e. aerobic cost. Positive rCST indicates relative glucose metabolism in excess of relative oxygen metabolism, which may imply mitochondrial dysfunction. (b) Z-scored regional weights that characterize the identified PD-related and exercise-modulated patterns. Only regions with $|z|>1.5$ for either pattern are shown for clarity; these are the regions that contribute most to the patterns. Note that "ventral DC" is a Freesurfer region consisting of the hypothalamus, mammillary body, subthalamic nuclei, substantia nigra, red nucleus, lateral geniculate nucleus, and medial geniculate nucleus. Positive weights indicate relative hypermetabolism whereas negative weights indicate relative hypometabolism. The projection of these weights onto the data of each subject yields subject scores; in the PD-related pattern these scores separate PDs vs. HCs ($p<0.00005$) and in the exercise-modulated pattern the PD subject scores decrease post-exercise ($p<0.005$, c.f. Fig. 1c). (c) Pattern expression (subject scores) of the exercise-modulated pattern for PD subjects pre- and post-exercise. VAF = variance accounted for in the data by the pattern. Note that post-exercise subject data are not used for the identification of the patterns; these data are independently projected onto identified patterns to yield unbiased subject scores.

COVID-19 Omicron variant spike protein infects primary cultures of endothelial and pericytes derived from Sprague-Dawley rats

Eugene Park[1] and Andrew Baker[2]

[1]*Unity Heatlh, St. Michael's Hospital*
[2]*Unity Health, St. Michael's Hospital*

Abstract

Background: Evidence suggests that SARS-CoV2 infection contributes to persistent neurological symptoms. The mechanisms of COVID-19 pathogenicity in the brain are not well understood. However, mounting evidence points towards the neurovascular unit as a target of infection.

Aim: The aim was to validate the use of a non-transgenic rodent as a model organism to study the effects of SARS-CoV2 infection in neural tissues and elucidate potential mechanisms of brain pathogenesis. We examined expression of ACE2 in adult Sprague-Dawley rats *in vivo* and the infectivity of Omicron variant B1.1.529 in rat endothelial and pericyte cells *in vitro*.

Method: Double-label immunohistochemistry was performed in coronal brain sections from adult Sprague-Dawley rats to identify cells expressing ACE2 receptors. A recombinant-GFP tagged spike protein receptor binding domain (RBD) of the omicron variant (B.1.1.529) was used to evaluate COVID-19 infectivity *in vitro*. Cells were cultured from P1 rat pups. Endothelial cells and pericytes were cultured on transwell inserts. Permeability of the cell monolayer following RBD incubation was determined using a tetramethylrhodamine isothiocyante dextran permeability assay.

Results: In brain tissues ACE2 colocalized with PDGFR-B labelled cells. There was no colocalization of ACE2 with endothelial cells. Increasing concentrations (0.2–1.0 μg/ml) of RBD applied *in vitro* resulted in increased GFP fluorescence intensity. In transwell experiments, preliminary data indicates RBD uptake resulted in increased permeability in pericytes to 70 k dextran. Incubation of cultures with LL37 (cathelicidin) an antimicrobial peptide that has a high affinity to the S1 domain of the SARS-COV2 spike protein reduced the permeability of cell monolayers compared to RBD alone.

Conclusions: The results suggests that the Omicron variant is infectious in cultured cells derived from Sprague-Dawley rats. Moreover, there is preliminary evidence that the spike protein is sufficient to cause changes in pericyte and endothelial cell-cell function resulting in increased permeability.

The Biological Basis of Cerebroprotection

Patrick Lyden[1], Padmesh Rajput[1] and Allison Brookshier[1]

[1]*University of Southern California*

Abstract

Background: Preclinical assessment of new stroke treatments typically emphasize neuronal salvage. No neuron-specific protectant has yet succeeded in clinical stroke trials.

Aim: We hypothesized that outcome after stroke depends on saving glia and vasculature as well as neurons.

Method: We used oxygen-glucose deprivation (OGD) in cell type-specific monocultures of neurons, astrocytes, endothelial cells, and pericytes, $n = 6$ wells per time point. Also, a standard filament rodent MCAo model was used. All p values are from 2-way ANOVA after Tukey's.

Results: Astrocyte cultures tolerated OGD for many hours, with a 50% lethal dose rate (LD_{50}) of 6 hours, endothelial and pericyte LD_{50} 4 h, and neuron LD_{50} 1.5 h ($p < 0.0001$ across all cell types). Then cultures ($n = 3$ wells per drug dose) were subjected to their specific LD_{50} and treated with test drugs at 3 doses (1, 10, 100 nM or μM). We found highly differential effects: e.g., argatroban (direct thrombin inhibitor) protected neurons at all 3 doses ($p < 0.0001$) but astrocytes and endothelial cells only at the highest dose ($p < 0.01$). SCH79797 (PAR1 agonist) protected neurons at the lowest dose ($p < 0.0001$) but at higher doses killed all cell types ($p < 0.0001$). We then confirmed similar differential effects in the MCAo model ($n = 8$–10 per group). For example, argatroban protected neurons but also reduced BBB damage ($P < 0.001$) and improved Barnes Maze performance ($p < 0.05$). In contrast, activated protein C (APC, PAR1 agonist) protected neurons but worsened BBB damage at higher doses ($p < 0.01$). Several other candidate protectants confirmed differential responses across cell types.

Conclusions: Differential vulnerability to ischemia and differential response to cytoprotective treatment among cell types in the NVU provides a biological rationale for shifting from a search for neuroprotectants to finding cerebroprotectants that protect neurons, glia, and vasculature. Future pre-clinical studies should characterize effects on all elements of the neurovascular unit.

Agomelatine Promotes Differentiation of Oligodendrocyte Precursor Cells and Preserves White Matter Integrity after Cerebral Ischemia

Shisi Wang[1], Xinmei Kang[1], Zhengqi Lu[1] and Wei Cai[2]

[1]*Department of Neurology, Mental and Neurological Disease Research Center, the Third Affiliated Hospital of Sun Yat-sen University*

[2]*the third affiliated hospital of sun yat-sen university*

Abstract

Background: White matter injury contributes to neurological disorders after acute ischemic stroke (AIS). Reparation of white matter injury is dependent on the re-myelination by oligodendrocytes. Both melatonin and serotonin antagonist have been proved to protect against post-stroke white matter injury. Agomelatine (AGM) is a multi-functional therapy which is both a melatonin receptor agonist and selective serotonin receptor antagonist. Whether AGM protects against white matter injury after stroke and the underlying mechanisms remain elusive.

Aim: To evaluate the therapeutic effects of AGM against post stroke white matter injury and the underlying mechanisms.

Method: Male adult C57BL/6J mice were subjected to 60-minute transient middle cerebral artery occlusion (tMCAO). AGM (10mg/kg) was injected intraperitoneally once daily for 28 days beginning at 24 h after reperfusion. Magnetic resonance imaging and cognitive functions were evaluated at 7d, 14d, 21d, and 28d after tMCAO. Transmission electron microscopy and immunostaining were used to assess infarct volume, myelin loss, and white matter integrity. BrdU was injected to view the numbers of newly generated mature oligodendrocytes. Organotypic slice cultures (OSCs) and nanofibers system were used to confirm the effects of AGM on oligodendrocyte differentiation and re-myelination.

Results: AGM efficiently preserved white matter integrity, reduced brain lesion loss, attenuated long-term sensorimotor and cognitive deficits in tMCAO models ($N = 8$, $P < 0.05$). AGM treatment promoted OPC differentiation and enhanced re-myelination both *in vitro* ($N = 3$, $P < 0.05$) and *in vivo* ($N = 8$, $P < 0.05$). On the other hand, OPC proliferation was unaffected by AGM treatment. Mechanistically, AGM activated LRP1-PPARγ signaling thus promoted maturation of OPCs. Inhibition of PPARγ and knock-down of LRP1 in OPCs reversed the beneficial effects of AGM.

Conclusions: Our data indicated that AGM promoted OPC differentiation and re-myelination after ischemic stroke through LRP1-PPARγ signaling. Therefore, AGM represents a novel therapy to protected against white matter injury after cerebral ischemia.

Microglia Initiated Astrocyte-Mediated Ischemic Tolerance

Toru Tateoka[1,2], Hideyuki Yoshioka[1], Takuma Wakai[1], Koji Hashimoto[1], Norito Fukuda[1], Schuichi Koizumi[2] and Hiroyuki Kinouchi[1]

[1]Department of Neurosurgery, Interdisciplinary Graduate School of Medicine and Engineering, University of Yamanashi
[2]Department of Neuropharmacology, Interdisciplinary Graduate School of Medicine, University of Yamanashi

Abstract

Background: Astrocyte-mediated ischemic tolerance has attracted much attention recently as a neuroprotective mechanism induced by ischemic preconditioning (IPC). The interaction between microglia and astrocytes is expected to play an important initiator; however, it has not been elucidated.

Aim: We investigated the effects of pharmacological microglial depletion on the neuroprotective efficacy and the phenotype of reactive astrocytes after IPC.

Method: Transient focal cerebral ischemia using mice was induced by intraluminal filament occlusion. Using a colony stimulating factor 1 receptor antagonist PLX5622, we created a situation of microglial depletion at the induction of IPC, and recovered to the normal levels at the loading of lethal ischemia, 7 days after IPC.

Results: This controlled microglial depletion diminished protective effects of IPC against lethal ischemia, with larger infarction volume (control 37.9 ± 19.5 vs PLX $64.0 \pm 16.5\,mm^3$, $P < 0.05$) and worse neurological Longa's scores (control 1.2 ± 0.78 vs PLX 2.4 ± 0.88, $P < 0.05$). Reactive astrocytes were observed after IPC, which was significantly more enhanced with microglial absence during IPC (control 11.4 ± 3.0 vs PLX $21.8 \pm 4.4/3*10^{-2}\,mm^2$, $P < 0.01$). Furthermore, IPC without microglia enhanced the proliferation of neurotoxic C3d-positive astrocytes (control 3.0 ± 3.1 vs PLX $12.1 \pm 4.5/3*10^{-2}\,mm^2$, $P < 0.05$), and suppressed the induction of neuroprotective P2X7 receptor-positive astrocytes (control $8.8 \pm 4.1\,mm^2$ vs PLX $4.4 \pm 2.9/3*10^{-2}\,mm^2$, $P < 0.01$).

Conclusions: The present study demonstrates that Microglia are essential for the induction of ischemic tolerance by cross-talk with astrocytes in a sophisticated manner.

250/250 words

Human glutamate NMDA receptor subunit GluN2B spatial coexpression to corresponding mRNA expression patterns

Matej Murgaš[1], Murray Bruce Reed[1], Lisa Aichinger[1], Clemens Schmidt[1], Gregor Dörl[1], Godber Mathis Godbersen[1], Andreas Hahn[2] and Rupert Lanzenberger[1]

[1]Division of General Psychiatry, Department of Psychiatry and Psychotherapy, Medical University of Vienna, Vienna, Austria; Comprehensive Center for Clinical Neurosciences and Mental Health (C3NMH), Medical University of Vienna, Vienna, Austria

[2]■

Abstract

Background: Glutamatergic N-methyl-d-aspartate receptor (NMDAR) is involved in numerous biological processes in the human brain. Various neuropsychiatric disorders (e.g. Alzheimer's dementia) are linked to the pathophysiologies of NMDAR subunit 2B (GluN2B)[1]. However, the relationships between GluN2B distribution and associated mRNA expressions, which might help in mapping pathological alterations, remain unknown.

Aim: Here, we aim to compare the GluN2B distribution to transcriptomic data of different NMDA receptor subunits in the human brain.

Methods: We made use of data measured by positron emission tomography with *(R)*-[^{11}C]-Me-NB1 as a part of our already published study[2]. The GluN2B total volume of distribution was quantified using the Logan plot with the arterial input function. Microarray data of the NMDAR subunit 1, 2A, 2B(GRIN2B), 2C and 2D mRNA expressions were adopted from Allen Human Brain Atlas[3] and were processed as previously described[4]. The associations between GluN2B protein distribution and the above-mentioned gene expression patterns, represented by 105 cortical and 18 cerebellar regional values, were evaluated using Spearman's correlation.

Results: To compare proteomic and transcriptomic data, we used the average GluN2B distribution map created from 6 healthy male subjects. Comparison between GluN2B and GRIN2B revealed highest correlation $r_s = 0.26$ ($p_{BHcorr} < 0.05$) among tested NMDAR subunits. Subsequential correlation analysis of GluN2B and other NMDAR subunit mRNA expression patterns revealed only weaker (ranging from $r_s = -0.06$ to $r_s = 0.15$) and non-significant associations(Figure1).

Conclusions: We compared GluN2B distribution to mRNA expressions of NMDAR subunits. Our results are in line with recent findings[4], showing a low correlation between mRNA expression patterns and glutamatergic receptor distributions. In light of the presented results, transcriptome in its current state should be considered as complementary information to protein distribution rather as its surrogate.

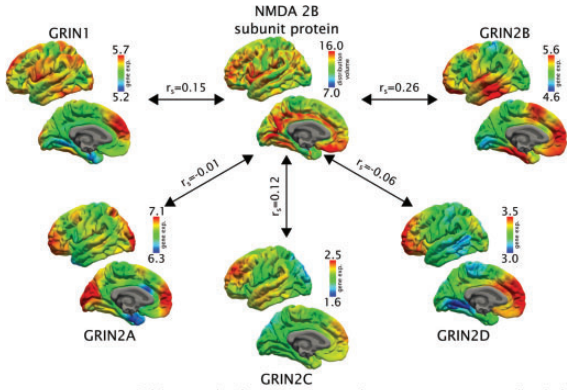

Figure 1: Comparison of of the cortical surface representation of mRNA expression patterns (log2) of NMDAR subunit 1 (GRIN1), 2A (GRIN2A), 2B (GRIN2B), 2C (GRIN2C) and 2D (GRIN2D) and NMDAR subunit 2B distribution volume (V_T; mL.cm^{-3}) overlayed on the cortical surface of the left hemisphere.

Funding: Austrian Science Fund(FWF), KLI 1006 and DOC 33-B27 to R. Lanzenberger

References

1. Hardingham et al., 2010, Nature Reviews Neuroscience, 11.10: 682–696
2. Rischka et al., 2022, JNM, 63.6: 936–941
3. Hawrylycz et al., 2012, Nature, 489.7416: 391–399
4. Murgaš et al., 2022, NeuroImage, 256: 119214

Angiotensin II-mediated hippocampal hypoperfusion and vascular dysfunction impairs memory in aged spontaneously hypertensive rats

Abbie Johnson[1], Sarah Tremble[1], Conor McGinn[2], Ruby Guth[2], Nadia Scoppettone[2] and Kirtika Prakash[1]

[1]University of Vermont Larner College of Medicine
[2]University of Vermont

Abstract

Background: Chronic hypertension causes cerebrovascular disease and accelerates age-related cognitive decline. However, little is known about how hypertension impacts the arterioles supplying deep brain regions involved in memory and cognition, such as the hippocampus, that may contribute to vascular dementia.

Aim: The aim of the current study was to investigate the role of hippocampal hemodynamics in hypertension-induced memory decline.

Method: Memory function, hippocampal perfusion and hippocampal arteriole (HA) function were compared between adult (4–5 mo.) male Wistar rats and spontaneously hypertensive rats (SHR) and aged (14 mo.) SHR without and with captopril treatment (100mg/kg/day in drinking water, 11–14 mo.). A novel object recognition task was used and recognition index calculated to assess long-term memory function. Absolute hippocampal blood flow was measured using the hydrogen clearance method. Isolated and pressurized HAs were studied and myogenic tone determined at an intravascular pressure of 60 mmHg. Data are mean $\pm$ SEM. Differences between groups were determined by one-way ANOVA with post-hoc Tukey test.
Results: Memory was similar between adult SHR and Wistar rats that had recognition indices >0.70. However, memory was impaired in aged SHR that was rescued by the angiotensin converting enzyme inhibitor captopril (recognition indices 0.47 ± 0.05 vs. 0.76 ± 0.05; $p < 0.01$; $n = 6$/group). HAs from aged SHR were hyperconstricted and had $56 \pm 2\%$ tone compared to $40 \pm 3\%$ in Wistar and $45 \pm 5\%$ in adult SHR ($p < 0.01$; $n = 6$/group). Hippocampal perfusion was substantially lower in aged SHR; however, captopril treatment ameliorated HA hyperconstriction by lowering myogenic tone to $46 \pm 2\%$ and increased hippocampal blood flow to be similar to adult SHR and Wistar rats (Figure 1).
Conclusions: These data suggest impaired memory function in aged SHR was due to angiotensin II-mediated hippocampal hyperconstriction and hypoperfusion. Further, this study highlights that HAs are a therapeutic target to slow memory decline during aging and chronic hypertension, two primary causes of vascular dementia.

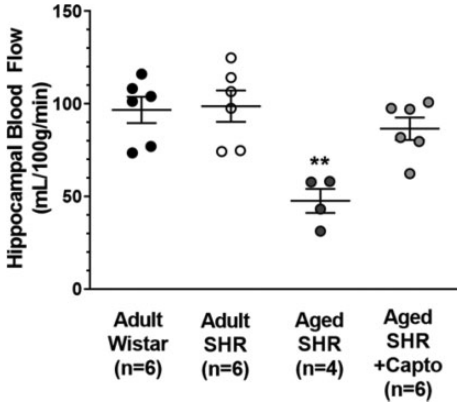

Enhancer RNAs and enhancer-centric gene regulatory networks in ischemic stroke

Sarra Limam[1], Ashirbad Guria[1], Sandeep Miryala[1], Ankit Patel[1], Maria Sara Cueto[1] and Ashutosh Dharap[1]
[1]*University of South Florida*

Abstract
Background: Enhancer RNAs (eRNAs) are a novel class of regulatory noncoding RNAs that are transcribed by enhancer elements in a stimulus-dependent manner. The eRNAs are known to play roles in enhancer-mediated gene regulation and phenotypic outcomes, but their expression and functions in stroke are largely unknown.
Aim: The goal of this study was to identify immediate-early stroke-responsive enhancers and eRNAs in the mouse cerebral cortex, pinpoint their cell-type localization, and map their interactions with target genes on a genome-wide scale with the overarching goal of elucidating the early gene regulatory processes that drive the post-stroke pathophysiology.
Method: Adult C57BL/6 mice underwent transient focal ischemia via middle cerebral artery occlusion (MCAO) followed by 6 h of reperfusion. Ipsilateral cortices were used for genome-wide H3K27ac ChIP-seq ($n = 3$/group), high-throughput RNA-seq ($n = 3$/group), and Hi-C ($n = 3$/group) to map active enhancers, transcribed eRNAs, and higher order chromatin interactions, respectively. The cellular localization of the eRNAs was mapped using single-molecule FISH, and the eRNA-protein interactions were identified using immunoprecipitation followed by mass spectrometry of the isolated proteins.
Results: We identified 77 eRNAs that were significantly upregulated in the adult cortex in response to stroke versus sham controls. Of these, 55 eRNAs were exclusively expressed during stroke. We identified direct, stroke-induced DNA-DNA looping between the enhancer elements and distal genes facilitated by higher-order chromatin organization (i.e., in 3D genomic space), illuminating potential gene regulatory relationships. Finally, we identified directly interacting proteins that may form the functional riboprotein complexes that drive eRNA function and the activity of the underlying enhancer elements.
Conclusions: This study presents the first report identifying stroke-responsive eRNA expression, stroke-dependent enhancer-gene looping across the 3D genome, and eRNA-protein complex formation that together may comprise an immediate-early gene regulatory response that contributes to the subsequent post-stroke pathophysiology.

Investigating single-subject dopamine synthesis capacity alterations in psychosis using normative modelling

Alessio Giacomel[1], Daniel Martins[1], Giovanna Nordio[1], Rubaida Easmine[1], Oliver Howes[2], Steven C.R. Williams[1], Federico Turkheimer[1], Marius De Groot[3], Ottavia Dipasquale[1] and Mattia Veronese[4]

[1]Centre for Neuroimaging Sciences, IoPPN, King's College London, London, UK
[2]Department of Psychosis Studies, IoPPN, King's College London, London, UK
[3]Clinical Imaging, Clinical Pharmacology and Experimental Medicine, GSK R&D, Hertfordshire, UK
[4]Centre for Neuroimaging Sciences, IoPPN, King's College London, London, UK; Department of Information Engineering, University of Padova, Padova, IT

Abstract

Background: Normative modelling (NM) is an emerging statistical framework which uses the between-subject variability expressed by covariates of interest (e.g., demographics or clinical measures) within a reference cohort as foundation to identify deviations from the expected variability on an individual basis (e.g., patient sample). Despite growing use of NM in MRI studies, its application to PET is still limited since the typical smaller sample sizes of these studies raise concerns about its feasibility and robustness.

Aim: To investigate the feasibility of NM in multi-site [^{18}F] FDOPA PET to quantify dopamine synthesis capacity deviations from normality in patients with psychosis.

Method: A voxel-wise Bayesian linear model was trained in a cohort of [^{18}F]FDOPA PET healthy controls (HC, $n = 143$) scans, where age and sex were used as covariates. This model was applied to data from both HC (under cross-validation) and psychosis patients ($n = 136$) from 4 previously published datasets. The voxel-wise Z-score maps quantifying deviations from normality were used to define individual spatial patterns of extreme deviations ($|Z| > 2$). Diagnosis and dataset effects were then tested with a two-way ANOVA.

Results: The grouped Z-score distributions of HCs and patients were close to 0 in terms of mean, whereas the patient distribution showed an increase ($\sim$1.4-fold) in terms of standard deviation. Patients exhibited significant differences from HCs ($F = 53.069$, $p < 0.001$), consistently with literature cross-sectional findings of dopamine alteration in psychosis. However, the analysis of individual patients' alterations from NM showed that only a small fraction of extreme deviations ($\sim$20%) colocalised in similar regions and outside the main dopaminergic regions (e.g., striatum), suggesting more complex and heterogeneous patterns of dopamine alternation in disease (**Fig. 1**).

Conclusions: In conclusion, NM can be successfully applied to PET imaging. This methodology offers the possibility to gain individualised mechanistic abnormalities which will hopefully shine upon the characteristic heterogeneity of psychosis patients.

Figure:

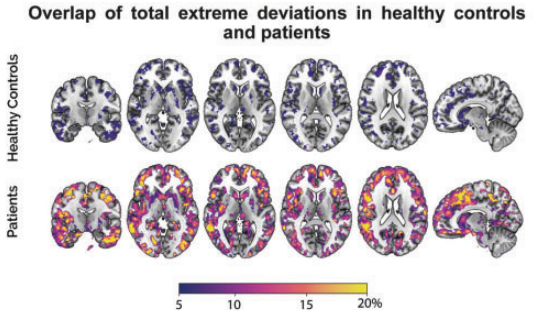

Figure 1: Healthy Controls and Patients differences in extreme deviations. *Percentage of subjects with extreme deviations (|Z|>2) in HC (top) and patients (bottom). The figure is thresholded above the level of chance (5%). Maps are superimposed on a standard MNI152 template.*

Developing a new small-molecule NLRP3 inflammasome inhibitor to treat intracerebral haemorrhage.

Emily McMahon[1], Victor Tapia[1], Siobhan Crilly[1], Jack Green[1], Christopher Hoyle[1], Adrian Parry-Jones[2], Stuart Allan[3], Sally Freeman[1], Catherine Lawrence[4], David Brough[1] and Paul Kasher[1]

[1]Geoffrey Jefferson Brain Research Centre, Manchester Academic Health Science Centre, Northern Care Alliance and the University of Manchester
[2]Division of Cardiovascular Sciences, University of Manchester
[3]■■■
[4]Geoffrey Jefferson Brain Research Centre, School of Biological Sciences. Faculty of Biology, Medicine and Health, University of Manchester, United Kingdom

Abstract

Background: The assembly of NLRP3 inflammasomes within immune cells plays a key role in the acute, injurious inflammatory response to intracerebral haemorrhage (ICH) and represents a promising therapeutic target. Indeed, NLRP3 inflammasome inhibition is protective in

rodent ICH models, however, no safe inflammasome inhibitors have been approved for clinical use to date. We have previously shown that zebrafish disease modelling represents an advantageous platform for pre-clinical ICH research (PMID: 30473780). Our published large-scale zebrafish larval drug screen identified 150 organic/repurposable compounds that inhibit brain cell death after spontaneous ICH (PMID: 35098999). Although the mechanisms underlying the protective properties of these drugs remain unknown, we hypothesised some may be protective by inhibiting the NLRP3 inflammasome response to ICH.

Aim: To further screen these candidate drugs and identify a potential organic/repurposable NLRP3 inflammasome inhibitor for ICH treatment.

Methods: Compounds were screened for NLRP3 inflammasome inhibition in mouse bone-marrow-derived macrophages (150 drugs, 10 μM). We subsequently tested the ability of one candidate inhibitor to modify the inflammasome response *in vivo*, using a mouse model of LPS/ATP-induced inflammation. Finally, using a transgenic cell death reporter zebrafish strain, we treated larvae with the candidate inhibitor after ICH and used live imaging to quantify the effect of treatment on brain injury.

Results/Conclusions: We identified one natural compound 'Brazilin' that potently inhibits NLRP3 inflammasome activation evoked by numerous standardised stimuli *in vitro* (Fig1A). Brazilin treatment can also significantly attenuate inflammasome activation in a mouse model of acute inflammation (Fig1B: $^{**}p < 0.01$, $N = 5$/group) and treatment significantly reduces acute brain injury after spontaneous ICH in two zebrafish models (Fig1C_i: $^{****}p < 0.0001$, $n = 17$–20/group; Fig1C_{iii}: $^{**}p < 0.01$, $n = 7$–8/group). Our future plans include assessing the effect of Brazilin on the inflammasome response of human microglia, identifying the molecular targets of this compound and evaluating the therapeutic efficacy of Brazilin in rodent models of ICH.

Figure

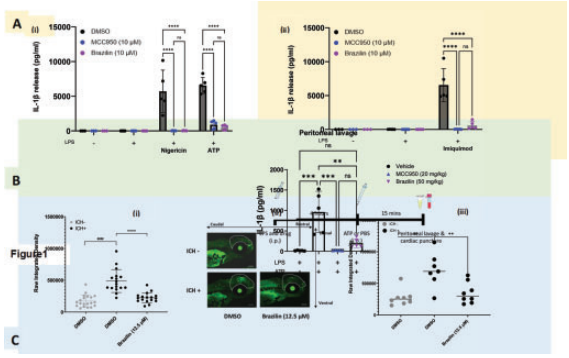

Validation of cardiac image-derived input function for cerebral quantitative [^{18}F] FDG functional PET imaging

Murray Reed[1], Lisa Aichinger[1], Clemens Schmidt[1], Matej Murgaš[1], David Gomola[1], Sebastian Klug[1], Benjamin Eggerstorfer[1], Patricia Handschuh[1], Christian Milz[1], Rupert Lanzenberger[1] and Andreas Hahn[2]

[1]Division of General Psychiatry, Department of Psychiatry and Psychotherapy, Medical University of Vienna, Vienna, Austria; Comprehensive Center for Clinical Neurosciences and Mental Health (C3NMH), Medical University of Vienna, Vienna, Austria

[2]■■■

Abstract

Background: Functional positron emission tomography (fPET) allows for the quantification of dynamics in cerebral glucose metabolism (CMRGlu)[1]. This however requires an arterial input function (AIF), whose acquisition includes additional challenges, effort and patient burden. Image-derived input functions(IDIF) offer a feasible noninvasive alternative, particularly when using large blood pools of the thorax[2]. However, for brain studies, these blood pools are not in the field of view and IDIF extraction from small intracranial blood vessels may lead to artifacts[3].

Aim: We aimed to develop a novel acquisition protocol, which allows for an accurate cardiac IDIF extraction without affecting quantification of task-related cerebral glucose metabolism.

Methods: Participants underwent a dynamic [^{18}F]FDG-fPET scan using a hybrid PET/MR system with simultaneous manual and arterial blood sampling. Utilizing the stop-and-go bed motion, each participant was moved between head and thorax positions to acquire data from both filed of views (Figure 1) while performing the monetary incentive delay task[4]. We compared different IDIFs (ascending and descending aorta, left ventricle, combination of all blood pools) to the AIF. Similarly, subcortical CMRGlu values (Harvard-Oxford atlas) were quantified with IDIFs and compared to those of AIF to evaluate the reliability of the different input functions.

Results: We observed high correlations between IDIFs and the AIF regarding area under the curve (AUC) ($r = 0.64$–0.92, $p < 0.01$) as well as for CMRGlu of both task regressors ($r = 0.8$–0.99, $p < 0.01$) for 10 healthy participants. The combined IDIF displayed the highest accuracy for AUC ($r = 0.92$, $p < 0.01$) and CMRGlu over all regions and task conditions ($r = 0.98$–0.99, $p < 0.01$).

Conclusion: We demonstrate a non-invasive alternative to accurately acquire task-specific quantitative CMRGlu values. This framework allows for a widespread and participant-friendly application of fPET and is extendable to numerous other PET applications.

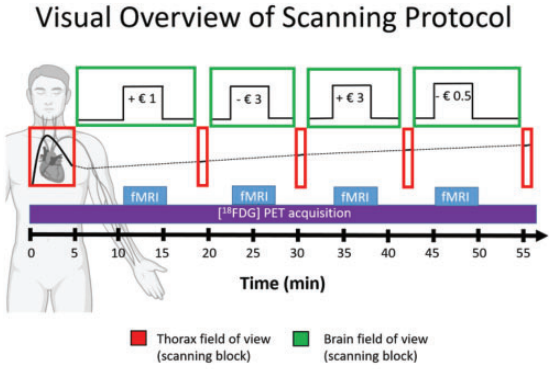

Figure 1: Graphical overview of the scanning timeline of each participant. fPET acquisition, tracer application and automatic arterial sampling were started simultaneously in the thoracic bed position to acquire the initial peak of the input function for 5:30min. Thereafter, the bed position was changed to the head, where the fPET baseline and task blocks are acquired (1st and 4th block 12:30; 2nd and 3rd block: 10:00). Succeeding each fPET block the bed position was moved to the thorax to obtain further data points for the image-derived input function (1:30min). Shortly after each thorax block, manual arterial samples were acquired.

Funding: Austrian Science Fund(FWF), KLI 1006 and DOC 33-B27 to R. Lanzenberger

References

1. Hahn A., JNM, 2016; 57(12): 1933.
2. van der Weerdt AP., JNM, 2001; 42(11): 1622–9.
3. Zanotti-Fregonara P., JCBFM, 2011; 31(10): 1986–98.
4. Hahn A., JCBFM, 2021;41(11):2973–85.

Numerical model for early warning of cerebrovascular vasospasm and delayed cerebral ischemia in SAH patients

Edgaras Misiulis[1], Alina Barkauskiene[2], Vytenis Ratkunas[3], Aidanas Preiksaitis[2], Saulius Lukosevicius[3], Robertas Alzbutas[4], Tomas Iesmantas[4], Mindaugas Serpytis[2], Indre Lapinskiene[2], Algis Dziugys[1], Vilma Putnynaite[4] and Vytautas Petkus[4]

[1]*Lithuanian Energy Institute*
[2]*Vilnius University Hospital Santaros Klinikos*
[3]*Lithuanian University of Health Science*
[4]*Kaunas University of Technology*

Abstract

Background: Cerebral vasospasm (CV) and delayed cerebral ischemia (DCI) are typical life-threatening phenomena occurring in the human brain within 3–21 days after subarachnoid haemorrhage (SAH). The novel methodology providing the early warning of CV and DCI is critically needed for personalised management of SAH patients.

Aim: The aim of the study was to evaluate the feasibility of developed numerical model for the early warning of CV/DCI after SAH by exploring the association between the computed 3D distribution of the blood breakdown products (BBPs) concentration in the cerebrospinal fluid with the detected CV of large cerebral arteries, cerebral ischemia's and patients' outcome.

Method: The developed model is based on numerical modelling of the spatial BBPs distribution within the detailed cerebrospinal fluid space according to patient clinical data (CT, MRI, blood test results). CV/DCI are predicted according to estimated concentration of blood breakdown products in specific areas of subarachnoid space.

Results: Preliminary results of 16 SAH patients demonstrated that higher BBPs concentration close to cerebral arteries cause formation of several cerebral vasospasms which later can develop to delayed cerebral ischemia (Fig. 1). The accumulation of higher BBPs concentration in vascular territories can cause formation of ischemic zones (marked in yellow, Fig. 1b). Leaked blood volume after SAH was found associated with unfavourable outcome (GOS $\leq$ 3) of SAH patients ($P < 0.01$).

Conclusions: Ongoing pilot study demonstrates possibility of developed model to predict critical cerebral zones with higher probability of CV and DCI formation. Further development and larger clinical studies are necessary to validate the created numerical model of CV/DCI prediction.

Figure:

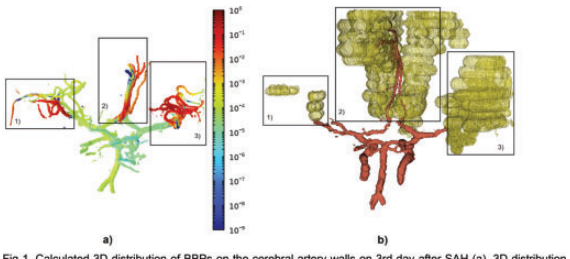

Fig 1. Calculated 3D distribution of BBPs on the cerebral artery walls on 3rd day after SAH (a). 3D distribution and scale of BBPs is represented by colormap legend. Three ischemic zones identified from CT scan (at 9th day) are marked in yellow (b).

Fig 1. Calculated 3D distribution of BBPs on the cerebral artery walls on 3rd day after SAH (a). 3D distribution and scale of BBPs is represented by colormap legend. Three ischemic zones identified from CT scan (at 9th day) are marked in yellow (b).

Kinetic Modelling of 5-HT Release Following a Non-pharmacological Stimuli Using a Modified Reference Tissue Model

Nina Fultz[1], Joseph B Mandeville[2], Gitte Moos Knudsen[1] and Hanne Demant Hansen[1]

[1]*Neurobiology Research Unit and NeuroPharm, Copenhagen University Hospital, Rigshospitalet*
[2]*Athinoula A. Martinos Center for Biomedical Imaging, Department of Radiology, Massachusetts General Hospital, Massachusetts General Hospital*

Abstract

Background: Measuring neurotransmitter release after pharmacological interventions with PET can be performed using a single-scan intervention in combination with modified simplified reference tissue models. Such models have been used to determine dopamine release following amphetamine challenges[1] and behavioral tasks[2].

Aim: In the present study, we evaluate whether the DBPND model[3] can be used to quantify 5-HT release due to a non-pharmacological challenge and to improve the temporal resolution of the non-displaceable binding potential (BP_{ND}) of [^{11}C]AZ10419369.

Method: Participants (n = 11) were scanned twice either with their eyes closed or during a visual stimulus (Fig.1A) with the radioligand [11C]AZ10419369[4]. Preprocessing was done using FreeSurfer[5] and PETSurfer[6,7]. Kinetic modelling was done using the DBPND model[8,9] with FASTMAP[10]. For kinetic modelling, PET time-activity curves from occipital cortex were partitoned into three 15-minute segments (35–50min, 50–65min, 65–81min).

Results: The occipital cortex exhibited a stepwise decrease in the BP_{ND} (Fig.1B), with a small decrease (2.5% ± 7.2%) during the first time interval (50–65min), followed by a larger decrease (5.6% ± 9.3%) during the 65–81 minute interval. A Wilcoxon rank-sum test revealed that these latter changes were significantly different from the first 35–50 minute time bin ($p = 0.02$) and are similar to results reported using the ESTRM model[4]. The percent change in BP_{ND} within the stimulus condition exhibited a higher degree of variance than the control conditions, suggesting that the stimulus condition may have induced varying 5-HT release.

Conclusions: Overall, we found that DBPND model improves BP_{ND} temporal resolution, and that state transitions from rest to increased vigilance appear to increase synaptic 5-HT. Future work should examine this analysis method using microdialysis in animal models to determine if BP_{ND} can be measured at sub-15 minute intervals.

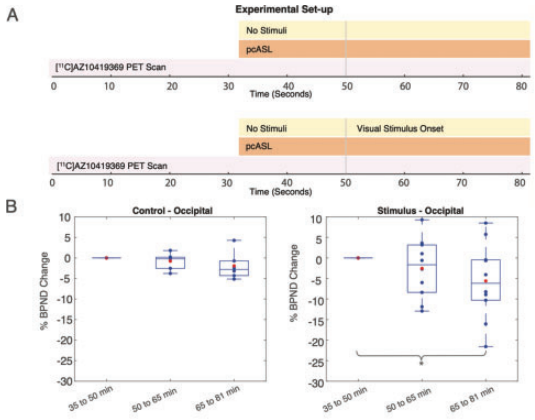

Figure 1: Improving temporal resolution of binding potentials. A) Experimental PET/MR design. B) Occipital binding potentials in 15-minute bins for no stimulus and visual stimulus conditions. Significant differences were seen between stimulus conditions indicated by grey bracket (Wilcoxon rank-sum, p=0.02). Blue dots represent individual subjects, red dots indicate group average.

References:

1. Hansen, 2022, preprint.
2. Levine, 2022, *JCBFM*.
3. Sander, 2013, *PNAS*.
4. Hansen, 2020, *HBM*.
5. Desikan, 2006, *Neuroimage*.
6. Greve, 2014, *Neuroimage*.
7. Greve, 2016, *Neuroimage*.
8. Alpert, 2003, *NeuroImage*.
9. Ichise, 2003, *JCBFM*.
10. "FastMap." https://www.nmr.mgh.harvard.edu/~jbm/fastmap/.

Female Sex and Age Dependent Paradoxical Alterations of Mouse Brain Microvascular Bioenergetics

Venkata Sure[1], Siva Sakamuri[1], Lokanatha Oruganti[1] and Prasad Katakam[1]

[1]*Tulane University School of Medicine*

Abstract

Background: Small cerebral arteries (SCA) from female animals have been shown to display increased mitochondrial respiratory parameters compared to male SCAs. Previously, we demonstrated aging-induced diminution of both glycolysis and oxidative phosphorylation (OxPhos) in male mouse brain microvessels (BMVs).

Aim: The objective of the study was to study the female sex and aging-related alteration of bioenergetics in female mouse BMVs.

Methods: BMVs were isolated from young (3–4 months) and aged (18–20 months) female and male mice (C57Bl/6) using a combination of 300μm and 40μm pore sizes filters followed by gradient centrifugation. Extracellular acidification rate (ECAR) and oxygen consumption rate (OCR) were measured utilizing Seahorse XF^{e}24 analyzer. Citrate synthase (CS) enzyme activity and ATP levels were estimated.

Results: Realtime ATP rate assay observed reduced Total ATP production rate (**A**) in female BMVs that was confirmed by lower ATP levels measured (**D**). In addition, female BMVs showed reduced ATP derived from both glycolysis and OxPhos despite a significant increase in contribution of %glycolysis to overall energy production relative to %OxPhos. Mito Stress test in female BMVs showed reduced basal and maximal respiration that was accompanied by reduced spare respiratory capacity and proton leak (**B**) despite the unchanged CS activity (**E**) versus male BMVs. Similarly, glycolytic rate assay observed diminished basal and compensatory glycolysis compared to male BMVs (**C**). Paradoxically, old female BMVs displayed greater total ATP production rate with increased ATP generation from mitochondria and reduced contribution to energy production from %glycolysis (**F, G**) ($n = 9–11$ each group, $p < 0.05$-$p < 0.001$).

Conclusions: In female mice, BMVs displayed sex and age dependent paradoxically diminished mitochondrial respiration and glycolysis compared to SCAs. Reduced spare respiratory capacity and compensatory glycolysis in female BMVs compared to males imply an inability to meet the stress-related energy demands consistent with the clinical presentation of stroke-related microvascular vulnerability in females.

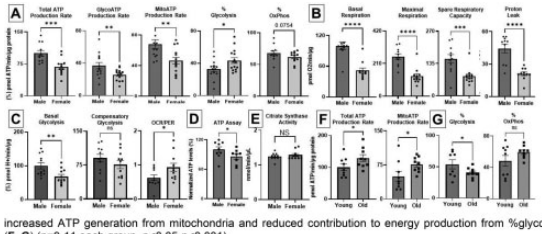

increased ATP generation from mitochondria and reduced contribution to energy production from %glycolysis (**F, G**) (n=9-11 each group, p<0.05-p<0.001).
Conclusions: In female mice, BMVs displayed sex and age dependent paradoxically diminished mitochondrial respiration and glycolysis compared to SCAs. Reduced spare respiratory capacity and compensatory glycolysis in female BMVs compared to males imply an inability to meet the stress-related energy demands consistent with the clinical presentation of stroke-related microvascular vulnerability in females.

A MATLAB toolbox implementing a blood-free and automatic IDIF extraction algorithm for brain [^{18}F]FDG PET

Mattia De Francisci[1], Erica Silvestri[2], Andrea Bettinelli[3], Tommaso Volpi[4], Diego Cecchin[5] and Alessandra Bertoldo[6]

[1]Department of Information Engineering, University of Padova, Padova, Italy
[2]Department of Information Engineering, University of Padua, Padua, Italy
[3]Department of Information Engineering, University of Padova, Padova, Italy;Medical Physics Department, Veneto Institute of Oncology – IOV IRCCS, Padova, Italy
[4]Yale University, Department of Radiology and Biomedical Imaging
[5]Nuclear Medicine Unit, Department of Medicine (DIMED), University of Padova; Padova Neuroscience Center, Padova, Italy
[6]Padova Neuroscience Center; Dept. of Information Engineering, University of Padova, Padova, Italy

Abstract

Background: The advent of biomarkers research has recently led to a renewed interest in the absolute quantification of PET tracer kinetics, which requires the knowledge of the arterial input function (AIF). A non-invasive alternative to arterial cannulation, the gold standard for AIF assessment, is represented by the Image-Derived Input Function (IDIF), which exploits the presence of vascular territories in the image Field-of-View.

Aim: To present and share an automatic MATLAB toolbox for IDIF extraction from [^{18}F]FDG brain PET scans, which includes a totally blood-free procedure for *spillover* correction.

Method: The toolbox only requires as inputs the dynamic PET images, their time grid and the following clinical covariates: sex, height, weight, age, injected [^{18}F]FDG dose. The user can choose between two extraction sites: the internal carotid arteries (ICA) and the common carotid arteries (CCA). Carotids segmentation is performed automatically directly from PET images and is followed by the selection of an optimal subset of arterial voxels. Denoising of the raw IDIF is obtained by tri-exponential model fitting. Finally, tracer kinetics after arterio-venous equilibrium is predicted through a population model based on the provided clinical covariates and used to correct the IDIF from the *spillover*.

Results: The toolbox was tested on [18F]FDG PET dynamic acquisition from 20 glioma patients (10 F, age: 57.5 ± 17 y.o.). IDIF curves have been extracted from both ICA and CCA: the differences between the two are coherent with the vessels' different location and

caliber. Within each site, the shape of the extracted curves exhibits a low across-subjects standard deviation.
Conclusions: The proposed toolbox simplifies the procedure to obtain an input function for [^{18}F]FDG quantification. Compared to the existing alternatives, it has the advantage of not requiring any multimodal registration with structural MR images.

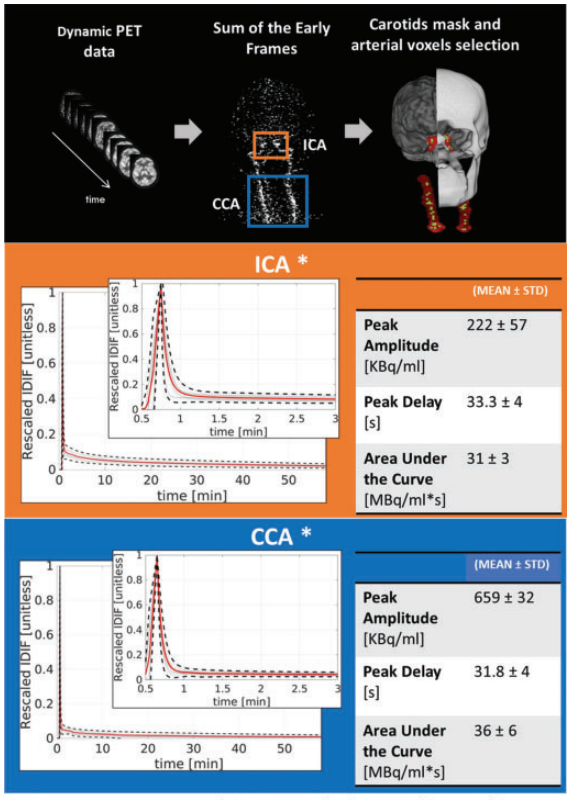

Validation of within-individual Metabolic Connectivity from dynamic [^{18}F]FDG PET data as an imaging biomarker in gliomas

Giulia Vallini[1], Tommaso Volpi[2], Erica Silvestri[3], John Lee[4], Andrei Vlassenko[4], Manu Goyal[4], Diego Cecchin[5], Maurizio Corbetta[6] and Alessandra Bertoldo[7]

[1]Dept. of Information Engineering, University of Padova, Padova, Italy
[2]Yale University, Department of Radiology and Biomedical Imaging
[3]Department of Information Engineering, University of Padua, Padua, Italy
[4]Neuroimaging Laboratories at the Mallinckrodt Institute of Radiology, Washington University School of Medicine, St Louis, MO, USA
[5]Nuclear Medicine Unit, Department of Medicine (DIMED), University of Padova; Padova Neuroscience Center, Padova, Italy
[6]Padova Neuroscience Center; Dept. of Neuroscience, University of Padova, Padova, Italy
[7]Department of Information Engineering, University of Padua, Padua, Italy; Padova Neuroscience Center, University of Padua, Padua, Italy

Abstract

Background: Static [^{18}F]FDG PET measurements are used to derive metabolic connectivity (MC) matrices at the group-level as the covariation of metabolic information across individuals, and these are proposed as biomarkers of neurological disorders. However, in case of lesions with high between-individual variability, like gliomas and strokes, a group-level approach is not appropriate. Therefore, individual-level analysis is necessary for clinical applications of MC, but definition of methodological best practices and validation are critical open issues.
Aim: We aim to validate a novel method to estimate within-individual MC (wi-MC) from dynamic [^{18}F]FDG PET data, applying it to glioma patients. We tested wi-MC as a biomarker for discriminating pathological alterations in brain metabolic connections.
Method: wi-MC was calculated as the Euclidean similarity between PET time-activity curves of each pair of regions of interest (ROI). The average healthy control matrix was used as reference. For each patient, a region-wise impairment index was obtained as one minus the Pearson's correlation coefficient (range [0 2]) between the corresponding ROI-wise connectivity patterns in the patient wi-MC and in the reference. Individual alteration maps consisting of regions with high impairment index (>0.8) were built. The potential association between mean global impairment of each patient and lesion volume was tested via Pearson's correlation.
Results: The dataset included 52 healthy participants and 51 with glioma (different locations, grade I-IV). Patients' alteration maps show how the proposed method successfully detects impairments in the lesioned areas and to a lesser extent in contralateral homologues, as expected by the underlying anatomical architecture (commissural fibers). Moreover, individual global impairment strongly relates to lesion volume ($r = 0.83$, $p < 10^{-10}$).
Conclusions: We reported a first validation of the approach developed for within-individual MC, proposing it as a biomarker capable of correctly detecting network abnormalities in clinical groups where traditional across-individual covariance would not be reliable.

Figure:

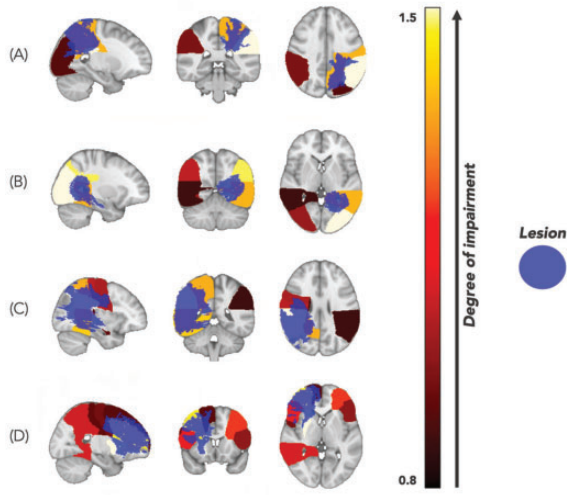

Figure: Sagittal, coronal and axial slice of the Alteration Map (ROIs with Impairment Index > 0.8 plotted on the Hammers atlas) and the lesion (tumour and oedema) of 4 subjects (A, B, C, D).

Exceptional PET Images from the First Human Scan on the NeuroEXPLORER, a next-generation ultra-high performance brain PET imager

Richard Carson[1], Takuya Toyonaga[2], Ramsey Badawi[3], Simon Cherry[3], Junwei Du[3], Kathryn Fontaine[1], Jean-Dominique Gallezot[1], Paul Gravel[1], Liuchun He[4], Ansel Hillmer[1], Nathanial Holderman[1], Praveen Honhar[1], Jocelyn Hoye[5], Lingzhi Hu[4], Terry Jones[3], Nikkita Khattar[1], Edwin Leung[4], Tiantian Li[3], Yusheng Li[4], Chi Liu[1], Peng Liu[4], Zhenrui Lu[4], Stanislaw Majewski[3], David Matuskey[1], Evan Morris[1], Tim Mulnix[1], Nakul Raval[1], Suranjana Samanta[4], Aaron Selfridge[3], Ekaterina Shanina[3], Xishan Sun[4], Tommaso Volpi[1], Zhaoheng Xie[3], Tianyi Xu[4], Tianyi Zeng[1], Jiazhen Zhang[1], Xuezhu Zhang[3], Andrea Franco[6], Joseph Masdeu[6], Masahiro Fujita[6], Jinyi Qi[3] and Hongdi Li[4]

[1]*Yale University*
[2]*Yale University, Department of Radiology and Biomedical Imaging*
[3]*UC Davis*
[4]*United Imaging Healthcare America*
[5]■■
[6]*Houston Methodist Research Institute*

Abstract

Background: The state-of-the-art for brain PET has not progressed beyond the 20-year-old HRRT and there is a compelling need to build the next generation of human brain PET systems.

Aim: The goal of the NeuroEXPLORER (NX) project is to develop a next-generation dedicated brain PET system. The NX design focused on ultra-high sensitivity (10-fold greater than the HRRT) and resolution (<2 mm FWHM).

Method: A 66 y.o. cognitively normal male participated in an IRB-approved protocol for [^{18}F]FDG-PET of the brain. The subject was administered 5 mCi and a 30-min emission scan was conducted at 30 min postinjection on the Siemens Vision. Emission data were reconstructed with standard parameters (OSEM, TOF, 8 iterations, 5 subsets, $512 \times 512 \times 88$ voxels with $0.7 \times 0.7 \times 3.0$ mm). The subject was then transported to the site of the NX and began a 60-min scan at 90 min postinjection. Reconstructed NX images contained $1024 \times 1024 \times 825$ voxels ($0.4 \times 0.4 \times 0.6$ mm). OSEM was used with 7 iterations and 10 subsets.

Results: Reconstructed transverse NX images are shown in Fig. A, demonstrating exceptionally high resolution. Fig. B shows matched slices from the Vision and the NX, exhibiting the improved resolution of the NX. Fig. C depicts the full FOV of the two systems, with the long axial FOV of the NX. Figures D-G show inter-scanner comparison of zoomed-in portions including subthalamic nuclei(STN), red nuclei(RN), superior colliculi(SC), and mamillary bodies(MB) (Fig. D), inferior colliculi(IC, Fig. E), and cerebellar dentate nuclei(DN, Fig. F). Coronal images of the cervical spinal cord (CC) show clear separation between left and right horns in NX images (Fig. G). In each case, the NX images have clearly superior resolution.

Conclusions: The NeuroEXPLORER consortium has successfully designed, built, and started initial tests of the NX system. We believe that the NX will dramatically expand the scope of brain PET studies.

Research support: U01EB029811

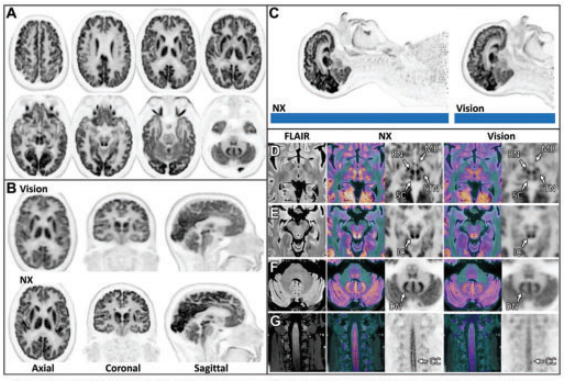

NeuroEXPLORER (NX) images in comparison to the Vision. A: Transverse NX images. B: Matching axial, coronal, and sagittal images from the Vision and the NX. C: Sagittal images showing the long axial FOV of the NX. D-G: Inter-scanner comparison of zoomed-in portions of the images (color image shows PET overlaid with MR). RN: red nuclei. MB: mamillary bodies. SC: superior colliculi. STN: subthalamic nuclei. IC: inferior colliculi. DN: dentate nuclei. CC: cervical cord.

Assessing the relationship between hemodynamic alterations and [18F]FDG PET microparameters in brain gliomas

Giulia Pagnin[1], Giorgia Baron[1], Erica Silvestri[2], Alessandro Chiuso[2], Diego Cecchin[3], Maurizio Corbetta[4] and Alessandra Bertoldo[5]

[1]Dept. of Information Engineering, University of Padova, Padova, Italy
[2]Department of Information Engineering, University of Padova
[3]Department of Medicine DIMED, Nuclear Medicine Unit, Padova Neuroscience Center, University of Padova
[4]Department of Neuroscience, Padova Neuroscience Center, University of Padova
[5]Department of Information Engineering, Padova Neuroscience Center, University of Padova

Abstract

Background: Multimodal approaches that combine fMRI, which measures activation changes in blood flow and oxygenation, and quantitative [^{18}F]FDG PET, which assesses both tissues tracer influx(a proxy of cerebral blood flux, K_1) and glucose metabolism(phosphorylation, k_3), provide new tools to investigate functional and pathological brain processes. In this study, for the first time, we assessed how the hemodynamic response function(HRF), which models the neurovascular coupling, is affected by gliomas, by relating HRF changes to cerebral blood flux and metabolic measures.

Aim: The aim of this work was to characterize HRF alterations and relate them to metabolic activity in patients with *de novo* brain tumours.

Method: A sparse DCM method was applied to the rs-fMRI signal to obtain the parcel-wise linear estimate of each single-individual HRF. Next, HRFs were distinguished between those characterizing parcels not involved in the lesion, which should have a hemodynamic pseudo-normal profile(reference), and those possibly affected by the lesion(overlapping). Then, overlapping HRFs were clustered into 4 classes according to two main shape indexes which better distinguish them from the reference: *amplitude*(AMP) and *full width at half maximum*(FWHM). [^{18}F] FDG PET K_1 and k_3 microparameters were estimated for each parcel, computed by averaging across parcels and zscoring across individuals. Finally, microparameters were compared between classes. Differences between the five groups(i.e. reference and 4 classes) were assessed through the ANOVA test(significance level 1%, Holm-Bonferroni correction for multiple comparisons).

Results: Statistically significant differences between the reference and class1 were obtained for the K_1 microparameter, whereas k_3 significantly differed between the reference and all the classes(12 individuals' dataset).

Conclusions: Our results suggest that HRF alterations, as measured by DCM in overlapping regions, reflect k_3 impairment, related to the rate of glucose consumption. On the contrary, K_1 variations seem to be less sensitive to the HRF variations induced by the brain lesions.

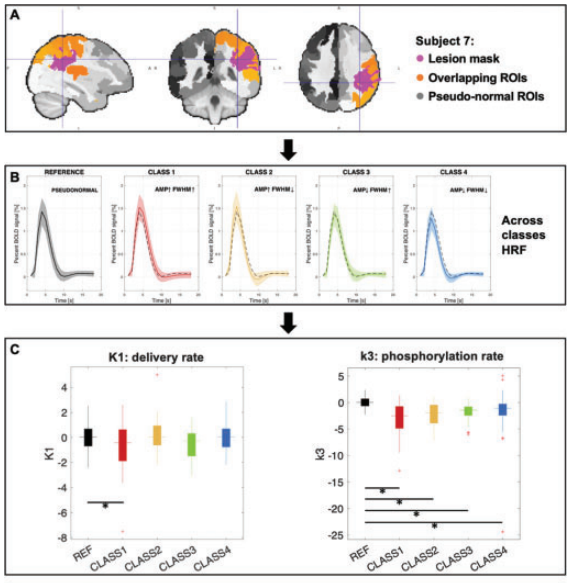

Figure: Workflow of key processing steps. A) Spatial distribution of lesion mask and both overlapping and non-overlapping Schaefer's cortical regions of interest (ROIs) for an example subject. B) HRF profile through non-overlapping and overlapping ROIs. C) K1 and k3 PET microparameter values through the classes.

Effective-metabolic coupling discriminates brain lesion localisation in patients with gliomas

Giorgia Baron[1], Giulia Vallini[1], Giulia Pagnin[1], Alessandro Chiuso[1], Diego Cecchin[2], Maurizio Corbetta[3] and Alessandra Bertoldo[4]

[1]*Dept. of Information Engineering, University of Padova, Padova, Italy*
[2]*Nuclear Medicine Unit, Department of Medicine (DIMED), University of Padova; Padova Neuroscience Center, Padova, Italy*
[3]*Padova Neuroscience Center; Dept. of Neuroscience, University of Padova, Padova, Italy*
[4]*Padova Neuroscience Center; Dept. of Information Engineering, University of Padova, Padova, Italy*

Abstract

Background: The directionality of functional-metabolic coupling is crucially relevant for the full understanding of human brain cognition. Recent studies combined undirected functional connectivity and local metabolism to provide a measure of the directional information flow, but whole-brain interdependent alterations in metabolic demands and directed brain communication have not been yet investigated at the individual level, especially in patients with localized brain lesions.

Aim: We investigated the association between effective connectivity(EC) and brain metabolism (measured both as metabolic connectivity(MC) and SUVR) in glioma patients to assess if tumour localisation is somewhat related to whole-brain effective-metabolic coupling.

Method: For each patient, the EC matrix was inferred from rs-fMRI through sparse DCM, while the MC map was computed as Euclidean similarity between each pair of PET time-activity curves. The effective-metabolic coupling was first evaluated as the Spearman distance(= 1-Spearman's correlation) between each pair of functional (incoming/outgoing EC strength) and PET(MC strength/SUVR) variables. The across-patient distance distributions were compared through an ANOVA+Tukey-Kramer post-hoc test. Individual samples were then tested for significance(FDR correction) and, when significant, employed to classify each patient based on the highest-correlation pair.

Results: At group-level(44 patients) coupling distributions were not significantly different, except for MC-ECout, which yielded the highest distance values. Assessing the statistical reliability of the strongest coupling pairs for each individual(MC-ECin, SUVR-ECin, SUVR-ECout) allowed identifying two clusters composed of patients expressing the highest effective-metabolic correlation in terms of MC-ECin(20%) or SUVR-ECout(18%). The remaining 62% does not show any statistically significant effective-metabolic coupling. In all tests, critical $\alpha = 5\%$.

Conclusions: When statistically significant, the effective-metabolic coupling divides patients into two spatially distinct group-lesion clusters, revealing that MC-ECin (network metabolism) coupling mostly characterizes temporal-parietal tumours, while SUVR-ECout (local metabolism) coupling is more pronounced in frontal lesions. This suggests that tumour localisation differentially impairs effective-metabolic coupling, potentially implying the emergence of distinct pathophysiological mechanisms.

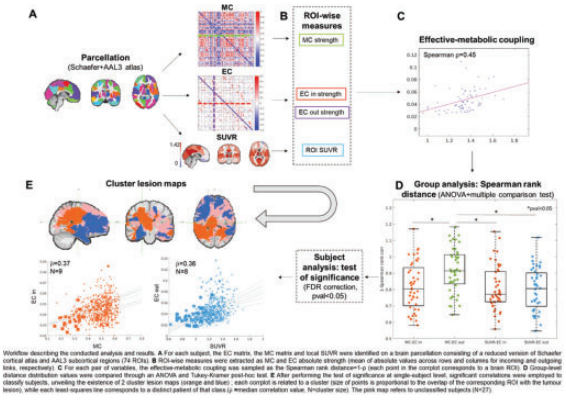

PET-based illustration of longitudinal changes of neuroinflammation under medical challenges: zonisamide

Yasuomi Ouchi[1], Tatsuhiro Terada[2], Tomoyasu Bunai[1], Takanori Hashizume[3] and Tomokazu Obi[2]

[1]*Hamamatsu University School of Medicine*
[2]*Shizuoka Institute of Epilepsy and Neurological Disorders*
[3]*Osaka Ohtani University*

Abstract

Background: In vivo evidence of zonisamide purportedly exerting a neuroprotective effect on the brains of Parkinson's disease (PD) patients has yet to be elucidated specifically under the long-term observation.

Aim: To examine long-lasting changes in microglial activation along with nigrostriatal degeneration after zonisamide medication in early PD patients using positron emission tomography (PET).

Method: Annual changes in neuroinflammation, dopamine transporter availability and clinical severity in a zonisamide^{+} and zonisamide^{-} groups were examined with [^{11}C]DPA713 PET, [^{11}C]CFT PET and various clinical tests for three years.

Results: Sixteen PD patients were randomly divided into two groups mentioned above. Voxelwise differentiations in the binding of [^{11}C]DPA713 (BP_{ND}) and [^{11}C]CFT (SUVR) were compared with normal data and between the zonisamide^{+} and zonisamide^{-} PD groups. The cerebral [^{11}C]DPA713 BP_{ND} increased with time predominantly over the parieto-occipital region in PD patients irrespective of treatment. Between-group comparisons showed lower levels (smaller changes) in the cerebral [^{11}C]DPA713 BP_{ND} in the zonisamide^{+} group ($p < 0.001$) annually. While the striatal [^{11}C]CFT SUVR decreased chronologically, the [^{11}C]CFT SUVR in the nucleus accumbens showed higher binding in the zonisamide^{+} group than in the zonisamide^{-} group ($p < 0.05$), suggesting the zonisamide mitigates the presynaptic dopaminergic terminal loss there. A significant annual increase in attention score and a tendency of motor recovery were found in the zonisamide^{+} group.
Conclusions: While neuroinflammation progresses over the parieto-occipital cortex along with nigrostriatal degeneration during the early stage of PD, zonisamide intervention may ameliorate proinflammatory responses and delay the demise of the dopaminergic terminals.

Cerebral vascular transcriptome profiling reveals intermittent fasting modulates chronic cerebral hypoperfusion-induced disease pathways

Quynh Nhu Dinh[1], Yibo Fan[2], Nishat Tabassum[2], Cecilia Lo[2], Grant R. Drummond[3], Christopher G. Sobey[3], Thiruma V. Arumugam[2] and T. Michael De Silva[1]

[1]Department of Microbiology, Anatomy, Physiology, & Pharmacology, Centre for Cardiovascular Biology and Disease Research, La Trobe University, Melbourne, VIC, Australia
[2]Centre for Cardiovascular Biology and Disease Research, Department of Microbiology, Anatomy, Physiology and Pharmacology, La Trobe University, Bundoora, VIC, Australia
[3]Centre for Cardiovascular Biology and Disease Research, Department of Microbiology, Anatomy, Physiology & Pharmacology, La Trobe University, Melbourne, VIC, Australia

Abstract
Background: Chronic cerebral hypoperfusion (CCH) is a major contributor to the development of vascular dementia, the second most common form of dementia. The pathophysiology of vascular dementia is not well understood, making it difficult to develop effective therapies. Intermittent fasting (IF) has been found to be neuroprotective against vascular dementia.
Aim: To identify potential mechanistic pathways, this study aimed to understand the transcriptomic changes induced by CCH in cerebral arteries and the effect of IF on these transcriptomic changes.
Method: Male C57Bl/6 mice were subjected to either ad libitum (AL) feeding or IF (fasting between 16:00-8:00). After 3 months of AL or IF, experimental CCH was induced in mice through bilateral carotid artery stenosis (BCAS) surgery to model vascular dementia. Transcriptomic changes in cerebral arteries were assessed using RNA sequencing after 1, 14, 21 and 30 days of BCAS or sham (control) surgery.
Results: IF mice had lower body weight and plasma glucose, and higher plasma ketone levels compared to AL mice ($n = 10$, $P < 0.05$). BCAS AL mice had elevated systolic blood pressure 1 day after surgery compared to sham AL mice (145 mmHg vs 126 mmHg, $n = 8$, $P < 0.05$) which was prevented by IF (130 mmHg vs 145 mmHg $n = 8$, $P < 0.05$). In cerebral arteries, BCAS induced differential expression of genes related to endothelial cell migration and cytoplasmic pattern recognition receptors (day 1), angiogenesis, stress and inflammation (day 14), morphogenesis and cytokinesis (day 21), and vascular structure, hypoxia, inflammation and DNA repair (day 30) ($n = 4$, P-adjusted < 0.05). IF altered expression of genes induced by BCAS that are involved in inflammation and cellular stress ($n = 4$, P-adjusted < 0.05).
Conclusions: CCH induces transcriptomic changes in cerebral arteries from as early as day 1 which may be reversed by IF. Novel pathways identified in this study could be targeted as a potential therapeutic for vascular dementia.

Neuroinflammation and blood-brain barrier breakdown in acute, clinical intracerebral haemorrhage

Olivia Jones[1], Saffwan Mohamed[2], Rainer Hinz[3], Ben Dickie[3], Laura Parkes[1] and Adrian Parry-Jones[2]

[1]Division of Psychology, Communication and Human Neuroscience, University of Manchester
[2]Division of Cardiovascular Sciences, University of Manchester
[3]Division of Imaging, Informatics and Data Science, University of Manchester

Abstract

Background: Inflammation is a promising target in intracerebral haemorrhage(ICH). [^{11}C](*R*)-PK11195-PET can map the translocator protein 18kDa(TSPO), expressed on activated microglia. Dynamic contrast-enhanced (DCE)-MRI tracks the movement of contrast-agent through and out of leaky vessels to quantify blood-plasma volume(v_p) and BBB permeability(K^{trans}).

Aim: The aims of this study are to test whether K^{trans} and [^{11}C](*R*)-PK11195 binding potential(BP_{ND}) 1) are elevated in the perihematomal oedema(PHO) surrounding the ICH, 2) are associated with peripheral inflammatory markers and functional outcome after stroke, and 3) are co-localised in the ICH brain, which has important implications for delivery of anti-inflammatory drugs that cannot cross an intact BBB.

Method: A cohort of acute, spontaneous, supratentorial ICH patients underwent DCE-MRI 1–3 days post-onset and 16 returned for [^{11}C](*R*)-PK11195-PET 2–7 days post-onset. Plasma C-reactive protein(CRP) and interleukin-6(IL-6) were measured at each scan. K^{trans} and BP_{ND} maps were co-registered with anatomical imaging. The PHO region and contralateral control regions were defined and median K^{trans} and BP_{ND} values extracted. Outcome was evaluated with the modified Rankin Scale(mRS) at 3-months.

Results: 36 subjects were included in the final analysis, example imaging data is shown in Figure 1. K^{trans} and BP_{ND} were significantly elevated in the PHO compared to the control region($P < 0.0001$); v_p was decreased($P < 0.0001$). Lobar haemorrhages had greater K^{trans} than deep ($P = 0.01$). Regions of elevated K^{trans} and BP_{ND} overlapped by 5% of the high-BP_{ND} region, ranging from 0–21% across patients. No measures correlated with IL-6 or CRP. mRS was negatively correlated with K^{trans}($P = 0.003$), but not v_p or BP_{ND}.

Conclusions: BBB leakage and neuroinflammation are observed acutely after ICH. In terms of drug development, anti-inflammatory drugs may not cross the BBB in areas of inflammation in most patients. Patients with greater BBB breakdown had better functional outcomes. The influence of neuroinflammation on patient outcome after brain injury is complex and requires further investigation.

Figure:

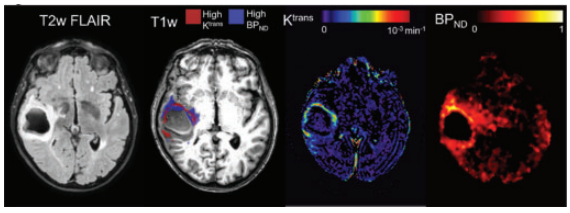

Modeling the relationship between PET measures of synaptic density from [^{11}C] UCB-J and [^{18}F]SynVesT-1 tracers

Tommaso Volpi[1], Mika Naganawa[1], Henry Huang[1] and Richard E. Carson[1]

[1] *Yale University, Department of Radiology and Biomedical Imaging*

Abstract

Background: [^{11}C]UCB-J has been the most widely used SV2A PET tracer. Among ^{18}F SV2A tracers, [^{18}F]SynVesT-1 has comparable kinetic properties[1].

Aim: With the aim of harmonizing [^{11}C]UCB-J and [^{18}F] SynVesT-1 PET data, we evaluated the relationship between their synaptic density estimates, i.e., distribution volume (V_T) and distribution volume ratio (*DVR*).

Method: 7 healthy subjects (44 ± 13yo, 2F) underwent 60-min [^{11}C]UCB-J and 120-min [^{18}F]SynVesT-1 PET acquisitions on a HRRT scanner. A 1-tissue compartment model with metabolite-corrected input function was used to estimate V_T for 22 anatomical regions. *DVR* with cerebellum as reference was obtained with SRTM2 and k_2' population average[2]. Within-subject across-region Pearson's correlations were calculated. Naïve pooled data (NPD) analysis[3] was performed by least squares fitting of [^{18}F]SynVesT-1 data (V_T or *DVR*) using [^{11}C] UCB-J V_T or DVR only as predictors, or adding covariates (age, sex, weight, injected dose). Model selection was performed with adjusted R^2 (R^2_{adj}) and Bayesian Information Criterion (BIC). Linear mixed-effects (LME) modeling was also performed with brain regions as the random factor.

Results: High individual-level spatial correlations were detected ($R > 0.97$), with V_T having higher slope variability (**Fig.A**). NPD modeling demonstrated that [^{11}C]UCB-J could explain a large proportion of variance in both [^{18}F]SynVesT-1 V_T ($R^2 = 0.66$, $BIC = 738$) and *DVR* data ($R^2 = 0.90$, $BIC = -343$). [^{18}F]SynVesT-1 dose ($\beta_{dose} = -0.006$) slightly improved the *DVR* model ($R^2_{adj} = 0.93$, $BIC = -390$), while including both [^{18}F] SynVesT-1 dose ($\beta_{dose} = -0.13$) and age ($\beta_{age} = -0.10$) significantly improved the V_T model ($R^2_{adj} = 0.82$, $BIC = 638$) (**Fig.B**). LME models were insensitive to brain region (random effects$\sim$0).

Conclusions: We found high consistency between V_T and *DVR* estimates of the two tracers. Including subject-specific information (i.e., injected dose, age) is a simple way to improve the match for V_T. LME modeling suggests [^{11}C]UCB-J regional ranking is sufficient to explain [^{18}F] SynVesT-1 variability. Further work is required to assess the impact of mixing [^{11}C]UCB-J and [^{18}F]SynVesT-1 data in one analysis.

[1]https://doi.org/10.2967/jnumed.120.249144

[2]https://doi.org/10.1002/alz.12097
[3]https://doi.org/10.3109/03602538409015063

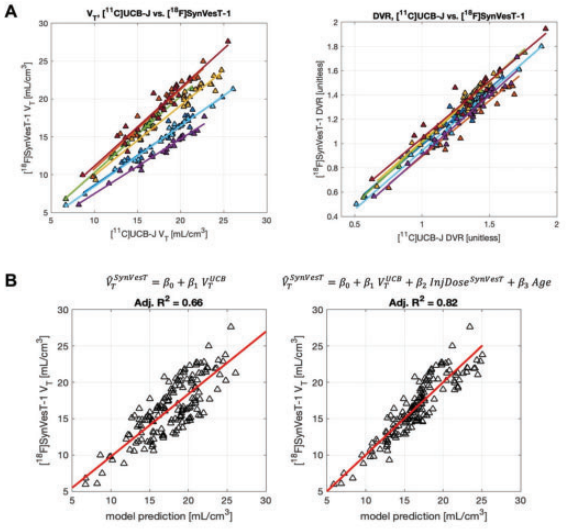

A: Scatter plots of [^{11}C]UCB-J vs. [^{18}F]SynVesT-1 V_T [ml/cm^3] (*left*), *DVR* [unitless] (*right*) values across 22 ROIs at individual level (n = 7) (data points and regression line shown in a different color for each subject). **B**: NPD model fitting all [^{18}F]SynVesT-1 V_T data pooled together using only [^{11}C]UCB-J V_T (*left*) or adding two covariates (*right*). The linear regression model equations and adjusted R^2 are reported above each plot.

Asymmetries of synaptic density, blood flow and glucose metabolism in temporal lobe epilepsy

Tommaso Volpi[1], Imran Quraishi[2], Sjoerd J. Finnema[3], Kamil Detyniecki[4], Dennis D. Spencer[5], Richard E. Carson[1] and Takuya Toyonaga[1]

[1]*Yale University, Department of Radiology and Biomedical Imaging*
[2]*Yale University, Department of Neurology*
[3]*AbbVie, North Chicago*
[4]*University of Miami Miller School of Medicine, Department of Neurology*
[5]*Yale University, Department of Neurosurgery*

Abstract

Background: Temporal lobe epilepsy (TLE) often originates from the medial temporal lobe. Higher hippocampal asymmetry for [^{11}C]UCB-J SV2A PET than [^{18}F]FDG was found in TLE patients with medial temporal sclerosis (MTS), which might support preoperative seizure onset zone localization [1].

Aim: Here, we explore asymmetries in other regions of interest (ROIs) potentially affected by TLE, e.g., the thalamus[2].

Method: In eleven patients with TLE and MTS (39 ± 11yo, 5F), [^{11}C]UCB-J PET data were acquired on a HRRT scanner for 60min, and [^{18}F]FDG data either on the HRRT (n = 8, 30–60min window) or Discovery PET/CT (n = 3, 50–60min window). Iterative Yang partial volume correction (PVC) of [^{11}C]UCB-J dynamic images was performed [3]. One-tissue compartment modeling with metabolite-corrected input function was used to estimate distribution volume (V_T) and delivery (K_1), while binding potential (BP_{ND}) was calculated with centrum semiovale as reference region[4]. [^{18}F]FDG data, after PVC, were converted into standardized uptake values (SUV). Average BP_{ND}, K_1 and SUV values were obtained for 12 ROIs, and their asymmetry indices (AIs) were calculated as 100%x[contralateral–ipsilateral]/contralateral. For each ROI, between-parameter AI correlations were assessed across patients.

Results: Positive median AIs were found in most regions for K_1 and [^{18}F]FDG SUV. For BP_{ND}, AI was positive in thalamus, hippocampus, amygdala, temporal pole, but negative in remaining ROIs (**Fig.A**). Strong relationships ($R^2 > 0.7$) were observed in the thalamus between BP_{ND}, K_1 and SUV AIs (with and without PVC), higher than those in hippocampus (**Fig.B**).

Conclusions: The negative BP_{ND} AIs in insula and posterolateral temporal cortex indicate higher synaptic density in the ipsilateral hemisphere, suggestive of compensatory synaptic remodeling. We also found consistent thalamic asymmetries in measures of *synaptic structure* (BP_{ND}) and *function* (K_1 and SUV), and future work should explore how these relate to clinical scores (e.g., seizure severity).

[1]https://doi.org/10.1111/epi.16653
[2]https://doi.org/10.1111/epi.12520
[3]https://doi.org/10.1016/j.neuroimage.2021.118248
[4]https://doi.org/10.1177/0271678x19879230

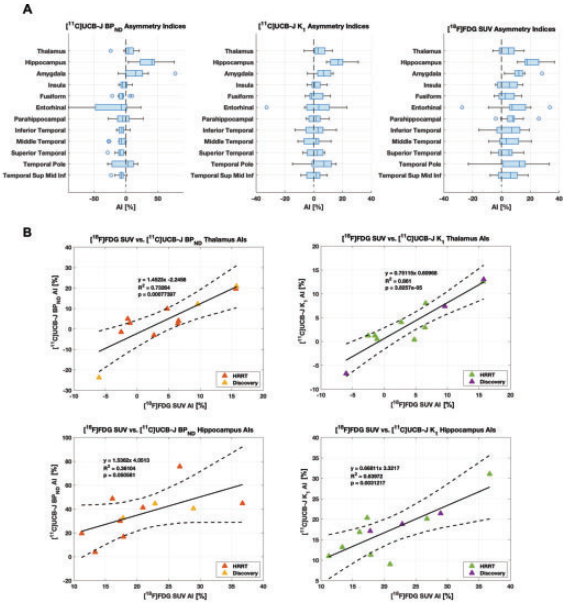

A: Boxplots of the AIs [unitless] for 12 ROIs: [^{11}C]UCB-J BP_{ND} [unitless], [^{11}C]UCB-J K_1 [mL/cm^3/min] and [^{18}F]FDG SUV [kg/mL]. The median AI values across subjects are shown by the central marks for each boxplot/region. **B**: Scatter plots of the relationship between the AI values of SUV vs. BP_{ND} (*left panels*), and SUV vs. K_1 (*right panels*) in thalamus (*top*) and hippocampus (*bottom*) across TLE patients (partitioned according to the scanner where [^{18}F]FDG PET was acquired, i.e., HRRT or Discovery). The regression line (*continuous*) is shown with its 95% confidence intervals (*dashed lines*).

Characterising the immune-rich perihaematomal microenvironment over time after ICH

Mary Newland[1], Michael Haley[1], Catherine Lawrence[1] and Stuart Allan[2]

[1]*Geoffrey Jefferson Brain Research Centre, School of Biological Sciences. Faculty of Biology, Medicine and Health, University of Manchester, United Kingdom*
[2]■■■

Abstract

Background: No individual medical treatments have shown improved functional outcome after intracerebral haemorrhage (ICH). Translation of preclinical findings into meaningful patient outcomes may be improved through more detailed characterisation of the immune microenvironment in the ICH brain.

Aim: Our aim was to examine changes in microglia, astrocyte, and vessel morphology in perihaematomal tissue over time after ICH in rats. We aimed further to characterise temporal changes in cell morphology and immune marker expression within perihaematomal regions of human post-mortem ICH using Imaging Mass Cytometry (IMC).

Methods: ICH was induced in male/female rats ($n = 36$, ICH) by intrastriatal injection of bacterial collagenase (or sham, $n = 12$). Brain sections (100μm) taken over the time-course after ICH (24 h, 3d, 7d, 14d, 28d, and 56d) were immunostained for Iba1, GFAP and lectin. Perihaematomal and contralateral regions were imaged using confocal microscopy for automated analysis of 3D cellular morphology, obtaining measures of 56 morphological parameters.

For IMC, perihaematomal tissue of human post-mortem ICH cases ($n = 9$; acute, subacute, chronic) and age/region-matched controls ($n = 3$) were stained using heavy metal isotope-conjugated antibodies against 40 different antigens. Imaged regions were analysed using established programming pipelines.

Results: At 24 h after ICH, perihaematomal microglia transition to a less branched, amoeboid morphology compared to contralateral microglia ($P < 0.0001$), which recovers up to 56d after ICH. A similar temporal pattern of morphological changes was observed in astrocytes across the brain, however, there were no significant differences between contralateral and perihaematomal astrocytes. Principal Component Analysis indicated that post-ICH changes in microglia morphology are more localised, whereas those of astrocytes are more global.

IMC revealed organised patterns of cellular expression post-ICH **(Figure 1)**, and ongoing analyses will provide further detail of cell-cell interactions and molecular/cellular phenotypes within the immune-rich perihaematomal microenvironment.

Conclusion: Parallel rat and human studies reveal distinct temporal and spatial profiles of the immune response post-ICH.

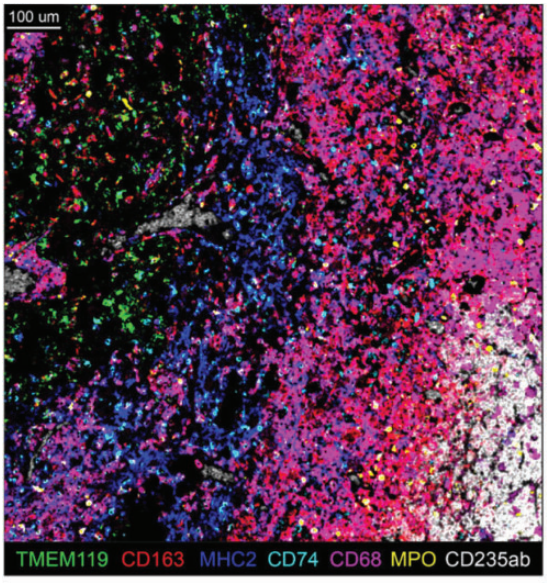

Figure 1: Example IMC image of perihaematomal tissue from one case of chronic ICH. displaying selected markers (TMEM119; CD163; MHC2; CD74; CD68; MPO; CD235ab, red blood cells) from a total of 40 co-stained antigens.

Ultrastructural and Functional Characterization of Microthrombosis-Mediated BBB Disruption in the Traumatic Penumbra Using Ultrabright Nanocarriers

Antonia Wehn[1], Martina Fetting[2], Maximilian Dorok[3], Sodai Yoshimura[3], Andrey Klymchenko[4], Plesnila Nikolaus[3] and Igor Khalin[3]

[1]*Departement of Neurosurgery, University Hospital Munich*
[2]*German Center for Neurodegenerative Diseases*
[3]*Institute for Stroke and Dementia Research, University Hospital Munich*
[4]*Laboratoire de Biophotonique et Pharmacologie, University of Strasbourg*

Abstract

Background: Traumatic brain injury (TBI) is characterized by reductions of cerebral blood flow and increased permeability of the blood-brain-barrier (BBB), however,

the mechanisms underlaying these processes are not well understood. We hypothesize that the formation of microvascular occlusions (mVOs) in peri-contusional tissue (traumatic penumbra) may be involved.

Aim: To characterize the composition of mVOs in an experimental TBI model and investigate their role for BBB opening.

Method: mVOs were visualized in C57BL/6 mice by systemic administration of super-bright 30 nm lipidic nanodroplets (LnDs) one hour following controlled cortical impact (CCI). Brains were investigated by fluorescent confocal imaging and correlative light-electron microscopy (CLEM). Additionally, caveolin (Cav1) knockout mice (*Cav1*^{tm1Mls}/J) and wildtype controls (WT) were used to investigate the mechanisms of BBB opening at the site of mVOs.

Results: We could show that 50% of mVOs formed in the traumatic penumbra were associated with extravasation of albumin, fibrinogen, IgG, and LnDs into the brain parenchyma. Further, immunohistochemistry revealed that mVOs consisted of erythrocytes, platelets, fibrin, and leukocytes, indicating the formation of microthrombosis. Extravasation of blood-borne molecules was positively correlated with the number of cells within mVOs ($n = 426$ clots; $R = 0.31$, $p = 0.02$) and negatively with the amount of fibrin ($R = -0.64$, $p < 0.001$). Genetic deletion of Cav1 significantly reduced extravasation of LnDs across the BBB as compared to WT controls ($n = 5$ animals per group, $p = 0.002$). Finally, CLEM revealed a shift of trans- to endocytosis in Cav1 deficient mice.

Conclusions: Our results show that microthrombosis occurs in the traumatic penumbra and results in an increased permeability of the BBB at the specific site of mVOs. Further, the caveolin transport system seems to be one of the leading transcytotic mediators for BBB opening. Taken together, we propose a novel diagnostic and therapeutic (theranostic) approach to specifically target the traumatic penumbra and treat traumatic brain injury.

Further evaluation of PET/MRI [^{18}F]MK-6240 delivery and ASL perfusion: bias with [^{15}O]water and reliability

Jessie Fang-Lu Fu[1], Meher Juttukonda[1], Arun H. Garimella[1], Andrew N. Salvatore[1], Hasan Sari[1], Cristina Lois[2], Bradford C. Dickerson[1], Keith A. Johnson[2], David Izquierdo Garcia[1], Ciprian Canata[1] and Julie C. Price[1]

[1]*Athinoula A. Martinos Center for Biomedical Imaging, Massachusetts General Hospital, Charlestown, MA, USA*
[2]*Department of Radiology, Harvard Medical School, Massachusetts General Hospital, Boston, MA, USA*

Abstract

Background: Assessing radioligand delivery and neuropathological protein accumulation in a single dynamic PET session informs on vascular health and amyloid/tau load. Using PET/MRI, we verified agreements between [^{15}O]water and [^{18}F]MK-6240 relative-delivery indices in tau-rich regions across young/elderly cognitively normal (yCN/eCN) and Alzheimer's disease (AD) subjects, with lower correlations between PET and arterial-spin-labeling (ASL) MRI.

Aim: To extend our evaluation using quantitative PET/MRI, including perfusion indices and Test-Retest reliability.

Methods: Seventeen subjects underwent *Test* [^{18}F]MK-6240 PET (4 yCN:28 ± 5 years; 10 eCN:68 ± 6 years; 3 AD:57 ± 6 years; 0–120min, Biograph-mMR, $n = 9$ arterial sampling). Subsets of subjects underwent multi-delay ASL ($n = 15$, post-label-delay:1.8–2.4s), *Retest* [^{18}F]MK-6240 and ASL ($n = 8$: 7eCN, 1AD; 22 ± 10 days after Test), and [^{15}O]water ($n = 11$, 0–3min, partial-volume-corrected carotid input). Outcomes included delivery K_1 ($mL \cdot cm^{-3} \cdot min^{-1}$) estimated using 2- or 1-tissue-compartmental models (2TCM:[^{18}F]MK-6240; 1TCM:[^{15}O]Water) in FreeSurfer-defined tau-rich regions. Relative delivery ($R_1 = K_{1,target}/K_{1,reference}$) was computed using reference-tissue modeling (SRTM, $n = 17$) or 2TCM ($n = 9$) using cerebellar-grey-matter reference, with high 2TCM-R_1 versus SRTM-R_1 agreement ($\rho = 0.85$). ASL cerebral blood flow (CBF, $mL \cdot g^{-1} \cdot min^{-1}$) and relative-CBF ($CBF_{target}/CBF_{reference}$ using occipital-cortex reference) were computed. Comparative assessments utilized Spearman correlations and Bland-Altman plots, with [^{15}O]water as reference standard. Reliability was assessed as $T \cdot RT(\%) = 100 * \frac{|Test - Retest|}{(Test + Retest)}$.

Results/Conclusions: 1) Correlations: [^{18}F]MK-6240 K_1 and ASL CBF were moderately-to-weakly correlated with [^{15}O]water K_1 (*Fig.1A*), with stronger correlations noted for relative-perfusion indices (*Fig.1B*). **2) Bias compared to [^{15}O]water:** Underestimation was high for [^{18}F]MK-6240 K_1 (50%, *Fig.1C-left*) and lower for [^{18}F]MK-6240 R_1 (10%, *Fig.1D-left*). Overestimation was high for ASL relative-CBF (30%, *Fig.1D-right*), but not for ASL-CBF. Negative proportional bias was observed for [^{18}F]MK-6240 K_1 and ASL-CBF. **3) Cross-regional reliability** was greatest for [^{18}F]MK-6240 SRTM-R_1 (2–13%), followed by ASL CBF (10–28%) and relative-CBF (5–25%). Results further support [^{18}F]MK-6240 R_1 as reliable relative-perfusion indices, but not [^{18}F]MK-6240 K_1 as perfusion indices. Future studies will explore agreements

between ASL, [^{18}F]MK-6240 and [^{15}O]water perfusion indices in flow territories.

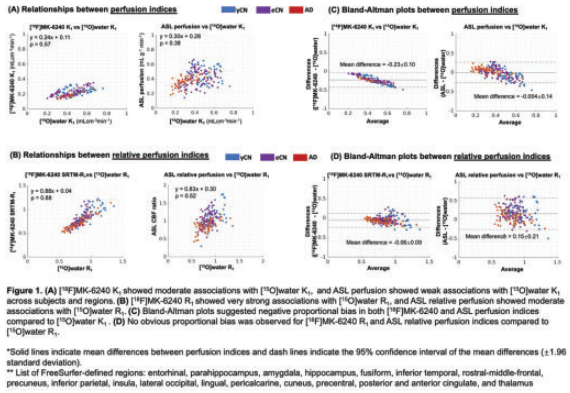

Figure 1. (A) [^{18}F]MK-6240 K_i showed moderate associations with [^{15}O]water K_1, and ASL perfusion showed weak associations with [^{15}O]water K_1 across subjects and regions. (B) [^{18}F]MK-6240 R_1 showed very strong associations with [^{15}O]water R_1, and ASL relative perfusion showed moderate associations with [^{15}O]water R_1. (C) Bland-Altman plots suggested negative proportional bias in both [^{18}F]MK-6240 and ASL perfusion indices compared to [^{15}O]water K_1. (D) No obvious proportional bias was observed for [^{18}F]MK-6240 R_1 and ASL relative perfusion indices compared to [^{15}O]water R_1.

*Solid lines indicate mean differences between perfusion indices and dash lines indicate the 95% confidence interval of the mean differences (±1.96 standard deviation).
** List of FreeSurfer-defined regions: entorhinal, parahippocampus, amygdala, hippocampus, fusiform, inferior temporal, rostral-middle-frontal, precuneus, inferior parietal, insula, lateral occipital, lingual, pericalcarine, cuneus, precentral, posterior and anterior cingulate, and thalamus

Differential diagnosis of parkinsonism using PE2I-PET and machine learning

Mark Lubberink[1], My Jonasson[2], Charles Widström[2], Elin Lindström[2], Lieuwe Appel[1], Joel Kullberg[1], Jens Sörensen[1], Dag Nyholm[1] and Torsten Danfors[2]

[1]*Uppsala University*
[2]*Uppsala University Hospital*

Abstract

Background: We are routinely using ^{11}C-PE2I-PET for differential diagnosis of parkinsonism using ^{11}C-PE2I-PET, replacing the combination of DaTSCAN SPECT and FDG using relative cerebral blood flow (rCBF) and dopamine transporter (DAT) availability images based on a single dynamic scan.

Aim: To develop supervised machine learning (ML) to support differential diagnosis with ^{11}C-PE2I.

Method: Since 2015, approximately 1400 patients underwent 40 min dynamic ^{11}C-PE2I-PET/CT scans. Data were analyzed using an in-house developed automated pipeline including motion correction, spatial normalization, VOI template, computation of DAT (SUVR-1) and rCBF images using a basis function implementation of SRTM, and comparison to a normal database. DAT and rCBF images were read by an experienced nuclear medicine physician providing a diagnosis based on images and referral information. Images of patients with unambiguous diagnosis were used to compute disease-specific DAT and rCBF patterns. The contribution of each pattern to individual patients' images was estimated using regression and regression parameters were used to train a classification tree algorithm.

Results: Approximately 60% of evaluable patients received an unambiguous diagnosis, of whom 34% normal scan, 31% PD, 16% DLB, 5% PSP, 4% CBD, 4% vascular parkinsonism, 2% MSA-P, 2% Alzheimer's and 1% MSA-C or FTD. ML-based classification accuracy varied from 96% for PD vs normal to 76% when including PD, DLB, and PSP subjects. Accuracy was always higher when including both DAT and rCBF images than for either image separately. For the other diseases, too few scans were available for ML training.

Conclusions: ML-based differential diagnosis of parkinsonism with ^{11}C-PE2I shows promising results considering the inherent inaccuracy of the ground truth diagnosis. More data is needed to train ML for the rarer diagnoses and clinical follow-up is needed to improve the ground truth diagnosis.

Figure:

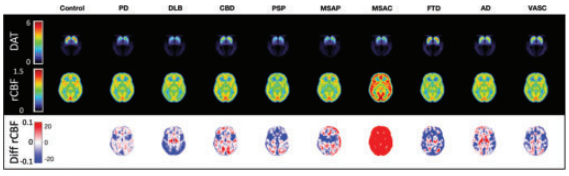

Disease-specific DAT and rCBF images, as well as difference rCBF images compared to controls.

Astrocytic nitric oxide in response to cholinergic stimulation in mouse somatosensory cortex.

Benjamin Le Gac[1], Xuewei Wang[2], Diane Vallerand[3], Andrée Lessard[4], Elvire Vaucher[5] and Hélène Girouard[3]

[1]*Physiologie et pharmacologie, Univ. de Montréal, Montréal, QC, Canada; Groupe de Recherche Universitaire sur le médicament (GRUM); Groupe de Recherche sur la signalisation neurale et la circuiterie (SNC), Montréal, QC, Canada; Ctr. interdisciplinaire de recherche sur le cerveau et l'apprentissage (CIRCA), Montréal, QC, Canada*
[2]*Physiologie et pharmacologie, Univ. de Montréal, Montréal, QC, Canada; Groupe de Recherche Universitaire sur le médicament (GRUM)*
[3]*Université de Montréal*
[4]*Ctr. interdisciplinaire de recherche sur le cerveau et l'apprentissage (CIRCA), Montréal, QC, Canada;Sherbrooke University*

[5]Groupe de Recherche sur la signalisation neurale et la circuiterie (SNC); École d'optométrie, Univ. de Montréal, Montréal, QC, Canada

Abstract

Background: Astrocytes are the main brain homeostasis regulators through their endfeet wrapping synapses and blood vessels. They release gliotransmitters and vasoactive molecules triggered by intracellular calcium elevation to modulate synaptic transmission and blood brain perfusion. Among the molecules whose production is calcium-dependant and play both roles, nitric oxide (NO) is a neuromodulator and vasodilator produced by neurons and endothelium through the so-called calcium-dependant neuronal (nNOS) and endothelium NO synthase (eNOS), respectively. Interestingly, astrocytes express eNOS but this pathway has never been explored. Acetylcholine has the potential to activate this pathway in cardiomyocytes.

Aim: The aim of this study was to investigate astrocytic NO production by eNOS in response to acetylcholine stimulation in mouse somatosensory cortex.

Methods: eNOS was identified and localized using electronic microscopy and immunohistochemistry. NO production in response to acetylcholine and glutamate was monitored with the NO indicator, DAF-FM, *in vitro* and *ex vivo* in brain slices of wild-type (WT) mice and knockout mice for eNOS ($eNOS^{-/-}$) and nNOS ($nNOS^{-/-}$).

Results: eNOS is preferentially distributed in perineuronal astrocytic processes rather than in perivascular processes ($n = 3$, $p < 0.001$) and is spatially connected to cholinergic terminals. Acetylcholine, but not glutamate, specifically increases NO production from eNOS both *in vitro* and *ex vivo*. In response to acetylcholine, there was no production in $eNOS^{-/-}$ mice astrocytic culture. As NO can be released from S-nitrosothiol pools, we removed it by N-ethylmaleimide and prevented NO production by acetylcholine only in $eNOS^{-/-}$ brain slices ($n = 3$ mice). *In vivo,* astrocytic NO production using biphotonic microscopy, fluorophore labeling, and electrical stimulations of the nucleus basalis of Meynert is under investigation.

Conclusions: These results demonstrate that astrocytes are a source of eNOS-derived NO responding to acetylcholine. Astrocytic NO which is both a neurotransmitter and a powerful vasodilator may thus play a role in the tripartite synapse or neurovascular coupling.

Mild pericyte loss induces a fatigue-like phenotype in adult mice.

Jake Cashion[1], Lachlan S. Brown[2], Gary P. Morris[2], Jo-Maree Courtney[2], Kalina Makowiecki[3], Carlie L. Cullen[3], Kaylene M. Young[2] and Brad A. Sutherland[2]

[1]Tasmanian School of Medicine, College of Health and Medicine, University of Tasmania
[2]University of Tasmania
[3]Menzies Institute for Medical Research, University of Tasmania

Abstract

Background: Central fatigue is a chronic and poorly understood condition. One suggested mechanism of central fatigue is inadequate delivery of oxygen and nutrients to the brain due to microvascular dysfunction. Pericytes are contractile cells which enwrap capillaries allowing them to control blood flow, maintain the blood-brain barrier and regulate immune cell trafficking in the CNS. Therefore, pericyte dysfunction may impair microvascular integrity in the brain resulting in an energy deficit and central fatigue.

Aim: Our aim was to determine the impact of pericyte ablation on blood-brain barrier integrity and glial activity, and whether pericyte ablation could induce a central fatigue phenotype.

Method: We delivered tamoxifen to *PDGFRβ-CreER^{T2}: : Rosa26-DTA* transgenic mice to genetically ablate pericytes. Mice were challenged with open field and beam walk tasks to measure fatigue and motor function respectively. Immunohistochemistry was used to investigate blood-brain barrier integrity (albumin) and glial activity (IBA1 for microglia and GFAP for astrocytes).

Results: Pericyte depletion was achieved in a dose dependent manner, with one dose of 100mg/kg tamoxifen depleting 43% of pericytes (mild depletion, $n = 15$, $p < 0.0001$), and two consecutive daily doses of 300mg/kg tamoxifen depleting 97% of pericytes (ablation, $n = 7$, $p < 0.0001$). Mice with mild pericyte depletion travelled half the distance ($n = 15$, $p = 0.0010$) and moved for half the time ($n = 15$, $p = 0.0010$) compared to control mice in the open field task. Mice with ablated pericytes also slipped more frequently (32-fold, $n = 7$, $p < 0.0001$) in the beam walk task compared to control mice. Labelling of brain sections revealed pericyte-ablated mice have more sites of albumin leakage (2.8-fold, $n = 7$, $p = 0.0029$) and increased microgliosis (1.7-fold, $n = 7$, $p < 0.0001$) and astrogliosis (4.5-fold, $n = 7$, $p = 0.0088$) compared to control mice.

Conclusions: Our results highlight the importance of pericytes for brain health and identifies mechanisms by which pericyte loss may contribute to central fatigue.

Biomarker interplay between CSF p-tau and 18F-PI-2620 PET in Alzheimer's disease and 4R-tauopathy

Roxane Dilcher[1], Stephan Wall[2], Nicolai Franzmeier[2], Sabrina Katzdobler[2], Henryk Barthel[3], Olivia Wagemann[2], Carla Palleis[2], Endy Weidinger[2], Urban Fietzek[2], Carolin Kurz[2], Christian Ferschmann[2], Maximilian Scheifele[2], Florian Eckenweber[2], Mirlind Zaganjori[2], Johannes Gnörich[2], Adrian Danek[2], Katharina Bürger[2], Daniel Janowitz[2], Boris-Stephan Rauchmann[4], Sophia Stöcklein[5], Robert Perneczky[2], Florian Schöberl[2], Andreas Zwergal[2], Günter Höglinger[6], Peter Bartenstein[2], Victor Villemagne[7], John Seibyl[8], Osama Sabri[3], Johannes Levin[2] and Matthias Brendel[2]

[1]*Monash Uni*
[2]*University Hospital of Munich*
[3]*University Hospital Leipzig*
[4]*University of Augsburg*
[5]*University Hospital of Munich*
[6]*Hannover Medical School*
[7]*Austin Health*
[8]*InviCRO*

Abstract

Background: Reliable biomarkers for detecting different abnormal tau protein isoforms between neurodegenerative diseases are currently missing. Phosphorylated tau (p-tau) in the cerebrospinal fluid (CSF) is acknowledged as a 3/4R tau biomarker in AD but not in other tauopathies. The positron emission tomography (PET) radiotracer ^{18}F-PI-2620 has the potential to detect abnormal 3/4R-tau in patients with Alzheimer's disease (AD) and 4R-tau in other tauopathies.

Aim: This study investigates the interplay between tau-PET and CSF p-tau in AD and 4R-tauopathies.

Methods: In this cross-sectional analysis, 52 patients with AD, 55 patients with PSP/CBS, and 8 controls underwent lumbar puncture and 0–60 min dynamic ^{18}F-PI-2620 PET scanning. Independent t-tests assessed group differences in standardized uptake value ratios for the 20–40min time window ($SUVr_{20–40}$) and p-Tau. Multiple regression analyses tested the association between $SUVr_{20–40}$ and p-tau and group interactions. ROC analyses evaluated biomarker performance in differentiating patient groups. Quantitative and voxel-wise analyses were performed with R, SPM, and VoxelStats, controlling for age and sex.

Results: Patients with AD showed elevated p-tau levels ($p < 0.05$; >61 pg/ml) and $SUVr_{20–40}$ in cortical regions, cingulate, insula, hippocampus, and amygdala ($p < 0.005$) in contrast to 4R and controls. Patients with clinically suspected 4R-tauopathies demonstrated low p-tau levels but high $SUVr_{20–40}$ in the globus pallidus compared to controls and AD ($p < 0.05$). P-tau levels predicted temporal $SUVr_{20–40}$ in AD ($p < 0.005$). ROC analyses showed that temporal $SUVr_{20–40}$ (85–90%) as well as CSF p-tau (79.5%) had high power to discriminate AD from 4R, and $SUVr_{20–40}$ in the globus pallidus had low to medium power to discriminate 4R from control in (60–65%) or from AD (50–55%). Interestingly, differences and discriminatory power increased when excluding patients with CBS.

Conclusion: The specific combination of CSF p-tau levels and ^{18}F-PI-2620 PET SUVR in disease-specific regions facilitates biomarker-guided stratification of AD and clinically suspected 4R-tauopathies.

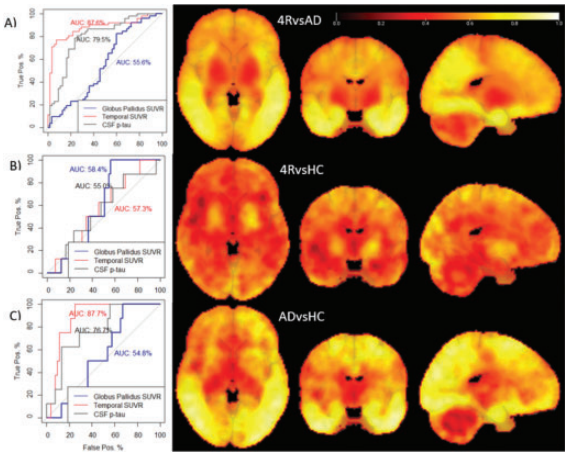

Sexually dimorphic effects of chronic cerebral hypoperfusion in mice.

Tarunpreet Rajput[1], Thiruma V. Arumugam[1], T. Michael De Silva[1] and Quynh Nhu Dinh[1]

[1]*Department of Microbiology, Anatomy, Physiology, & Pharmacology, Centre for Cardiovascular Biology and Disease Research, La Trobe University, Melbourne, VIC, Australia*

Abstract

Background: Vascular dementia (VaD) is a cerebrovascular disease resulting from compromised cerebral blood flow (CBF) causing white matter lesions and neuronal death. VaD is more prevalent in men compared to women, suggesting that sex may be an important determining factor. However, the mechanism(s) accounting for this is unclear.

Aim: To determine the effect of biological sex on cognitive function and brain injury in a model of chronic cerebral hypoperfusion.

Method: Bilateral common carotid artery stenosis (BCAS) was used to induce chronic cerebral hypoperfusion in 12-week-old male and female C57Bl6 mice. Cortical CBF was measured via laser speckle contrast imaging (before/after BCAS surgery and at day 36). Cognitive function was assessed using Barnes maze from day 28 post-surgery for 7 consecutive days. Days 1–3 were acquisition phase and days 4–6 were reversal task. Neuron (NeuN) and microglia (IBA-1) cell numbers were quantified in pre-frontal cortex using immunofluorescence.

Results: After BCAS, CBF reduced by $\sim$35% in male and female mice from baseline ($P < 0.05$, $n = 11–12$). However, this reduction in CBF recovered by $\sim$17% at day 36 in both male and female BCAS groups ($P < 0.05$, $n = 11–12$). Escape latency for male BCAS group was significantly higher compared to male sham animals on days 2 (61.8 ± 39.3s) and 3 (50.6 ± 36.5s) ($P < 0.05$, $n = 11–12$), however, there was no difference in primary latency. Female BCAS and sham groups had no difference in escape or primary latency. The number of NeuN positive cells were reduced by $\sim$50% in BCAS male mice compared to sham ($P < 0.05$, $n = 5–6$) but were not different between BCAS and sham female mice. The number of IBA-1 positive microglia was not affected in male or female mice after BCAS ($n = 5–6$).

Conclusion: This suggests that female mice are protected against some deleterious effects of chronic cerebral hypoperfusion. Further studies are required to identify the precise mechanisms underlying this protection.

In vivo characterization of the antipsychotic aripiprazole as a "partial antagonist" by PET/fMRI

Irena Bass[1], Hongping Deng[1], Bruce R. Rosen[1], Joseph B. Mandeville[1] and Christin Y. Sander[1]

[1]Athinoula A. Martinos Center, Massachusetts General Hospital

Abstract

Background: Aripiprazole is among the first in a new class of antipsychotic drugs with high clinical efficacy. *In vitro*, aripiprazole behaves as a D_2 receptor partial agonist that triggers receptor internalization. Yet, *in vivo*, the balance between its agonistic and antagonistic properties remains largely unknown.

Aim: We aimed to evaluate whether aripiprazole induces receptor signaling and internalization similar to full agonists using simultaneous PET/fMRI.

Methods: Simultaneous [^{11}C]raclopride-PET/fMRI (bolus+infusion) was acquired over 100 minutes. Anesthetized nonhuman primates ($n = 2$) were injected intravenously with 0.01, 0.02, 0.05, or 0.1 mg/kg of aripiprazole as a within-scan challenge at $\sim$35min (followed by a second injection at $\sim$70min in 6 scans). fMRI data were analyzed with a GLM and iron oxide contrast injections enabled quantifying relative cerebral blood volume (CBV) changes. Binding potentials (BP_{ND}) were derived from PET data using a simplified reference tissue model that included a sigmoidal term for dynamic binding changes (with cerebellum as the reference region).

Results: Kinetic modeling of PET data showed that aripiprazole produced D_2/D_3 receptor occupancies ranging from 22.6–89.5% and positive CBV peak changes between 0.1%–11.0% in the putamen (Figure 1). CBV timecourses displayed long-lasting dynamics, matching the PET occupancy timecourses. The four doses of aripiprazole produced average receptor occupancies of $33.9\% \pm 15.9\%$ (mean $\pm$ SD), $57.3\% \pm 9.6\%$, $73.2\% \pm 0.6\%$ ($n = 3$), and $80.4\% \pm 5.7\%$ in the putamen. Average peak CBV changes were $1.4\% \pm 1.8\%$, $5.2\% \pm 1.2\%$, $7.9\% \pm 2.7\%$, and $4.8\% \pm 0.2\%$, plateauing once 50% receptor occupancy was reached.

Conclusions: Our findings demonstrate that aripiprazole displays characteristics consistent with D_2/D_3 "partial antagonism" *in vivo*. Aripiprazole elicits a positive CBV response with a substantially lower magnitude compared to full D_2 antagonists at similar receptor occupancies. Matching PET and fMRI timecourses indicate that receptors are not internalized, further supporting partial antagonistic properties of aripiprazole. This study provides novel insights into *in vivo* functional signatures of antipsychotics, helping predict their therapeutic effects.

Figure:

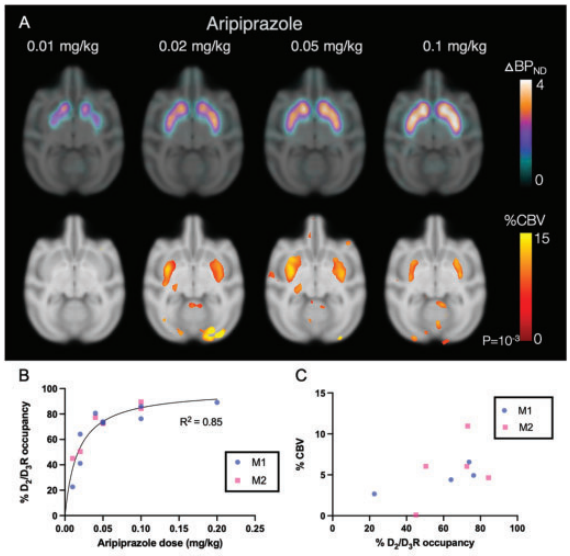

Figure 1. Changes in PET and fMRI signal in nonhuman primates treated with aripiprazole. A) Map of BP_{ND} (top row) and positive CBV (bottom row) changes. B) Occupancy of D_2/D_3 receptors in the putamen plotted against dosage of aripiprazole given. C) Change in CBV vs D_2/D_3 receptor occupancy in the putamen. Abbreviations: M1 = Monkey 1, M2= Monkey 2, D_2/D_3R = D_2/D_3 receptors

Noninvasive Vagus Nerve Stimulation Reduces Cortical Edema and Improves Outcomes in a Rat Model of Brain Injury.

Afshin Divani[1], Pascal Salazar[2], Colin Wilson[1], Denis Bragin[3] and Michel Torbey[1]

[1]*University of New Mexico*
[2]*Canon Medical Informatics, Inc*
[3]*Lovelace Biomedical Research Institute*

Abstract

Background: Traumatic brain injury (TBI) continues to be a major cause of death and disability.

Aim: Assessing the effect of different doses of non-invasive VNS (nVNS) on reducing lesion volume, cerebral edema, and neurobehavioral deficits in a rat model of TBI.

Methods: TBI was induced using a standard CCI (Impact one, Leica) model. Rats were randomized into three groups: TBI Control, TBI with five 2-min nVNS stimulations, and TBI with five 4-min nVNS stimulations using the gammaCore device (electroCore, Inc., NJ, USA) initiated 30 minutes post-injury. Rotarod, beam walking, elevated plus maze (EPM), and MRI studies were performed on days 1 and 7. A p-value of 0.05 was considered statistically significant.

Results: The overall difference of lesion volume (log_{10} transformed) among 'Control' (N = 13), VNS-2min (N = 13), and VNS-4min (N = 14) groups was highly significant for day 1 ($P < 0.0001$) and day 7 ($P < 0.0001$).

The apparent diffusion coefficient (ADC) %differences (between ipsilateral and contralateral cortex) on day 1 were significantly smaller for the higher dose (4-min) nVNS group compared with the Control group ($P = 0.024$). The ADC %difference on day 1 for the lower dose (2-min) nVNS group was almost but not significantly different from the Control group ($P = 0.058$). The variances of ADC %difference on day 7 were significantly different between the Control group and the higher dose nVNS group ($P = 0.028$).

Beam-walking time on day 1 was reduced for the higher dose nVNS group compared to Control ($P = 0.0036$). The overall inter-group beam-walking time difference on day 7 was not significant.

EPM anxiety index for the higher dose nVNS group was reduced compared with Control group on day 1 ($P = 0.0165$) and day 7 ($P = 0.0001$).

Conclusions: Both nVNS treatments (2 min and 4 min) were associated with lesion volume reduction compared to the control group. Moreover, VNS-4 min stimulations lead to significantly smaller lesions than VNS-2 min.

Recovery of the vasculature and blood flow within the ischaemic core two weeks post-photothrombotic stroke

Hannah Coombe[1], Gary P Morris[1], Catherine G Foster[1], Emma K Gowing[2], Jo-Maree Courtney[3], Natalie E King[1], Phillippa C Taberlay[1], Dino Premilovac[1], David W. Howells[1], Andrew N Clarkson[2] and Brad A. Sutherland[1]

[1]*Tasmanian School of Medicine, College of Health and Medicine, University of Tasmania, Hobart, Tasmania, Australia*
[2]*Department of Anatomy, Brain Health Research Centre and Brain Research New Zealand, University of Otago, Dunedin, New Zealand*
[3]*University of Tasmania*

Abstract

Background: Following ischaemic stroke, the core has severely compromised blood flow resulting in irreversible neuronal death and long-lasting changes to the cellular milieu. Recent evidence suggests vascular repair processes are active within the core and vascular recovery of this region may be possible.

Aim: To determine whether restoration of the vasculature and blood flow occurs within the ischaemic core following stroke.
Method: C57BL/6 mice ($n = 13$) were perfused with FITC-albumin at 3- or 14-days following Rose Bengal photothrombotic stroke, and immunohistochemistry was performed on sections to determine the extent of perfused (FITC-albumin-positive) vessels compared to total vessels (CD31-positive) within the ischaemic core. An additional cohort of mice ($n = 21$) underwent photothrombotic stroke, and post-stroke blood flow was assessed using repeated *in vivo* laser speckle contrast imaging on days 0, 3, 7 and 14.
Results: Within the core, only 3% ($n = 3$) of CD31-positive vessels contained FITC-albumin 3-days post-stroke. However, 14 days following stroke, 94% of CD31-positive vessels within the core contained FITC-albumin ($n = 10$, $p < 0.0001$), suggesting blood flow had returned between 3- and 14-days post-stroke. Interestingly, length of perfused blood vessels in the core on day 14 was 47% less compared to the uninjured contralateral hemisphere ($n = 13$, $p < 0.0001$). However, the average width of perfused vessels was 32% greater in the core compared to the contralateral side ($n = 13$, $p < 0.0001$). *In vivo* imaging 3-days following stroke revealed a 33% decrease in blood flow compared to day 0 ($n = 11$, $p = 0.0008$), with restoration close to baseline at 7-days (93%, $n = 6$) and 14-days (99%, $n = 4$).
Conclusions: Collectively, this study suggests blood flow may partially return to the ischaemic core, through the neovascularisation of larger vessels, within 14 days post-stroke. Whether therapeutic interventions targeting ischaemic core revascularisation are effective at improving neural repair following stroke remains to be elucidated and is the focus of future studies.

Transcriptional analysis of regions undergoing post-stroke plasticity after photothrombotic stroke in mice

Dene Betz[1], Kielen Zuurbier[2], Matthew Kenwood[1], Erik Plautz[3], Peter Douglas[2] and Mark Goldberg[1]

[1]*UT Health San Antonio*
[2]*Molecular Biology, UT Southwestern Medical Center*
[3]*Neurology and Neurotherapeutics, UT Southwestern Medical Center*

Abstract
Background: Chronic disability affects over half of stroke survivors. After motor cortical stroke, robust plasticity occurs in multiple distinct regions, including the peri-infarct and contralesional motor (cM1) cortex. In rodent models of stroke, these regions exhibit overlapping cellular responses such as increased neuronal activity and immune activation. However, the overlap of molecular mechanisms between these regions has not been extensively studied.
Aim: To compare the transcriptomes of peri-infarct and contralesional motor cortex undergoing post-stroke plasticity in mice.
Methods: This study utilized 8-week-old male C57/Bl6 mice that received photothrombotic stroke (PT) ($n = 3$) or sham surgery ($n = 3$) targeted to primary motor cortex (M1). One week later, the peri-infarct and cM1 were dissected and processed for RNA isolation. Quality control, mRNA purification, and paired-end 150 bp Illumina sequencing were performed by Novogene, and analysis was conducted using Qiagen's CLC genomics workbench.
Results: Differentially expressed genes (stroke vs sham) in the peri-infarct region greatly outnumbered the cM1 (911 vs. 182, p-adj < 0.1). Top upregulated genes in the peri-infarct suggested high phagocytic activity and immune cell infiltration, while cM1 genes involved a wider spectrum of processes, including regeneration, angiogenesis, and leukocyte activation. Compared to peri-infarct, cM1 gene expression was enriched for pathways related to post-stroke plasticity, such as synaptic signaling and actin cytoskeletal reorganization (p-adj < 0.1). Transcriptional regulatory network analysis of the genes comprising plasticity-related pathways identified two transcriptional regulators, Restrictive element-1 Silencing Transcription Factor (REST) and specificity protein 1 (SP1), whose roles in the cM1 have not been previously established.
Conclusions: At 7 days post-stroke, gene expression in peri-infarct cortex is dominated by inflammatory processes. In contrast, contralesional cortex includes differential pathway activation of neuronal regeneration and vascular proliferation. These results provide insights into transcriptional regulation in uninjured cortical regions that undergo post-stroke plasticity.

Estradiol, through the Estradiol Receptor β and GPER, Protects Females from Neurovascular Coupling Impairment Induced by Interleukin-17A

Jessica Youwakim[1], Diane Vallerand[1] and Hélène Girouard[1]

[1]*Université de Montréal*

Abstract

Background: Menopause is associated with a higher risk of cerebrovascular diseases and increased levels of pro-inflammatory markers. An important mechanism of cerebral blood flow regulation (CBF) altered in cerebrovascular diseases is neurovascular coupling (NVC), the dynamic link between neuronal activity and local CBF. NVC is altered in male hypertensive mice while females are protected by estradiol. NVC alteration in hypertensive male mice is mediated by interleukin (IL)-17A. Since reduced estradiol levels as seen in menopause have been associated with a higher risk of cerebrovascular diseases and altered NVC, our hypothesis stipulates that estradiol protects females from NVC impairment caused by IL-17A.

Aim: The objective of this study is to examine the protective role of estradiol and its receptors on NVC in female mice in the context of pro-inflammatory conditions involving IL-17A.

Method: Male and female mice were perfused with IL-17A through an osmotic pump. A subgroup of female mice was ovariectomized (OVX) and another subgroup was OVX and received estradiol for 7 days. To investigate which receptor is implicated in the protection seen in female receiving IL-17A, antagonists against the estradiol receptor α (MPP), the estradiol receptor β (PHTPP) or the GPER (G15) were administered. NVC was assessed by monitoring CBF changes by laser Doppler flowmetry in response to whiskers stimulations.

Results: IL-17A administration decreases the vascular responses to whiskers stimulations in male compared to female mice ($n = 6$–7, $p < 0.05$). In OVX mice, this protection is lost but restored by an estradiol treatment ($n = 7$, $p < 0.05$). PHTPP and G15, but not MPP administration let to the NVC alteration induced by IL-17A ($n = 6$–9, $p < 0.05$).

Conclusions: These results suggest that estradiol through its receptors β and GPER prevent cerebrovascular dysfunctions induced by pro-inflammatory conditions involving IL-17A. These results provide a better understanding of the mechanisms linking menopause to cerebrovascular diseases

Small extracellular vesicles-COCKTAIL based therapy for traumatic brain injury

Khan Haroon[1], Haoran Zhang[1], Yaohui Tang[2], Guo-Yuan Yang[2] and Zhijun Zhang[2]

[1]*Med-X Research Institute, School of Biomedical Engineering, Shanghai Jiao Tong University, Shanghai 200030, China*
[2]*Shanghai Jiao Tong University*

Abstract

Background: Blood brain barrier (BBB) is the major challenge in treating traumatic brain injury (TBI) as it preclude the entry of therapeutic molecules from blood to the brain. Neuroprotective peptide NR2B9C have potential to mitigate TBI long term sequalae but its poor brain penetrability through BBB, intrigues a need to develop an effective, natural, and non-immunogenic brain targeted delivery approach.

Aim: To develop sEVs-COCKTAIL, comprised of rabies virus glycoprotein 29 (RVG29) conjugated small extracellular vesicles (RVG-sEVs), loaded with NR2B9C for TBI treatment.

Method: sEVs were isolated and characterized for size, morphology, yield and sEVs markers expression. RVG29 was decorated on sEVs surface via Bio-orthogonal click chemistry reactions, followed by loading of NR2B9C, generating brain specific therapeutic COCKTAIL. Primary neurons and Neuro-2a cells were cultured to evaluate cellular uptake, Anti-oxygen glucose deprivation and anti-reactive oxygen species potential of sEVs-COCKTAIL *in-vitro*.

TBI mouse model ($n = 90$) was developed, and brain lesion volume was evaluated after sEVs treatment. sEVs live tracking for brain targeting, neurobehavioral tests, apoptosis assay and western blots were performed to confirm TBI recovery in rodents.

Results: RVG-sEVs were selectively up taken by neurons but not glial cells ($p = < 0.001$). *In-vitro* results confirmed the neuroprotective potential of sEVs-COCKTAIL against oxygen glucose deprivation and reactive oxygen species induced cytotoxicity in Neuro-2a cell ($p = < 0.001$). *In-vivo* studies further demonstrated the biocompatibility, prolong circulation and specific targeting of NR2B9C to the lesion area, reducing lesion volume and improving neurobehavioral outcomes ($p = < 0.05$) in TBI bearing mice. Co-immunostaining results showed NR2B9C specific binding to N-methyl-D-Aspartate receptor of neurons, mitigating BCL-2 and P-38 proteins expression. Our results provide an efficient and biocompatible approach of targeted delivery system, which is a promising modality for TBI therapy.

Conclusions: We ideate sEVs-COCKTAIL based remedy for TBI and present a natural and broadly applicable brain delivery approach.

Figure: (optional)

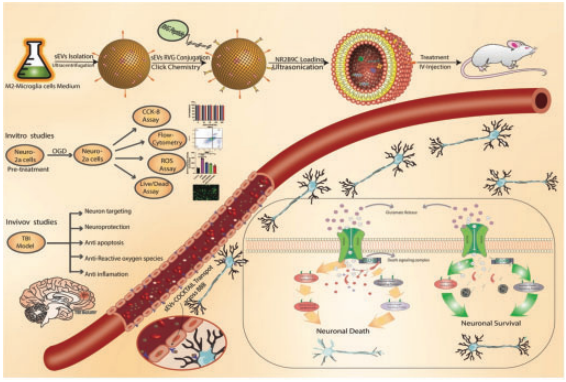

Dose-Dependent Modulation of Cerebral Perfusion and Oxygenation by Transcranial Alternating Current Stimulation an Awake and Anesthetized Mice

Olga A Bragina[1], Dmitriy Atochin[2], Alex O Trofimov[3] and Denis Bragin[1]

[1]*Lovelace Biomedical Research Institute*
[2]*Cardiovascular Research Center, Massachusetts General Hospital, Harvard Medical School*
[3]*Department of Neurological Diseases, Privolzhsky Research Medical University*

Abstract

Background: Transcranial alternating current stimulation (tACS) is a stimulation technique where a sinusoidal oscillating low-voltage electric current is applied to the brain. TACS is investigated for its potential to modulate cognition and treat brain disorders. However, the physiological mechanisms underlying tACS are underinvestigated. Previously, we demonstrated that transcranial direct current stimulation facilitates cerebral microcirculation and oxygenation in mice through nitric oxide-dependent vasodilation.

Aim: Since the effects of tACS and tDCS may be both similar or dissimilar, we tested the dose-dependent effects of tACS (5–20 Hz, 15 min) on regional cerebral blood flow (rCBF) and tissue oxygenation in anesthetized and awake mice using Laser Speckle Contrast Imaging (LSCI) and intrinsic optical signal imaging (IOSI).

Method: We imaged anesthetized wild-type C57BL6 mice ($n = 8$) under isoflurane anesthesia (~1.0%) delivered in 30% O_2 and 70% N_2O. Awake mice ($n = 8$) were pre-trained on a rotating ball for five days, starting on day three after optical window preparation. We conducted baseline imaging before and post-stimulation imaging during ~3 hours after tACS. Differences between groups were determined using a two-way ANOVA analysis for multiple comparisons and post hoc testing.

Results: Stimulation at 5–20 Hz increased cerebral blood flow and oxygen saturation in a dose-dependent manner. The time to peak and blood flow shape varied with stimulation intensity and duration, showing a linear correlation between stimulation dose and peak blood flow increase ($p < 0.05$). In awake mice, rCBF and oxygen saturation responses were more robust and prolonged compared to anesthetized mice, where the response was either weaker or shorter with overshoot.

Conclusions: The significant difference between anesthetized and awake mice emphasizes the importance of experiments conducted on awake mice, as anesthesia is not typical for human stimulation and significantly alters the results.

Neutrophil Extracellular Traps Induced by β-Amyloid Protein Damage Neurovascular Unit in Cerebral Amyloid Angiopathy

Huipeng Huang[1], Deng Xiaohui[2], Shishi Shen[2], Wei Cai[2] and Lu Zhengqi[2]

[1]*Sun Yat-sen University*
[2]*the third affiliated hospital of sun yat-sen university*

Abstract

Background: Deposition of Aβ40 in cerebral blood vessel leads to development of cerebral amyloid angiopathy (CAA). As a danger associated molecular pattern (DAMP), Aβ40 summons leukocytes and thus amplifies neuroinflammation. In response to stimulus including DAMPs, neutrophils release extracellular traps (NETs) and other pro-inflammatory factors thus mediate inflammatory injury. However, how Aβ40 affect neutrophil functions and the subsequent impacts on CAA outcomes remain elusive.

Aims: The study aims to unveil the response of neutrophil when encountering Aβ40 stimulus in CAA and the underlying mechanisms.

Methods: Tg-SwDI/B mice were used as CAA models. NETs were evaluated by CitH3 immunostaining and MPO-dsDNA ELISA. NETosis was inhibited by PADI4 inhibitor GSK484, and neutrophil infiltration was inhibited by CXCR2 inhibitor SB225002. Organotypic cerebellum cultures were obtained from WT and Tg-SwDI/B mice at P7-P10. Transwell-based B.end3 culture was used as *in vitro*

endothelial model. White matter injury was assessed with SMI32 and MBP staining while the tight junction protein integrity was evaluated with ZO1 expression.
Results: Evident neutrophil infiltration was detected in CAA brains. Abundant NETs were detected along brain blood vessels with Aβ40 deposition. Inhibiting neutrophil infiltration or NETs formation protected against neuronal loss, white matter damage and blood brain barrier (BBB) injury in CAA models. *In vitro* experiments revealed that Aβ40 efficiently induced NETs formation (Aβ40-NETs) ($N = 4$, $p = 0.0443$). With organotypic brain slice and transwell-based BBB model, we confirmed that Aβ40-NETs caused neuronal death, white matter injury and BBB breakdown. Mechanistically, Aβ40 activated STAT6 signaling in neutrophil, which inhibited apoptosis but switched the path towards cell death to NETosis ($N = 4$, $p = 0.0046$).
Conclusions: Aβ40 elicits NETs formation by activating STAT6 which switches neutrophil death from apoptosis to NETosis. Inhibition of NETs represents a novel therapeutic strategy against neurovascular unit injury in CAA.

Psilocybin as a potential treatment for traumatic brain injury? A study investigating effects on 5HT2A receptor binding in rats

Bianca Jupp[1], Mohammad Haskali[2], Richard Lin[1], Mujun Sun[1], Emma Klein[1], Robert Brkljaca[1], Rhys Brady[1], Pablo Casillas-Espinosa[1], Sandy Shultz[1] and Josh Allen[1]

[1]*Monash University*
[2]*Peter MacCallum Cancer Centre*

Abstract
Background: Traumatic brain injury (TBI) can result in long-lasting impairment of cognition and behaviour. The serotonin 2A receptor (5HT2A) is known to play a key role in regulating mood and cognition and emerging evidence suggests deficits in its function may underlie the neuropsychiatric complications of TBI. The 5HT2A agonist psilocybin has gained recent attention as a potential therapeutic based on its capacity to induce long-lasting improvement in cognitive and emotional function. While the mechanism/s of action underlying this effect remain largely unknown, evidence implicates an influence on 5HT2A function.
Aim: To examine the effect of psilocybin on 5HT2A binding using [18F]-altanserin PET and determine its influence on cognitive-behavioural outcomes in a rat model of TBI.
Method: Adult male rats received either TBI (fluid percussion injury, $n = 13$) or sham-injury ($n = 10$) and were allowed to recover for ~12 months. Rats received either a single dose of psilocybin (1mg/kg) or vehicle before undergoing a battery of cognitive/behavioural tests followed by an [^{18}F]-altanserin PET scan, two weeks post-treatment.
Results: TBI significantly reduced [18F]-altanserin binding (partial-volume corrected SUVR) across all regions investigated (vehicle: sham v TBI; $p < 0.0001$). Psilocybin treatment rescued this deficit (vehicle sham v psilocybin TBI, $p = 0.12$), significantly increasing binding at this receptor (TBI: vehicle v psilocybin; $p < 0.045$). Psilocybin had the opposite effect in sham-injured animals, decreasing 5HT2A binding (sham: vehicle v psilocybin; $p < 0.0001$). Prefrontal cortical binding was found to significantly correlate with sociability ($p < 0.045$). Notably, psilocybin treatment impaired this behaviour in sham-injured animals ($p < 0.006$). No other significant behavioural effects were observed.
Conclusions: These results support an effect of TBI to reduce 5HT2A receptor function and may potentially underlie the influence of injury on social withdrawal. Given the apparent divergent action of psilocybin on 5HT2A binding and sociability between TBI and sham-injured animals, the efficacy of this drug may depend upon 5HT2A receptor availability.

Effects of Human Amnion Epithelial Cells In Experimental Chronic Stroke

Shenpeng Zhang[1], Liz J Barreto-Arce[2], Siow Teng Chan[3], Grant Drummond[2], Hyun Ah Kim[4] and Christopher Sobey[2]

[1]*Centre for Cardiovascular Biology and Disease Research, Department of Microbiology, Anatomy, Physiology, & Pharmacology, La Trobe University, Melbourne, VIC, Australia*
[2]*Centre for Cardiovascular Biology and Disease Research, Department of Microbiology, Anatomy, Physiology & Pharmacology, School of Agriculture, Biomedicine & Environment, La Trobe University*
[3]*The Ritchie Centre, Hudson Institute of Medical Research, Clayton, VIC, Australia*
[4]*Centre for Cardiovascular Biology and Disease Research, Department of Microbiology, Anatomy, Physiology & Pharmacology, School of Agriculture, Biomedicine & Environment, La Trobe University*

Abstract

Background: Human amnion epithelial cells (hAECs) are neuroprotective when administered within 90 min of experimental stroke in mice. However, the broader therapeutic window for longer post-stroke timepoints is not yet defined.

Aim: To investigate the therapeutic window of hAECs therapy during chronic stroke in aged mice.

Method: Male ($n = 60$) and female ($n = 64$) C57BL/6 mice (12–16 months) were subjected to photothrombotic stroke in the left primary motor cortex. Mice were treated with saline or hAECs (1×10^6 cells, i.v.) at day 1, day 7, or on both days 14 and 35 post-stroke. Cylinder tests were performed before stroke and treatments, and after weeks 5 and 8 to assess motor asymmetry. Mice were euthanised at 8 weeks for infarct analysis.

Results: Mice treated with hAECs at day 1 following stroke recovered at a faster rate than those treated with saline ($N = 17$–18 per group, $P = 0.04$, linear mixed model analysis), and with 40% less functional impairment at 8 weeks ($p = 0.01$; linear mixed model analysis). Treatment with hAECs at day 7 following stroke was found to only promote recovery in females ($N = 9$–10 per group; $P < 0.01$, linear mixed model analysis), but not in males ($N = 7$ per group; $P > 0.05$). By contrast, treatment with hAECs on days 14 and 35 following stroke had no effect on motor impairment in either sex as assessed at 8 weeks. Thus, systemic treatment of aged mice at day 1 (but not from 14 days) after stroke can promote motor recovery ($N = 11$–13 per group; $P > 0.05$). Treatment with hAECs did not affect brain atrophy volume in any group ($P > 0.05$, unpaired t-test).

Conclusions: Treatment of males with hAECs at 1 day, and of females with hAECs up to 7 days following stroke appears to enhance long-term functional recovery. Ongoing studies aim to identify mechanisms underlying this sex difference in responsiveness to hAECs at 7 days post-stroke.

RNF213 loss of function reshapesvascular transcriptome andspliceosome leading to disruptedangiogenesis and aggravatedvascular inflammatory responses

Sherif Rashad[1], Liyin Zhang[1] and Kuniyasu Niizuma[1]

[1] *Tohoku University*

Abstract

Background: RNF213 gene mutations are the cause behind Moyamoya disease, a rare cerebrovascular occlusive disease. However, the function of RNF213 in the vascular system and the impact of its loss of function are not yet comprehended.

Aim: To elucidate the impact of RNF213 loss on vascular cells (endothelial cells and smooth muscle cells) function and biology.

Method: To understand RNF23 function, we performed gene knockdown (KD) in vascular cells and performed various phenotypical analysis as well as extensive transcriptome and epitranscriptome profiling using next generation sequencing. Co-culture techniques were used to study the potential role of RNF213 in regulating endothelial-smooth muscle cells communication and the implications on vascular wall biology. Flow analysis was used to elucidate the potential for RNF213 to act as a mechano-responsive gene.

Results: Our data revealed that RNF213 KD led to disrupted angiogenesis in HUVEC, in part due to downregulation of DNA replication and proliferation pathways. Furthermore, HUVEC cells became sensitive to LPS induced inflammation after RNF213 KD, leading to retarded cell migration and enhanced macrophage transmigration. This was evident at the level of transcriptome as well. Interestingly, RNF213 led to extensive changes in mRNA splicing that were not previously reported. In vascular smooth muscle cells (vSMCs), RNF213 KD led to alteration in cytoskeletal organization, contractility, and vSMCs function related pathways. Finally, RNF213 KD disrupted endothelial-to-vSMCs communication in co-culture models. Overall, our results indicate that RNF213 KD sensitizes endothelial cells to inflammation, leading to altered angiogenesis. Our results shed the light on the important links between RNF213 mutations and inflammatory/immune inducers of MMD and on the unexplored role of epitranscriptome in MMD.

Conclusions: Our results shed the light on the important links between RNF213 mutations and inflammatory/immune inducers of MMD and on the unexplored role of epitranscriptome in MMD.

iPSC-derived pericytes with APOE ε4/ε4 genotype are dysfunctional in vitro: implications for Alzheimer's Disease pathology

Natalie King[1], Jo-Maree Courtney[1], Lachlan S. Brown[1], Jake M. Cashion[1], Jana Talbot[1], Alice Pebay[2], Alex W. Hewitt[1], Gary P. Morris[1], Kaylene M. Young[1], Anthony L. Cook[1] and Brad A. Sutherland[1]

[1]*University of Tasmania*
[2]*University of Melbourne*

Abstract

Background: Dysregulation of the cerebrovasculature is an emerging feature of Alzheimer's Disease (AD). Pericytes are contractile cells residing on capillaries and are essential regulators of cerebral blood flow, but maladaptive pericyte contraction may contribute to vascular dysfunction in AD. The ε4 variant of the apolipoprotein E (*APOE*) gene is the strongest genetic risk factor for sporadic AD, and accelerated pericyte degeneration has been observed in *APOE* ε4, compared to *APOE* ε3 carriers.

Aim: To determine how the *APOE* ε4 genotype affects the proliferative capability, contractility and response to amyloid-beta (Aβ) of pericytes *in vitro*.

Method: Pericytes were differentiated using a published protocol from iPSCs via the mesoderm pathway using isogenic lines possessing an *APOE* ε3/ε3 and ε4/ε4 genetic background. Several assays assessing key pericyte functions were carried out including proliferation (response to PDGF-BB), contraction (xCelligence electrical impedance system), and exposure to Aβ40 to assess uptake and cell death.

Results: iPSC-derived pericytes expressed the canonical pericyte marker platelet-derived growth factor receptor β (PDGFRβ) and the contractile protein α-smooth muscle actin. iPSC-derived pericytes proliferated in response to the pericyte mitogen, PDGF-BB ($p < 0.0001$, $n = 8$) and contracted in response to endothelin-1 ($p = 0.0283$, $n = 4$). ε4/ε4 iPSC-derived pericytes had an impaired contractile response to endothelin-1 ($p = 0.0382$, $n = 4$), greater sensitivity to PDGFRβ inhibition (ε3 $p = 0.7295$, ε4 $p < 0.0001$, $n = 8$), increased death by fibrillar Aβ40 (ε3 $p > 0.9999$, ε4 $p = 0.0011$, $n = 8$) and a higher level of monomeric Aβ40 uptake relative to ε3/ε3 iPSC-derived pericytes ($p = 0.0413$, $n = 12$).

Conclusions: iPSC-derived pericytes expressing *APOE* ε4 have functional deficits compared with those expressing *APOE* ε3. These findings may explain why *APOE* ε4 carriers exhibit exacerbated pericyte and vascular dysfunction in AD.

Lipopolysaccharide is Associated with Corpora amylacea and White Matter Injury in AD and Aging Brains

Marisa Hakoupian[1], Xinhua Zhan[2], Lee-Way Jin[3] and Frank Sharp[1]

[1]*Department of Neurology, University of California Davis School of Medicine*
[2]*Department of Neurology, School of Medicine, University of California at Davis, Sacramento, CA, USA*
[3]*Department of Pathology, University of California Davis School of Medicine*

Abstract

Background: Previously, we found that Alzheimer's disease (AD) brains have more *Corpora amylacea (CA)* in the periventricular white matter (PVWM) compared to aging controls. CA are associated with neurodegeneration as indicated by colocalization of degraded myelin basic protein (dMBP) with periodic acid-Schiff (PAS), a CA marker. PAS stains CA due to their high polysaccharide content. However, the molecules that contribute to the polysaccharides in CA are still not known. We also found that bacterial lipopolysaccharide (LPS) is present in aging brains, with more LPS in AD compared to controls.

Aim: We determined whether LPS associates with CA and stain with PAS since LPS is a polysaccharide with lipid.

Methods: Immunohistochemistry, immunofluorescence, western blotting, Limulus Amoebocyte Lysate assay, and PAS staining were used.

Results: A total of 50 brains (30 AD and 20 age-matched controls) were studied. We found aging brains had a myelin deficit zone (MDZ) adjacent to the ventricles in PVWM. The MDZ contained more LPS^+ vesicles in AD brains compared to controls ($p = 0.0085$). LPS and dMBP levels were higher in AD than in control brains (LPS: $p = 0.0022$; dMBP: $p = 0.007$). LPS was colocalized with dMBP in the vesicles/CA. The vesicles also contained oxidized fibers, C-reactive protein, NG2, and GALC, markers of oligodendrocyte precursor cells (OPCs) and oligodendrocyte cells (OLs), respectively. LPS was co-localized with CA by double staining of PAS with LPS in aging brains. Purified LPS on nitrocellulose membranes stained with PAS.

Conclusions: These findings reveal that LPS is one of the polysaccharides found in CA which can be stained with PAS. The LPS in these vesicles/CA may have contributed to oxidative myelin damage and may have contributed to oxidative stress to OPCs and OLs which could impair the ability to repair damaged myelin in AD and control brains.

Investigating the Effect of Human Ischaemic Stroke on the mTOR Pathway in Cells of the Neurovascular Unit

Daniel Beard[1], Lily Watson[2], Brad Sutherland[3], Ain Neuhaus[2], Gabriele De Luca[2] and Alastair Buchan[2]

[1]*University of Newcastle*
[2]*University of Oxford*
[3]*University of Tasmania*

Abstract

Background: Ischaemic stroke remains a leading cause of death and disability. Given substantial injury occurs at the neurovascular unit during stroke, cytoprotectants with pleiotropic effects in the cells of the neurovascular unit may revolutionise stroke therapy and encourage neuronal survival. One potential target is mammalian Target of Rapamycin (mTOR). mTOR inhibition by hamartin (endogenous) or rapamycin (pharmacological) is cytoprotective following cerebral ischaemia in rat models. However, the effect of stroke on the mTOR pathway in the human brain has not been studied.

Aim: To investigate changes in the mTOR pathway in neurovascular cells of the human brain following ischaemic stroke.

Method: Expression of hamartin, mTOR and phosphorylated-mTOR (the active form) in the lesion area of human post-mortem ischaemic stroke brains were compared to non-stroke control cases. Stroke cases were classified as acute (<3 days post-stroke survival) or chronic stroke (>3 days), to determine temporal changes. We measured mTOR pathway positivity in neuronal, glial and vessel-associated cells in stroke and controls using immunohistochemistry.

Results: Strikingly, vessel-associated phos-mTOR significantly increased ($p < 0.001$), whilst hamartin and mTOR were unchanged ($p > 0.05$) in chronic ischaemia ($n = 4$) compared to control ($n = 5$). In acute ($n = 6$) and chronic ischaemia, glial hamartin decreased ($p = 0.002$) and glial phos-mTOR increased ($p < 0.001$), whilst glial mTOR increased in chronic ischaemia only ($p < 0.001$). In both acute and chronic ischaemia, neuronal mTOR and phos-mTOR decreased ($p < 0.001$), whilst hamartin decreased in chronic ischaemia only ($p < 0.001$). Interestingly, there was a significant increase in expression of glial mTOR and phos-mTOR ($p < 0.001$, $p = 0.008$, respectively) as well as vascular mTOR ($p = 0.002$), within the non-lesioned area of chronic stroke cases compared to control.

Conclusions: This is novel evidence of ischaemia-induced mTOR pathway changes in the human brain, and warrants further investigation to determine whether therapeutic inhibition of mTOR may benefit stroke patients

TET3-Mediated Epigenetic Regulation Restores Mitochondrial Function and Promotes Neuroprotection Following Cerebral Ischemia

Samantha Probelsky[1], Alexis Gaillard[1], Sylwia Pietrzak[2] and Kahlilia Morris-Blanco[3]

[1]*University of Wisconsin-Madison*
[2]*University of Pennsylvania*
[3]*University of Pennsylvania Perelman School of Medicine*

Abstract

Background: Mitochondria play a central in the pathogenesis of stroke injury. Thus, maintaining mitochondrial function is critical for promoting neuroprotection and improving neurological deficits after stroke. Epigenetics, modifications to DNA that regulate transcription and gene expression, have been shown to play a major role in modulating mitochondrial properties. We previously showed that ten-eleven translocase 3 (TET3), an enzyme that produces the 5-hydroxymethylcytosine (5 hmC) epigenetic modification, provides robust protection against ischemic brain damage and modulates 5 hmC in mitochondrial-related genes.

Aim: To investigate the role of TET3 in regulating post-stroke mitochondrial genes and mitochondrial function.

Method: Adult C57BL/6J mice were subjected to focal ischemia by transient by middle cerebral artery occlusion following brain specific TET3 knockdown/overexpression. Hydroxymethylation DNA immunoprecipitation sequencing (hMeDIP-seq) was used to assess 5 hmC changes in DNA from peri-infarct cortex. Mitochondrial gene expression and mitochondrial properties were analysed by fluorescent live-cell imaging, real-time PCR, and immunohistochemical analysis. Brain damage was quantified by MRI or TTC staining. Rotarod, beam-walk test and Treadscan were utilized to assess post-stroke motor function recovery.

Results: The hMeDIP-seq revealed hundreds of TET3-dependent 5 hmC changes on genomic loci associated with mitochondrial function ($n = 3$/group). Gene ontological analysis identified several mitochondrial processes related to the 5hmC-associated genes including mitochondrial membrane potential, mitochondrial bioenergetics, mitochondrial calcium homeostasis, mitochondrial structural components, and mitochondrial-mediated apoptosis (Fig.1). TET3 overexpression reduced oxidative stress, maintained mitochondrial integrity, and decreased apoptosis up to 24 h of reperfusion ($n = 9$/group). Knockdown of TET3 exacerbated secondary brain damage after stroke ($n = 6$/group), whereas overexpression of TET3 decreased

edema, infarct size, and brain damage from 1 to 7 days reperfusion (n = 7–9). Furthermore, TET3 overexpression enhanced motor function recovery up to 14 days of reperfusion (n = 7–9/group). Significance, p value < 0.05.
Conclusions: This evidence indicates that epigenetic regulation by TET3 may protect the brain after stroke by promoting mitochondrial stability.
Figure:

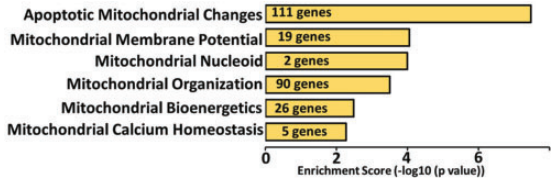

Differences in the peripheral immune response after intracerebral hemorrhage and ischemic stroke are driven by diagnosis-specific hub genes.

Paulina Carmona-Mora[1], Bodie Knepp[1], Fernando Rodriguez[1], Glen C. Jickling[2], Xinhua Zhan[1], Hajar Amini[1], Marisa Hakoupian[1], Heather Hull[1], Frank R. Sharp[1], Bradley P. Ander[1] and Boryana Stamova[1]

[1]Department of Neurology, School of Medicine, University of California at Davis, Sacramento, CA, USA
[2]Department of Medicine, Division of Neurology, University of Alberta, Edmonton, Alberta, Canada

Abstract
Background: Distinct peripheral blood gene expression (GE) profiles differentiate intracerebral hemorrhage (ICH) and ischemic stroke (IS) at the molecular level. Differences are seen across leukocyte types, like monocytes and neutrophils, which are key immune responders following ICH and IS.
Aim: Understanding the main drivers of GE changes seen after ICH and IS can help prioritize the investigation of strong candidates for differential diagnosis and treatment.
Method: RNA-seq was performed on peripheral blood (WB), and isolated monocytes (MON) and neutrophils (NEU) (n = 6 ICH; n = 33 IS, n = 9 vascular risk factors control (VRFC) subjects). Co-expression networks (WGCNA) were constructed using the GE results from ICH + VRFCs and IS + VRFCs, for MON, NEU and WB. Network modules of co-expressed genes significantly associated with ICH or IS were identified (disease genes). The most highly interconnected genes (hubs, or potential GE drivers) in the disease-significant modules were identified, and their functional significance assessed using gene ontology.
Results: There was little overlap in disease genes between IS and ICH (MON = ≤2%, NEU = ≤21%, WB = ≤16%). Some WB ICH and IS gene modules were enriched in immune function themes: regulation of T cell proliferation, leukocyte adhesion, and interferon-γ production for ICH, and for IS, these included complement activation, B cell receptor signalling, and humoral immune response. There was no overlap between ICH and IS hubs in MON and NEU, and ≤2% overlapped in WB. ICH hubs were associated with RNA splicing, cell adhesion and NF-κβ signalling; IS hubs were associated with cell migration, T cell chemotaxis and transcription factor activity.
Conclusions: The gene networks and their hubs help elucidate novel cell-specific pathophysiology, potential biomarkers and possibly novel treatment targets.

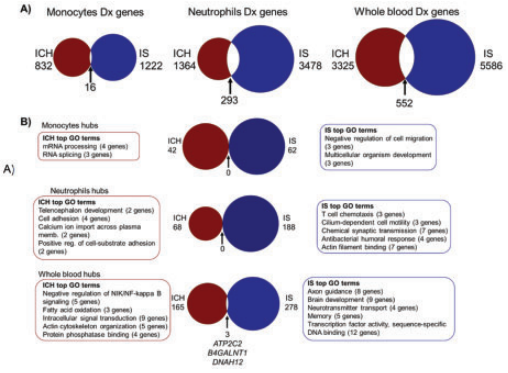

A) Diagnosis (Dx)-associated genes are highly specific for ICH or IS. B) Hubs are unique for ICH or IS. The top associated functions of these drivers are shown.

Correlations between decreased gray matter volume and changes in CBF in Cushing's disease: an arterial spin labeling and cross-sectional study

Hongchi Zhang[1] and Hong Jiang[2]

[1]Ruijin Hospital, School of Medicine Shanghai Jiao Tong University
[2]Ruijin Hospital, School of Medicine, Shanghai Jiao Tong University

Abstract

Background: The damaging effects of hypercortisolism, such as decreased gray matter volume (GMV) and altered cerebral blood flow (CBF), on the human brain in Cushing's disease (CD) have been highlighted in previous neuroscience studies. However, how these changes in GMV and CBF correlate with hypercortisolism remains unknown.

Aim: This study aimed to investigate the relationships between these alterations and hypercortisolism.

Method: Active CD patients ($n = 61$) and healthy control subjects ($n = 50$) matched for age, sex, and education were included in this study. The perfusion data of the subjects were assessed using 3D pseudo-continuous arterial spin labeling (PCASL), and structural data was obtained with T1 scanning. The differences in CBF and GMV between the two groups were examined using voxelwise group comparison analyses. Differences in CBF were determined before and after GMV correction, and the correlation between CBF and GMV in CD patients was explored at an overall level, voxel level, and atlas level.

Results: CBF was altered in multiple regions in active CD patients. However, these alterations were restricted to the thalamus and frontal gyrus after GMV correction. Clinical characteristics also correlated with CBF in these regions, and CBF was associated with GMV at the overall level and in some specific regions in CD patients.

Conclusions: Changes in CBF might be influenced by the decrease in GMV in CD. This study provides a new approach to investigating brain function abnormalities in CD and enhances our understanding of the complex effect of hypercortisolism on the human brain.

Influence of image reconstruction on quantitative brain ^{11}C-PE2I positron emission tomography

Elin Lindström[1], Torsten Danfors[1], Paul de Roos[1], Dag Nyholm[2], Martin Ingelsson[1] and My Jonasson[1]

[1]*Uppsala University Hospital*
[2]*Uppsala University*

Abstract

Background: There are many PET image reconstruction methods available for clinical use. Different reconstruction settings, such as time-of-flight (TOF), point-spread-function (PSF) modeling, and regularized reconstruction, have been shown to influence quantification of static acquisitions.

Aim: We investigated the impact of reconstruction settings on quantitative ^{11}C-PE2I PET, where dopamine transporter availability (BP_{ND}) and relative cerebral blood flow (rCBF) can be measured at the voxel level using dynamic acquisition and tracer kinetic analysis.

Methods: Twenty subjects (10 controls and 10 Parkinson patients) received an 80-min dynamic PET scan with ^{11}C-PE2I. Reconstructed images were obtained by ordered-subsets expectation maximization (OSEM; 3 iterations, 16/34 subsets, 3/5-mm filter, $\pm$TOF, $\pm$PSF) and block-sequential regularized expectation maximization (BSREM; TOF, PSF, β-value 100, 200, 300, 400). Parametric images showing rCBF and BP_{ND} were generated, and average regional voxel values were extracted.

Results: Figure 1 displays visual differences in parametric images with different reconstruction methods. Adding TOF and PSF to OSEM significantly increased BP_{ND} in putamen for both patients and controls (OSEM versus TOF-OSEM-PSF $P < 0.04$), while an increasing β-value with BSREM decreased BP_{ND} in putamen for both groups (BSREM β100 versus β400 $P < 0.001$). Mean BP_{ND} in putamen ranged between 7.3–8.9 depending on reconstruction method for controls, whereas the range was 1.7–1.9 for patients. Thus, corresponding Cohen's D between the groups were high for all reconstruction methods ($\geq$7.4). rCBF in putamen followed the same trend as BP_{ND} with a gradual increase when adding TOF and PSF to OSEM, although not significant ($P > 0.05$), and decrease with an increasing β-value with BSREM (β100 versus β400 $P < 0.0001$). rCBF in the cortical area resulted in significant differences between most reconstructions (OSEM versus TOF-OSEM-PSF $P < 0.001$ and BSREM β100 versus β400 $P < 0.0001$).

Conclusion: Quantitative ^{11}C-PE2I measures, rCBF and BP_{ND}, were found to be sensitive to reconstruction methods. Hence, consistency in reconstruction method is important.

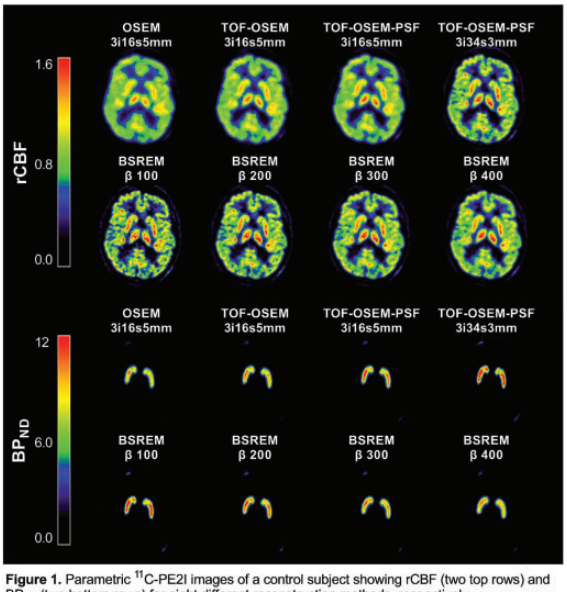

Figure 1. Parametric ^{11}C-PE2I images of a control subject showing rCBF (two top rows) and BP_{ND} (two bottom rows) for eight different reconstruction methods, respectively.

Plasma Exosomes from Remote Ischemic Post-Conditioned Rats Transfer a Specific Cluster of miRNAs and Attenuate Cerebral Ischemia-Reperfusion Injury

Ornella Cuomo[1], Pasquale Cepparulo[1], Paola Brancaccio[1], Antonio Vinciguerra[2], Serenella Anzilotti[3], Lucio Annunziato[1] and Giuseppe Pignataro[1]

[1]*Federico II University of Naples*
[2]*Università Politecnica Marche*
[3]*University of Sannio, Benevento*

Abstract

Background: Remote ischemic conditioning (RIC) represents an innovative and attractive neuroprotective approach in brain ischemia. The purpose of this intervention is to activate endogenous tolerance mechanisms by inflicting a subliminal ischemia injury to the limbs, or to another "remote" region, leading to a protective systemic response against ischemic brain injury. Among the putative mediators of the protective effect generated by the subthreshold peripheral ischemic insult, it has been hypothesized that microRNAs may play a vital role in the infarct-sparing effect of RIC. Recently, miRNAs have been isolated in exosomes. Exosomes, small lipid bilayer vesicles, are part of the transportable cell secretome that can be taken up by nearby recipient cells or can travel through the bloodstream to cells in distant organs.

Aim: The aims of the present study were:(1)To evaluate the effect of the systemic administration of exosomes isolated from plasma of animals subjected to remote ischemic postconditioning(RLIP) on cerebral ischemia-reperfusion injury;(2)To finely dissect exosomes content in terms of miRNAs;(3)To select those regulatory miRNAs specifically expressed in protective exosomes and to identify molecular pathways involved in their protective effects.

Method: Circulating exosomes were isolated from blood of animals exposed to RLIP and administered to animals exposed to tMCAO by intracerebroventricular, intraperitoneal or intranasal routes. miRNA signature in protective exosomes was evaluated by microarray analysis.

Results: Exosomes isolated from the plasma of rats exposed to RLIP attenuate cerebral ischemia-reperfusion injury and improved neurological functions ($n = 6$–8 per group; $p \leq 0.05$). By contrast, exosomes isolated from plasma of animals exposed to tMCAO alone failed to confer neuroprotection. Notably, protective exosomes were characterized by a peculiar miRNA signature.

Conclusions: Collectively, the results of the present work demonstrated that plasma released exosomes after RLIP may transfer a neuroprotective signal to the brain of ischemic animals thus representing a potentially translatable therapeutic approach in stroke.

Therapeutically Retrieved clots for an -Omic and Biochemical Understanding after ischaemic Stroke (THROMBUS) Study

Rebecca Hood[1], Prajwal Gyawali[2], Thomas Lillicrap[3], Carlos Garcia Esperon[4], Sushma Rao[5], Marten Snel[5], Paul Trim[5], Renée Turner[6], Pablo Garcia Bermejo[4], Christopher Levi[4], Neil Spratt[3] and Ferdinand Miteff[4]

[1]*Translational Neuropathology Laboratory (TNL), Discipline of Anatomy and Pathology, School of Biomedicine, Faculty of Health & Medical Sciences, The University of Adelaide, SA, Australia*
[2]*School of Health and Medical Sciences, University of Southern Queensland, QLD, Australia*
[3]*University of Newcastle School of Biomedical Sciences and Pharmacy, and Hunter Medical Research Institute, NSW, Australia*
[4]*Department of Neurology, John Hunter Hospital, Hunter New England Local Health District, NSW, Australia*

[5]Proteomics, Metabolomics and MS-Imaging Core Facility, South Australian Health and Medical Research Institute, SA, Australia
[6]International Society for Cerebral Blood Flow and Metabolism

Abstract

Background: Prevention of early secondary stroke is a key aspect of stroke management. However, the best treatment strategy depends on the origin of the thrombus. Cardioembolic strokes (25% of strokes; CE) are best prevented with anticoagulants, whereas thrombi from large artery atherosclerosis (LAA) are better prevented with antiplatelet medications. Early confirmation of stroke aetiology is therefore crucial to ensure most effective preventative therapy. However currently, approximately 25% of patients have an undetermined source of stroke after full investigation.

Aim: Identify proteins within endovascularly retrieved clots that can be used to determine stroke aetiology.

Method: A total of 45 thrombi ($n = 18$, LAA; $n = 27$, CE), extracted during routine thrombectomy at John Hunter Hospital, were fresh-frozen and examined using proteomic mass-spectroscopy (DIA-PASEF workflow). Proteomic data were analysed and grouped based on CE or LAA aetiology (defined according to the Trial of ORG 10172 in Acute Stroke Treatment (TOAST) criteria).

Results: Of the 1114 proteins identified (false discovery rate $\leq$ 1%), we identified 74 proteins with significantly higher relative abundance and 33 with significantly lower relative abundance in CE clots compared with LAA ($p < 0.05$). The top 5 proteins in each group are listed in Table 1.

Table 1. Top 5 proteins with higher and lower abundance in CE compared with LAA clots

	Protein Descriptions
Higher in CE	Actin, alpha skeletal muscle; Atlastin-1; RNA helicase aquarius; Myc target protein 1; Single-stranded DNA-binding protein
Lower in CE	Apolipoprotein C-I; Immunoglobulin heavy variable 1-18; C4b-binding protein alpha chain; 40S ribosomal protein S3; Apolipoprotein(a)

Table 1. Top 5 proteins with higher and lower abundance in CE compared with LAA clots

Conclusion: The proteins identified may be useful in determining CE or LAA aetiology, and for incorporation into a testing algorithm to determine whether patients should be prescribed anticoagulants or antiplatelets, respectively.

Characterizing regional Cerebral-Blood-Flow changes after successful thrombectomy: A prospective longitudinal clinical neuroimaging study

Felix Ng[1], Gagan Sharma[1], Prodipta Guha[1], Vijay Venkatraman[2], Chris Steward[2], Nawaf Yassi[1], Andrew Bivard[1], Vincent Thijs[3], Patricia Desmond[2] and Bruce Campbell[1]

[1]Melbourne Brain Centre at the Royal Melbourne Hospital, University of Melbourne
[2]Department of Radiology, University of Melbourne
[3]Department of Neurology, Austin Health

Abstract

Background: The mechanism of infarct growth after reperfusion is not well-characterised, and may involve secondary tissue injury from persistent tissue-level perfusion derangements.

Aim: To characterise the trajectory of post-treatment cerebral blood flow (CBF) in cerebral tissue using serial perfusion MRIs

Method: In this prospective multicentre study, 66 patients with successful thrombectomy (angiographic reperfusion eTICI 2b-3) for MCA occlusions underwent 3T-MRI immediately (Timepoint-1[TP1]) and 24–48hours (Timepoint-2[TP2]) post-thrombectomy. Pre-treatment CT-Perfusion, post-treatment TP1 and TP2 MRIs were co-registered to segment 3 Regions-Of-Interest: (1) Infarct-Growth – defined as regions of restricted diffusion at TP2 only (2) Established-Infarct–regions of restricted diffusion on TP1 and TP2, and (3) Salvaged-Penumbra–regions with critical ischemia (Tmax > 6) on pre-treatment CT-Perfusion with normal DWI at TP2. CBF in the regions-of-interest were compared to a mirror analogue and expressed as an interside-ratio.

Results: At TP1, CBF was elevated in the ischemic hemisphere in the Infarct-Growth (ipsilateral 42.2% vs. 35.2% contralateral; $p = 0.10$) and Established-Infarct (48.4% vs. 37.6%; $p = 0.014$) regions but not in the Salvaged-Penumbra (41.0% vs. 37.1%; $p = 0.096$). Infarct-Growth and Established-Infarct regions became more hyperperfused at TP2 (Infarct-Growth TP1 CBF interside-ratio 1.14 vs 1.29 TP2 $p < 0.001$; Established-Infarct 1.05 vs 1.30; $p = 0.022$).

Persistent hypoperfusion (CBF interside-ratio $\leq$0.85) despite successful thrombectomy was present in 18–28% of patients within the Infarct-Growth and Established-Infarct. In multivariable ordinal analysis adjusted for age, NIHSS and pre-morbid mRS, reduced CBF was associated with worse 3-month modified-Rankin-Scale in the

Established Infarct at both timepoints (TP1; $p = 0.024$, TP2; $p = 0.018$), but only at TP2 in the Infarct-Growth region (TP1; $p = 0.31$, TP2; $p = 0.038$).

Conclusions: Immediately post-reperfusion, ischemic cerebral tissue generally exhibited hyperperfusion which increased over time and appeared to be protective. Conversely, persistent hypoperfusion within infarcted tissue was associated with worse recovery. However hypoperfusion within non-infarcted tissue was not prognostic of future outcomes, suggesting the detrimental effect of hypoperfusion post-reperfusion may be preventable before tissue irreversibly evolves into infarction. Maintaining tissue perfusion and reversing persistent-hypoperfusion post-treatment may improve outcome.

Relationships between Haemostatic function, Vessel health, and Neurovascular function: The HAVEN Study

Gabriella Rossetti[1], Jonathan Gibbins[2], Joanne Dunster[2], Aamir Sohail[1] and Anastasia Christakou[1]

[1]*University of Reading, Centre for Integrative Neuroscience and Neurodynamics*

[2]*University of Reading, Institute for Cardiovascular and Metabolic Research*

Abstract

Background: Platelet reactivity is elevated in individuals with vascular dementia, but we don't know what mechanisms drive this association. At the same time, platelet reactivity is central to cardiovascular pathology, which is also associated with neurodegeneration.

Aim: Firstly, to determine whether individual variations in platelet reactivity are associated with functionally-relevant neurovascular measures in healthy older adults. Secondly, whether any effects of platelet reactivity on neurovascular function demonstrate regional specificity.

Method: Fourty-eight healthy older adults (52–81 years) completed this cross-sectional study. Platelet reactivity was assessed using plate-based aggregometry with three agonists (ADP, TRAP-6 (a thrombin receptor agonist), CRP (a GPVI collagen receptor agonist)) to determine relationships with (i) peripheral vascular reactivity to nitric oxide, (ii) cerebrovascular anatomy and function assessed by white matter hyperintensities (WMH), cerebral blood flow (CBF) and carbon dioxide-dependent cerebrovascular reactivity, and (iii) neurovascular function assessed by BOLD haemodynamic response functions (HRFs) in the precuneus and visual cortex (V1) during an episodic memory task.

Results: Higher platelet reactivity was associated with lower peripheral vascular reactivity to nitric oxide, longer BOLD HRF time to peak in the precuneus, and larger BOLD HRF peak height in the precuneus and V1. Specifically, higher platelet reactivity to ADP was associated with lower peripheral vascular reactivity to nitric oxide ($R = -0.41$, $P = 0.003$). Higher platelet reactivity was also associated with longer BOLD HRF time to peak in the precuneus (CRP, $R = 0.47$, $P = 0.003$; TRAP-6, $R = 0.35$, $P = 0.04$) but not in the V1 ($R \leq 0.21$, $P \geq 0.21$) and larger peak height in the precuneus (ADP, $R = 0.33$, $P = 0.04$, CRP, $R = 0.51$, $P = 0.001$) and V1 (ADP, $R = 0.45$, $P = 0.006$, CRP, $R = 0.45$, $P = 0.006$). Platelet reactivity was not associated with cerebrovascular anatomy and function assessed by WMH ($R \leq 0.28$, $P \geq 0.06$), CBF ($R \leq 0.3$, $P \geq 0.07$), or hypercapnic CVR ($R \leq 0.25$, $P \geq 0.09$).

Conclusions: In conclusion, platelet reactivity may influence neurovascular function through systemic effects on nitric-oxide-dependent vascular reactivity.

Figure:

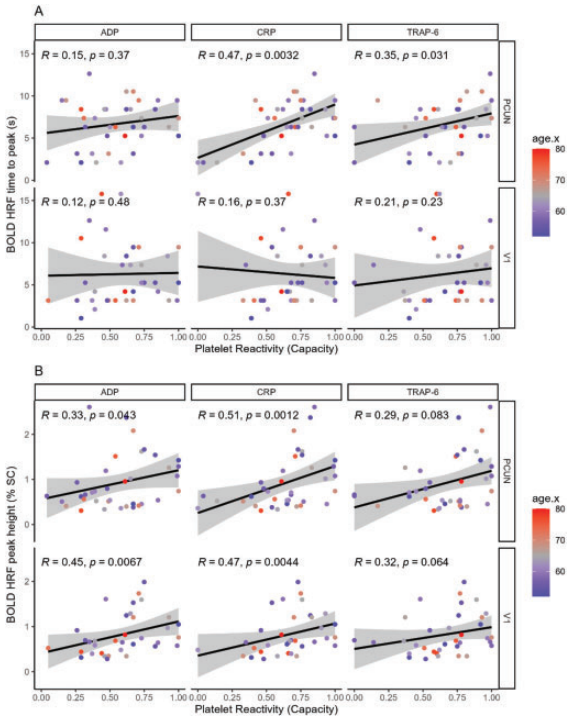

Induction of prominent subcortical white matter degeneration by renovascular hypertension

Byung Gon Kim[1], Xuelian Jin[1], Young Joo Oh[1], Hyo-Gyeong Seo[1], Hyung Soon Kim[1], Yuexain Cui[1] and Jun Young Choi[1]
[1]*Ajou University School of Medicine*

Abstract
Background: Chronic impairment of cerebral blood flow due to hypertension may underlie white matter degeneration in the elderly. The potential mechanisms of how ischemic stress leads to demyelination and axonal degeneration in the white matter are largely unknown. An animal model with reliable white matter pathology would help elucidate the pathomechanism of the ischemic white matter degeneration.
Aim: We describe a novel subcortical white matter degeneration model in renovascular hypertensive rats. We also sought to determine how RVH leads to white matter pathology.
Method: RVH was induced by clipping bilateral renal arteries with two kidneys preserved. Histological evaluations were made to verify the white matter degeneration and blood-barrier dysfunction. Single-cell RNA-sequencing (sc-Seq) was performed to profile cell-type specific gene expression in this model. To test a role of brain angiotensin II (AngII), angiotensin receptor blocker losartan was administered in an intracerebroventricular route.
Results: RVH markedly induced demyelination and axonal degeneration within the corpus callosum and cingulum. White matter hyperintensities on T2 MRI accompanied these white matter pathologies, and the fractional anisotropy in diffusion tensor imaging was also significantly reduced. A substantial extent of mature oligodendrocyte (OL) loss was accompanied by reactive astrogliosis and microglial activation. Furthermore, the deposition of fibrinogen and IgG extravasation in the subcortical white matter indicated blood-brain barrier (BBB) disruption. Sc-Seq revealed the overactivation of microglial phenotypes characterized as neurogenerative-disease-associated and defective protective mechanisms in OLs in this model. Intracerebroventricular infusion of losartan significantly attenuated the BBB disruption and white matter degeneration in the 2K2C RVHT model without affecting systemic hypertension.
Conclusions: RVH induces prominent subcortical white matter degeneration that is preceded by BBB impairment. Hyperactivation of disease-associated microglial cells may contribute to white matter pathology. Brain AngII may be responsible for the disruption of BBB and thereby trigger subcortical white matter degeneration.

Relationship between cerebral blood flow and dopamine transporter availability in healthy individuals

My Jonasson[1], Appel Lieuwe[1], Sara Roslin[1], Dag Nyholm[2], Torsten Danfors[1] and Mark Lubberink[2]
[1]*Uppsala University Hospital*
[2]*Uppsala University*

Abstract
Background: In a recent study we found a significant correlation between dopamine transporter (DAT) availability and relative tracer delivery (R_1) as a measure of relative cerebral blood flow (rCBF) in striatum with both ^{11}C-PE2I and ^{18}F-FE-PE2I PET (Jonasson *et al*, JCBFM, 2023, *in press*). This suggests that a more active dopamine system requires a higher striatal perfusion, or that the activity of the dopamine system is flow limited. However, to date, the relation between DAT availability and absolute blood flow has not been investigated.
Aim: To investigate the relation between cerebral blood flow (CBF) and DAT availability and tracer delivery using ^{15}O-water and ^{18}F-FE-PE2I PET.
Method: Seven healthy controls have been included so far in this ongoing study. Each subject underwent a 6-minutes dynamic ^{15}O-water PET scan and a 60-minutes dynamic ^{18}F-FE-PE2I PET scan. Parametric images, showing ^{15}O-water CBF and rCBF as well as ^{18}F-FE-PE2I BP_{ND} and R_1, were generated. Average regional voxel values were extracted from striatal VOIs (caudate and putamen, left and right) as well as cortical VOIs (frontal, temporal, parietal and occipital).
Results: A significant positive relationship was found between ^{15}O-water CBF and ^{18}F-FE-PE2I BP_{ND} in striatum ($r = 0.79$, $p < 0.0001$), Figure 1A. A strong correlation was also seen between rCBF and BP_{ND} ($r = 0.78$, $p < 0.0001$), Figure 1B. When comparing the relative measures ^{15}O-water rCBF to ^{18}F-FE-PE2I R_1, the correlation in striatal region was high ($r = 0.89$, $p < 0.0001$) but only moderate in the cortical regions ($r = 0.60$, $p < 0.001$) due to narrow range of cortical R_1 values, Figure 1C and D.
Conclusion: These preliminary results indicate an association between DAT availability and absolute blood flow and confirms that that relative tracer delivery correlates to relative blood flow. More data (controls and Parkinson's disease patients) will be included in the near future.

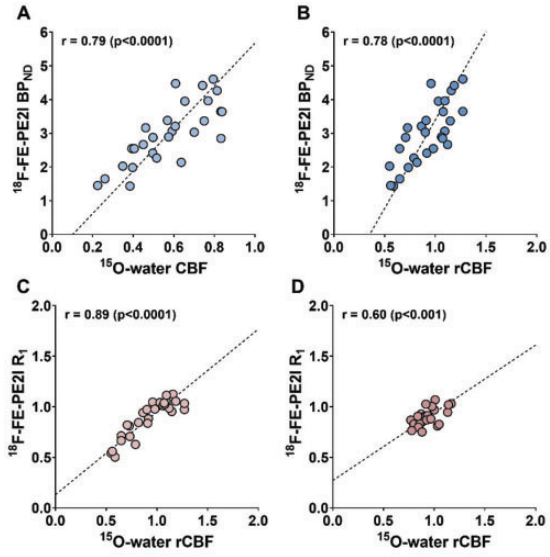

Figure 1. Relationships between ^{15}O-water CBF measures and ^{18}F-FE-PE2I BP_{ND} and R_1 values. (A) striatal CBF and BP_{ND}, (B) striatal rCBF and BP_{ND}, (C) striatal rCBF and R_1 and (D) cortical rCBF and R_1

Parametric imaging of neuroinflammation in multiple sclerosis with [^{11}C]L-deprenyl-D2 and [^{11}C]PK11195 PET

Karolina Hedman[1], My Jonasson[1], Andreas Tolf[1], Lieuwe Appel[1], Joachim Burman[1] and Mark Lubberink[1]

[1]*Uppsala University*

Abstract

Background: Multiple sclerosis (MS) is an inflammatory and neurodegenerative disease, characterised by inflammatory processes in the CNS. [^{11}C]L-deprenyl-D2 and [^{11}C]PK11195 are PET radioligands that may indicate immunity and compartmentalised inflammation characteristics of progressive MS. The former binds irreversibly to monoamine oxidase B (MAO-B) primarily found in astrocytes. The latter is a selective biomarker for the translocator protein (TSPO), upregulated in microglial activation. Quantitative parametric imaging of these biomarkers in MS patients using PET enables voxel-wise analysis and visualisation of disease pathology.

Aim: To assess differences in astrocyte reactivity and microglial activation in secondary progressive MS (SPMS) patients, MS patients treated with autologous haematopoietic stem cell transplantation (AHSCT) and healthy controls.

Method: This study involved 31 subjects: 10 SPMS, 10 AHSCT and 11 controls. Subjects underwent 60-minute dynamic PET scanning after intravenous bolus injection of [^{11}C]L-deprenyl-D2 and [^{11}C]PK11195 on consecutive days. Parametric images of MAO-B activity ($\lambda k_3 = K_1 k_3/k_2$; Fowler-1995) and TSPO binding (BP_{ND}; Yaqub-2012) were generated. Voxel-wise group comparisons were calculated with SPM12 two-sample *t*-test ($p < 0.01$, clusters >1 cm^3). In addition, mean BP_{ND} values in the calvarium were extracted using a skull template based on bone segmentation in the SPM12 tissue probability mask.

Results: Higher λk_3 and BP_{ND} were found in the white matter of SPMS patients compared to controls ($p < 0.01$), Figure 1A and B. No significant difference was seen in λk_3 values between the AHSCT group and controls. A small cluster of higher BP_{ND} was found in the AHSCT group compared to controls. A higher TSPO binding in the calvarium was found between SPMS and controls ($p < 0.001$), Figure 1C.

Conclusions: Elevated MAO-B and TSPO expression was found in SPMS patients compared to controls, but not in AHSCT patients. Furthermore, increased TSPO expression was found in the calvarium of SPMS patients. These results contribute to growing evidence of a long-lasting treatment effect of AHSCT.

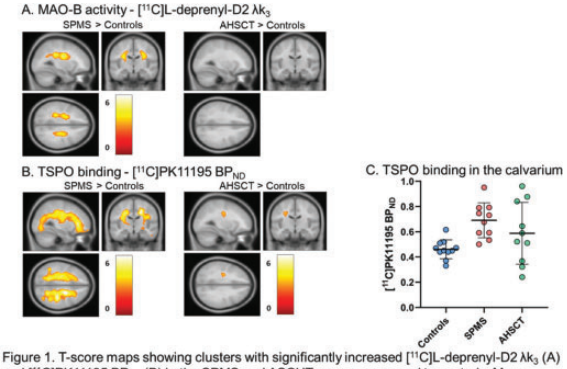

Figure 1. T-score maps showing clusters with significantly increased [^{11}C]L-deprenyl-D2 λk_3 (A) and [^{11}C]PK11195 BP_{ND} (B) in the SPMS and ASCHT groups compared to controls. Mean [^{11}C]PK11195 BP_{ND} values (C) in the calvarium for the three groups: healthy controls, SPMS and ASCHT.

Striatal and extrastriatal monoaminergic disruption in progressive supranuclear palsy: a ^{18}F-FP-DTBZ PET/CT study

Chong Dong[1], Jing-Hong Ma[1], Hong-Wen Qiao[2], Olivier Barret[3], Gilles D. Tamagnan[4], Wei Mao[1], Er-He Xu[1], Chun Zhang[2], Jie Lu[2], Piu Chan[5] and Shu-Ying Liu[6]

[1]*Department of Neurology, Xuanwu Hospital, Capital Medical University, Beijing, China*
[2]*Department of Nuclear Medicine, Xuanwu Hospital, Capital Medical University, Beijing, China*
[3]*Université Paris-Saclay, CEA, CNRS, MIRCen, Laboratoire des Maladies Neurodégénératives, Fontenay-aux-Roses, France*
[4]*XinglImaging LLC, 760Temple Street, New Haven, Connecticut 06510, United States*
[5]*Department of Neurology, Xuanwu Hospital, Capital Medical University, Beijing, China; National Clinical Research Center for Geriatric Diseases, Beijing, China*
[6]*Department of Neurology, Xuanwu Hospital, Capital Medical University, Beijing, China; Chinese Institute for Brain Research (CIBR), Beijing, China; National Clinical Research Center for Geriatric Diseases, Beijing, China*

Abstract

Background: As a biomarker targeting Vesicular Monoamine Transporter 2 (VMAT2), ^{18}F-FP-DTBZ PET/CT has shown high accuracy in the diagnostic ability and association of Parkinson's Disease (PD) severity. However, the evidence was unclear in patients with progressive supranuclear palsy (PSP).

Aim: The study aimed to evaluate the striatal and extrastriatal monoaminergic disruption of PSP and pattern difference with PD and healthy controls (HC) using ^{18}F-FP-DTBZ PET/CT, and its correlations with the clinical characteristics of PSP.

Method: We recruited 58 PSP patients, 23 age and duration-matched PD patients, and 17 HC, from the CHINA cohort. They were scanned with ^{18}F-FP-DTBZ PET/CT, which were spatially normalized and analyzed by volumes of interest (VOI). The caudate, putamen, substantia nigra (SN), thalamus, hippocampus, amygdala, NAc, dorsal raphe and median raphe were defined from an atlas in the MNI space, and the standardized uptake value ratios were calculated relative to the occipital cortex.

Results: The VMAT2 binding significantly differed in the striatum and SN among groups ($P < 0.01$). More severe disruption in the caudate of PSP ($P = 0.001$) was noted compared to PD, which was negatively correlated with the PSP rating scale (PSPRS) score. However, a lack of difference was found in the NAc, hippocampus, amygdala, thalamus, and raphe among groups. Within PSP group, the striatal VMAT2 binding showed significant correlations with the falls/postural stability sub-score of the PSPRS, especially the putamen. Besides, the VMAT2 binding in the hippocampus was correlated with Minimum Mental State Examination scores and Montreal Cognitive Assessment scores, the thalamus binding was correlated with the apathy sub-score of the Unified PD Rating Scale-I.

Conclusions: Striatal monoaminergic disruptions, especially the caudate, presented prominent differences among groups. The VAMT2 binding in the striatum, hippocampus, and thalamus could reflect the severity of falls/postural stability, cognition, and apathy, respectively.

Perivascular mascrophage-derived ApoE4 aggravates neurovascular function and hypoperfusion-induced white matter damage

Yorito Hattori[1], Ken Uekawa[2], James Seo[2], Laibaik Park[2] and Costantino Iadecola[2]

[1]*Feil Family Brain and Mind Research Institute, Weill Cornell Medicine; Department of Neurology, National Cerebral and Cardiovascular Center*
[2]*Feil Family Brain and Mind Research Institute, Weill Cornell Medicine*

Abstract

Background: Apolipoprotein E4 (ApoE4) is a risk factor for both Alzheimer's disease (AD) and white matter (WM) injury. In mice, ApoE4 induces neurovascular dysfunction through oxidative stress, and aggravates WM damage and cognitive deficits produced by bilateral carotid artery stenosis (BCAS). Perivascular macrophages (PVM) are a source of oxidative stress and mediate neurovascular dysfunction.

Aim: To test whether PVM are the source of the ApoE4 mediating neurovascular dysfunction and worsening of WM damage and cognitive function in BCAS.

Methods: Male wild-type (WT) mice were transplanted with WT bone marrow (BM) (WT→WT) or BM of mice expressing human ApoE4 (ApoE4-TR) (ApoE4→WT) to repopulate their perivascular space with ApoE4^{+} PVM. ApoE4→ApoE4 chimera were also studied. Cerebral blood flow (CBF) was assessed by laser-Doppler flowmetry in the somatosensory cortex ($n = 5$/group), 12 weeks after BM transplantation. In BCAS experiments, WM integrity ($n = 5$/group) and cognitive function ($n = 12$/group) were evaluated 1 month later.

Results: In WT→WT chimeras, whisker stimulation (WS) or neocortical application of the endothelial

vasodilator acetylcholine (ACh) increased CBF (WS: $+26 \pm 2\%$;) (ACh: $+23 \pm 1\%$; 10μM) ($p > 0.05$ from naïve WT). In ApoE4→ApoE4 chimeras, these responses were markedly attenuated (WS: $-47 \pm 5\%$; ACh: $-49 \pm 4\%$; $p < 0.05$ from WT). These responses were also attenuated in ApoE4 BM →WT chimeras (WS: $-46 \pm 4\%$; ACh: $-45 \pm 4\%$; $p < 0.05$ from WT). Two hours after BCAS, the CBF reduction was greater in ApoE4→WT ($-25 \pm 1\%$) compared to WT→WT mice ($-15 \pm 3\%$; $p < 0.05$), an effect associated with increased WM damage (MBP/SMI312 ratio, $+42 \pm 3\%$; Klüver-Barrera stain, $+66 \pm 1\%$; $p < 0.05$) and cognitive deficits (Y-maze, $+52 \pm 2\%$; Banes maze probe test, $+56 \pm 1\%$; $p < 0.05$) 28 days later.

Conclusions: ApoE4-positive PVM mediates neurovascular dysfunction and exacerbates hypoperfusion-induced WM damage and cognitive deficits. Targeting ApoE4 in PVM may reduce the risk of WM damage in ApoE4 carriers.

Metabolic dysfunction may underly secondary tissue injury after reperfusion in a rodent ischemic stroke model

Bart A.A. Franx[1], Milou Straathof[1], Caroline L. van Heijningen[1], Gerard M. van Vliet[1], Henk de Feyter[2], Annette van der Toorn[1], Willem M. Otte[1], Robin A. de Graaf[2] and Rick M. Dijkhuizen[1]

[1]Biomedical MR Imaging and Spectroscopy Group, Center for Image Sciences, University Medical Center Utrecht/Utrecht University, Utrecht, the Netherlands

[2]Department of Radiology and Biomedical Imaging, Magnetic Resonance Research Center, Yale University School of Medicine, New Haven, United States of America

Abstract

Background: Many acute ischemic stroke patients have poor outcome despite recanalization. Preclinical and clinical studies with diffusion-weighted MRI have shown normalization of the apparent diffusion coefficient (ADC) in the lesion after recanalization, reflective of cellular recovery, followed by secondary ADC reduction and ultimate infarction.

Aim: To elucidate pathophysiological or metabolic underpinnings of secondary deterioration of post-ischemic tissue after reperfusion.

Method: 45- or 90-min transient middle cerebral artery occlusion (tMCAO) was induced in female Long-Evans rats.[1] Tissue injury was assessed with diffusion- and T_2-weighted MRI[1], combined with deuterium metabolic imaging during [6, 6]-$^2H_2$-glucose infusion (2 g/kg, i.v.)[2] ($n = 20$), or perfusion imaging following Gd-DTPA-bolus injection (0.35 mmol/kg, i.v.)[1] ($n = 16$), 0–2 h or 24 h after recanalization. Downstream products of glucose metabolism were quantified from ^{2}H-MR spectra from the lesion area and its contralesional counterpart. Cerebral blood flow was quantified as previously described.[1]

Results: ADC in the post-ischemic lesion recovered to 99 ± 3 or $79 \pm 10\%$ (of contralateral) at 2 h after 45- or 90-min tMCAO, respectively (Fig. A). Successful reperfusion was evident immediately and 24 h after recanalization in both groups. Deuterated water, glucose and glutamate/glutamine (glx) levels after ^{2}H-glucose infusion were not significantly different between the lesional and contralesional area (Fig. B). Actively formed ^{2}H-lactate inside the lesion was significantly elevated in the 90-min tMCAO but not the 45-min tMCAO group (Fig. B; $p < .001$). After 24 h, the post-ischemic lesion displayed secondary ADC reduction and active ^{2}H-lactate formation in both groups (Fig. A, B), despite restored perfusion.

Conclusions: Disturbed energy metabolism despite reperfusion may explain incomplete ADC normalization after recanalization. This could be due to persistence of ischemia-induced upregulation of anaerobic glycolysis or reperfusion-associated hypermetabolism. Lactate formation in reperfused post-ischemic tissue after 24 h may be related to anaerobic glycolysis in infiltrated or activated immune cells.[3]

Figure:

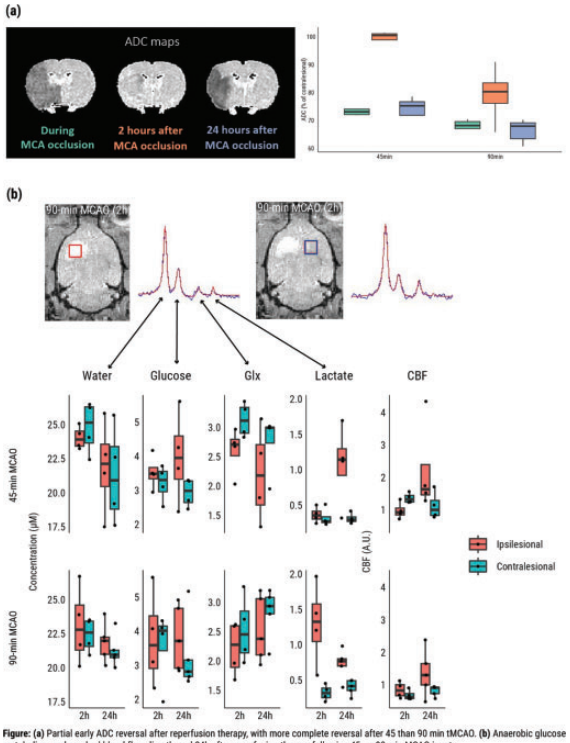

Figure: (a) Partial early ADC reversal after reperfusion therapy, with more complete reversal after 45 than 90 min tMCAO. **(b)** Anaerobic glucose metabolism and cerebral blood flow directly and 24h after reperfusion therapy following 45- or 90 min MCAO in rats.

Notes

1. Franx (2021); https://doi.org/10.1161/STROKEAHA.121.034910
2. Straathof (2021); https://doi.org/10.1016/j.neuroscience.2021.01.023
3. Meerwaldt (2023); https://doi.org/10.1177/0271678X221148970

Relative OGI based on calibrated fMRI as a complementary biomarker for AD diagnosis

Qikai Qin[1], Miao Zhang[2], Biao Li[2] and Garth Thompson[1]

[1]iHuman Institute, ShanghaiTech University
[2]Department of Nuclear Medicine, Ruijin Hospital, Shanghai Jiao Tong University School of Medicine, Shanghai, China

Abstract

Background: Alzheimer's disease (AD) is a neurodegenerative disease characterized by Amyloid β (Aβ) plaque deposition, affecting 50 million people worldwide. Many recent studies suggest that neuroinflammation may play an important role in AD pathology, which might influence the relative excess of glucose metabolism versus oxygen metabolism (aerobic glycolysis) in the brain in the early stages of the disease.

Aim: Since early diagnosis and timely intervention are critical to preserve cognition against AD progression, an imaging biomarker based on aerobic glycolysis is desirable.

Method: Cerebral metabolic rate of oxygen consumption relative to grey matter was acquired by calibrated fMRI. Combined with SUV of [^{18}F]FDG, we can calculate the relative Oxygen-Glucose Index (rOGI), reflecting the ratio of oxygen and glucose consumption. [^{18}F]AV45-PET was conducted on another day to image Aβ plaques. We used a pretrained neural network SynthSeg 2.0 to parcellate the cortex, before we compared the rOGI of healthy subjects and AD patients in frontal regions, anterior/posterior cingulate regions, lateral parietal regions, and lateral temporal regions.

Results: 31 healthy subjects (HC), 40 mild cognition impairment (MCI) patients, and 43 AD patients were in this study. According to a two-sample t-test, rOGI values are significantly different from healthy subjects and AD patients in frontal regions ($p = 0.0403$), anterior/posterior cingulate regions ($p = 0.0034$), and lateral parietal regions ($p = 5.4522 \times 10^{-7}$). The linear regression slope of rOGI vs $SUVR_{AV45}$ are also significantly different between healthy subjects and AD patients ($p = 4.0358 \times 10^{-7}$), according to a two-sample K-S test.

Conclusions: We propose rOGI as a complementary biomarker for AD diagnosis, which is correlated with Aβ plaque deposition. Additionally, rOGI could also potentially correlate with neuroinflammation.

Figure:

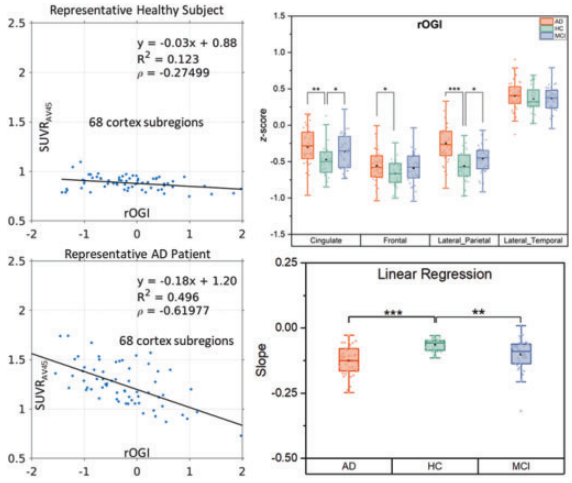

Cognitive severity markers of hemodynamic disruption in asymptomatic carotid artery stenosis/occlusion

Yorito Hattori[1], Yoshinori Kakino[1], Yuriko Nakaoku[1], Soshiro Ogata[2], Hidehiro Iida[3] and Masafumi Ihara[1]

[1]Department of Neurology, National Cerebral and Cardiovascular Center
[2]Department of Department of Preventive Medicine and Epidemiology, National Cerebral and Cardiovascular Center
[3]Turku PET Centre, University of Turku

Abstract

Background: Carotid artery stenosis or occlusion (CASO) is a major causative disease of not only ischemic stroke but also vascular cognitive impairment, which is considered to be because of cerebral hypoperfusion/metabolism or asymptomatic cerebral infarction. Thus, monitoring the cognitive status in patients with CASO might contribute to the early detection of cerebral blood flow and metabolism disruption.

Aim: We aimed to investigate what cognitive components correlated with cerebral circulation and metabolism and seek novel cognitive severity markers indicating exacerbation of cerebral perfusion/metabolism.

Method: This single-centre, cross-sectional study was performed at the National Cerebral and Cardiovascular

Centre (NCVC) in Japan. Patients with asymptomatic moderate or severe CASO visiting NCVC were enrolled in the study between July 2020 and June 2021. All patients underwent Montreal Cognitive Assessment (MoCA), and Alzheimer's Disease Assessment Scale-Cognitive Subscale 13 (ADAS-Cog) assessment, and ^{15}O-gas PET between July 2020 and June 2021. Cerebral blood flow (CBF), cerebral metabolic rate of oxygen ($CMRO_2$), and oxygen extraction fraction were measured by ^{15}O-gas PET.

Results: Altogether 98 patients' mean age was 76.8 ± 5.5 years, and 78 (79.6%) patients were male. The mean total MoCA and ADAS-Cog scores were 23.3 ± 3.6 and 15.9 ± 6.6, respectively, indicating that the patients had mild cognitive impairment to mild dementia. Disorientation was significantly correlated with cerebral hypoperfusion (left hemisphere: $\beta = 0.24$, $p = 0.033$); further visuospatial/executive dysfunction (right hemisphere: $\beta = 0.20$, $p = 0.049$) and disorientation (the right hemisphere: $\beta = 0.32$, $p = 0.004$; the left: $\beta = 0.23$, $p = 0.038$) were also significantly correlated cerebral hypometabolism even after adjusting for age, sex, and multiple conventional vascular risk factors, such as smoking, systolic blood pressure, haemoglobin A1c, low-density lipoprotein cholesterol, and triglyceride/high-density lipoprotein cholesterol ratio.

Conclusions: Disorientation and visuospatial/executive dysfunction are significantly correlated with cerebral hypoperfusion/hypometabolism, indicating that they can be novel cognitive severity markers of carotid artery disease in disruption of cerebral perfusion/metabolism.

Asymmetric Perivascular Space Distribution in Post Stroke Epilepsy

Benjamin Sinclair[1]
[1]*No*

Abstract

Introduction: Around 10% of stroke patients develop post-stroke epilepsy (PSE), leading to long-term impairments and higher mortality rates. Various risk factors for PSE have been reported, including stroke-severity, cortical-involvement, and carotid circulation territory involvement.

The glymphatic system is thought to be the brain's primary "waste" clearance system, eliminating soluble metabolites and proteins within the neuropil. It consists of cerebrospinal fluid, interstitial fluid, and a conduit between the two, perivascular spaces (PVS), which are channels formed by astroglial cells surrounding the blood vessels. PVS can be observed on high-resolution T1-weighted MRI images. This study investigates PVS as a novel imaging biomarker for PSE.

Methods: 25 patients with PSE following an acute ischemic stroke (AIS) were studied. They were matched with 31 patients who had had AIS but without PSE, and 27 healthy controls. All participants were recruited from the Hospital das Clinicas, Campinas, Brazil. They were scanned with T1-weighted MRI on a 3T Phillips MRI scanner, resolution 1.0x1.0x1.0mm. A deep-learning algorithm, U-Net, was trained and applied to segment PVS. The number of PVS and asymmetry in PVS were extracted and used as predictors of PSE in a logistic regression with hypertension, cardiopathy, dyslipidemia, NIHSS, vascular-territory, and cortical-involvement included as nuisance covariates.

$$Absolute\ Asymmetry\ Index\ (AAI) = \frac{PVS(lesion-side)\ -\ PVS(nonlesion-side)}{PVS(lesion-side)\ +\ PVS(nonlesion-side)}$$

Results: AAI was an independent predictor of PSE (beta (se) $= -18.19(8.77)$, $z = -2.074$, $p = 0.038$), but number of PVS was not (beta(se) $= -0.001(0.004)$, $z = -0.206$, $p = 0.837$).

Conclusion: These findings suggest that asymmetry in PVS is an independent predictor of PSE after an AIS (after accounting for several clinical characteristics associated with PSE). If confirmed in larger studies, PVS could potentially serve as a biomarker to predict high-risk AIS patients, be used to monitor antiepileptogenic trials closely, and eventually .assist the selection of more individualized treatment streams.

Assessment of prediabetes and chronic hyperuricemia on inflammation and motor recovery after ischemic stroke.

Andrew Clarkson[1], **Nikita Potemkin**[2] **and Ute Zellhuber-McMillan**[3]
[1]*1Department of Anatomy, Brain Health Research Centre and Brain Research New Zealand, University of Otago, Dunedin, New Zealand*
[2]*Department of Anatomy, Brain Health Research Centre and Brain Research New Zealand, University of Otago, Dunedin, New Zealand*
[3]*Department of Anatomy, Brain Health Research Centre and Brain Research New Zealand, University of Otago, Dunedin, New Zealand*

Abstract

Background: Recovery following a stroke is difficult to predict, with comorbidities such as diabetes and hyperuricemia contributing to poor neurological outcomes. A hallmark of both diabetes, hyperuricemia and stroke is inflammation. Further, hyperuricaemia and diabetes and are linked to metabolic impairments and poor vascular health. However, little is known about the role of diabetes and hyperuricemia on stroke outcome.

Aim: We aimed to assess whether obese prediabetic (POUND (Lepr(db/*lb*)) and chronic hyperuricemic, (PLT2) mice would have aberrant inflammation that would contribute to poor vascular health and impaired stroke recovery.

Method: Focal stroke to the motor cortex was induced using the photothrombosis method in POUND, PLT2 or wild-type (WT) mice. Circulating cytokines levels were assessed from tail tip blood samples as were blood lipids, HbA1c levels and basal fasting glucose. Behavioural assessments were performed weekly on both cylinder and grid-walking tasks.

Results: PLT2 mice (lean, hyperuricemic, $n = 10$) had significantly lower HbA1c and basal glucose levels compared to WT controls ($n = 10$) indicating they were hypoglycaemic ($P < 0.001$). Assessment of PLT2 mice revealed increased circulating cytokine levels, expansion of infarct volume and impaired motor recovery ($P < 0.001$). Further PLT2 mice had increased total cholesterol and LDL levels ($P < 0.01$). Assessment of POUND mice (obese, hyperuricemic, $n = 10$) revealed normal basal fasting glucose and elevated HbA1c levels confirming they are prediabetic ($P < 0.001$). A significant increase in total cholesterol and LDL level were observed compared to WT controls ($P < 0.001$). POUND mice also revealed increase in circulating cytokine levels and impaired motor recovery ($P < 0.001$).

Conclusions: These studies highlight that both POUND and PLT2 mice have aberrant inflammation and elevated lipids contributing to coronary risk and poor recovery.

Sex-based differences in B cell subsets & functional recovery after stroke

Katie Malone[1], Riley Franks[2], Jadwiga Turchan-Cholewo[2], Thomas Ujas[2], Katherine Cotter[3], Daimen Britsch[2], Edric Winford[2] and Ann Stowe[4]

[1]*University of Ky*

[2]*Department of Neuroscience, College of Medicine, University of Kentucky, Lexington, KY 2Center for Advanced Translational Stroke Science (CATSS), University of Kentucky, Lexington, KY*

[3]*University Of Kentucky*

[4]*Department of Neuroscience, College of Medicine, University of Kentucky, Lexington, KY Center for Advanced Translational Stroke Science (CATSS), University of Kentucky, Lexington, KY Department of Neurology, College of Medicine, University of Kentucky, Lexington, KY*

Abstract

Background: Brain-localized age-associated B cells (ABCs) occur during multiple sclerosis, performing pro- or anti-inflammatory roles depending on context, but their role(s) during stroke remain unclear.

Aim: To classify ABCs in the context of stroke using mouse and human tissue.

Method: Mice ($n = 60$;19–28 mos) were randomly assigned to 30-min middle cerebral artery occlusion surgery or uninjured controls for either flow cytometry or histology. Mice underwent rotarod (motor coordination), open field (anxiety), and catwalk (gait) behavioral assays to examine functional recovery. Flow cytometry antibodies CD45, CXCR5, CD23, TCRβ, CD27, CD11b, CXCR4, IgG2a/c, IL-21R, CD11c, CD80, CCR7, Mouse IgD, IgM, MHC II, CD138, and CD21/25 identified ABCs in splenic or brain-derived samples using high-dimensional clustering (UMAP). For histology, mouse (40μm coronal) or post-stroke human cortical tissue (20μm) was stained with B220 (B cells), T-Bet (ABCs), and DAPI. Confocal/epifluorescent imaging occurred on a Nikon Ti2 or Zeiss Axioscan Z.1. Statistics performed with GraphPad Prism.

Results: Aged male mice ($n = 15$) demonstrated motor coordination deficits ($p = 0.0029$, 0.0006, and 0.0010) but no gait deficits through 3 weeks post-stroke. Aged females ($n = 15$) showed no post-stroke deficits in either motor coordination or gait, but pre-stroke baseline was already worse ($p = 0.0001$) than young controls ($n = 15$). Clustering analysis comparing males vs. females showed varying B cell subsets ($p = 0.0001$), including CD11bhi ABCs in both males and females, though females demonstrated higher subset variability. Histology confirmed T-Bet+ ABCs in cortical, hippocampal, and cerebellar regions post-stroke. ABCs were also in the brains of healthy aged mice ($n = 15$), though without discernable patterns of diapedesis. Cortical ABCs were present in post-stroke in human parenchyma.

Conclusion: Our data are the first histological confirmation of ABCs in the aged brain pre- and post-stroke, with potential identification of unique ABC subsets. These populations are elevated in aged females, the population at greatest risk for stroke and vascular dementia.

Serotonin receptor HTR2B regulates phagocytic function of brain infiltrated monocyte/macrophages in the neuroinflammation after brain injury

Yueman Zhang[1] and Peiying Li[2]

[1]*Shanghai Jiao Tong University School of Medicine Affiliated Renji Hospital*
[2]*Renji Hospital, Shanghai Jiao Tong University School of Medicine*

Abstract

Background: Monocytes/macrophages infiltrating the brain after acute injuries play a critical role in resolving neuroinflammation through their phagocytic function. Neurotransmitter receptors on these cells may regulate this function, but the specific mechanism is not well understood.

Aim: This study aimed to investigate the role of HTR2B, a serotonin receptor upregulated after monocyte/macrophages brain infiltration, in the phagocytic function after brain injury.

Method: Single cell RNA sequencing, immunofluorescence and flow cytometry were used to examine the phenotypic change of immune cells in the ischemic area and bone marrow tissue following middle-cerebral-artery-occlusion (MCAO) and traumatic-brain-injury (TBI). Combined RNA-sequencing and metabolomics were used to elucidate the transcriptional and metabolic changes of the brain infiltrated monocytes/macrophages. Pharmacological inhibition and conditional knockout of HTR2B in Lyz2^{+}monocyte/macrophage (Lyz2^{cre}HTR2b$^{fl/fl}$ mice) were used to examine the role of HTR2B in regulating the phenotypic and metabolic changes of brain infiltrated monocyte/macrophages.

Results: We found brain infiltrated monocyte/macrophages exhibited significantly increased expression of HTR2B compared to peripheral monocytes/macrophages after MCAO and TBI. Activation of HTR2B using BW723C86 enhanced phagocytosis in cultured monocyte/macrophages after oxygen-glucose-deprivation (OGD), while pharmacological inhibition of HTR2B by SB204741 attenuated phagocytosis. RNA-sequencing and metabolomics showed that activation of HTR2B in the brain infiltrated monocyte/macrophages exhibited upregulated intracellular creatine levels and enhanced mitochondrial oxidative phosphorylation after MCAO. Administering creatine in cultured monocyte/macrophages increased oxidative phosphorylation and further enhanced their phagocytic function following OGD. Lyz2^{cre}HTR2b$^{fl/fl}$mice exhibited impaired phagocytosis, exacerbated neuroinflammation and increased infarction size after MCAO in both male and female mice.

Conclusions: Our findings suggest that upregulated HTR2B expression in monocyte/macrophages and is critical for the phagocytic function to reduce brain damage after MCAO and TBI. HTR2B activation increases creatine levels in these cells, enhancing their oxidative phosphorylation and phagocytic function. Modulating HTR2B and creatine metabolism may offer a novel therapeutic strategy to resolve neuroinflammation after acute brain injuries.

Neutrophil-derived CAMP promotes cerebral angiogenesis after ischemic stroke

Wanqin Xie[1], Tingting Huang[1], Yunlu Guo[1] and Peiying Li[1]

[1]*Renji Hospital, Shanghai Jiao Tong University School of Medicine*

Abstract

Background: Neutrophils play critical roles in the evolving of brain injuries following ischemic stroke. However, how neutrophils impact the brain repair in the late phase after stroke remain uncertain.

Aim: To investigate how neutrophil-derived cathelicidin antimicrobial peptide (CAMP) impact angiogenesis and brain repair after stroke.

Method: Using a prospective clinical stroke patient cohort and middle cerebral artery occlusion (MCAO) model, we collected the peripheral blood and brain sample to detect the CAMP level. We used CAMP$^{-/-}$ mice or intracerebroventricular injection (ICV) of CAMP recombinant protein (rCAMP) to explore the function of CAMP in stroke. Neurological function after MCAO was measured by cerebral blood flow, neurological function score and behavioral test. Endothelial cell proliferation and angiogenesis were evaluated by EdU proliferation assay and immunofluorescence staining. Using bEND3 cells subjected to oxygen-glucose deprivation (OGD), RNA sequencing and antagonists AZD-5069, JNJ-47965567, WRW4 treatment, we explored the mechanism of CAMP in promoting angiogenesis after MCAO.

Results: We found significantly increased CAMP in the peripheral blood of stroke patients compared to that of healthy controls. While in the mouse stroke model, CAMP was present in the peripheral blood, ischemic brain and significantly increased at day1, 3, 7, 14 after MCAO. CAMP$^{-/-}$ mice exhibited significantly increased infarct volume, exacerbated neurological outcome, reduced cerebral endothelial cell proliferation and vascular density at 7 and 14 days after MCAO. We found significantly increased angiogenesis-related gene expression with the treatment of rCAMP after reoxygenation. AZD-5069, the antagonist

of CAMP receptor CXCR2, or knockdown of CXCR2 impeded angiogenesis and neurological recovery after MCAO. Administration of rCAMP promoted endothelial proliferation and angiogenesis and attenuated neurological deficits 14 days after MCAO.

Conclusions: Neutrophil derived CAMP represents an important mediator that could promote post-stroke angiogenesis and neurological recovery in the late phase after stroke.